POLITECNICO
MILANO 1863

SCUOLA DI INGEGNERIA INDUSTRIALE
E DELL'INFORMAZIONE

Numerically Efficient Methods for Low-Thrust Collision Avoidance Maneuver Design in Multiple Orbital Regimes

Tesi di Laurea Magistrale in
Ingegneria Spaziale

Author: **Gabriele Dani**

Student ID: 968112
Advisor:
Prof. Pierluigi Di Lizia
Co-advisors:
Prof. Roberto Armellin
PhD Candidate Andrea De Vittori

Academic Year: 2021-22

Abstract

Due to the intensive exploitation of the space environment and the increasing number of debris present, the problem of collisions between the latter and active satellites is growing at a relentless pace. Given the new investments in CubeSats and the development of large constellations, it is difficult to expect a stabilization of this phenomenon. Compared to lower orbits, the geostationary regime is less crowded. However, the presence of debris remains considerable and despite the smaller number of active missions, the risk of a collision is rising concern in this area. For these reasons, the planning and implementation of Collision Avoidance Maneuvers (CAMs) is becoming a crucial task for the success of space missions. The above-mentioned problems are compounded by recent technological innovations in the field of space propulsion. The increase in the number of satellites equipped with low-thrust propulsion systems, presents a new perspective to the study of anti-collision maneuvers.

This thesis investigates the design of optimal and computationally efficient low-thrust CAMs in different orbital regimes. In the first part, a conjunction in Low Earth Orbit (LEO) is prevented thanks to two different CAM policies. The first one involves the execution of a maneuver enforcing a certain threshold on the collision probability (PoC) at the Time of Closest Approach (TCA), then safely letting the spacecraft re-enter in a point belonging to its nominal orbit. For this purpose, the conjunction dynamics of the two objects are presented in a Cartesian reference system and then projected onto the B-plane, centered on the secondary object. The second method simply forces the satellite to match the original orbit Keplerian parameters, neglecting the true anomaly.

In the second part, the thesis deals more specifically with collisions in the geostationary region. In this particular orbital regime, objects undergo gravitational perturbations that can cause a change in the satellite's motion violating its assigned slot, characterized by precise latitude and longitude boundaries. To cope with it, ad-hoc strategies keep the satellite confined within its assigned box through Station-Keeping (SK) maneuvers. The goal is to formulate a procedure that allows a station-keeping maneuver to be carried out and at the same time avoid a possible collision. Contrary to the first two envisioned methods, modeled considering a Keplerian motion, embedding CAMs and SK necessitates

the addition of geopotential perturbation in the dynamical model.

In each of the analyzed cases, fully analytical methods are based on the approximation of orbital motion thanks to the State Transition Matrix (STM). The effect of linearization in the LEO case is investigated by comparing it with a semi-analytical procedure capable of calculating the optimal maneuver through several successive linearizations. In order to fulfill the operational requirements, an iterative method able of finding the Bang-Bang transformation starting from the analytical solution of the control problem for continuous-thrust maneuvers is also showcased. Applying the previous iterative method to approximate an impulsive maneuver is succesively examined. Finally, a purely bang-bang solution was found, which does not use smoothing techniques starting from the approximate solution.
The different algorithms are compared in terms of efficiency and computational robustness.

Keywords: GEO, CAM, station-keeping, PoC, TCA, optimization.

Abstract in lingua italiana

A causa dello sfruttamento intensivo dell'ambiente spaziale e del crescente numero di detriti presenti, il problema relativo alle collisioni tra quest'ultimi ed i satelliti attivi è in forte aumento. Visti i nuovi investimenti in cubesat e nello sviluppo di grandi costellazioni, risulta difficile aspettarsi una stabilizzazione di questo fenomeno. Rispetto ad orbite più basse, il regime geostazionario risulta meno affollato. Tuttavia, la presenza di detriti rimane di notevole entità e nonostante il minor numero di missioni attive, il rischio di una collisione è preoccupante anche in questa zona. Per queste ragioni, la pianificazione e la realizzazione di manovre anticollisione sta diventando un compito fondamentale per il successo delle missioni spaziali. Ai problemi sopraelencati si aggiungono le recenti innovazioni tecnologiche nell'ambito dei sistemi propulsivi. L'aumento del numero satelliti equipaggiati con sistemi di propulsione a bassa spinta, pone di fronte ad una nuova prospettiva nello studio delle manovre.

Questa tesi indaga la progettazione di manovre anticollisione a bassa spinta ottime ed efficienti dal punto di vista computazionale in regimi orbitali differenti. Nella prima parte, viene impedita una congiunzione in LEO grazie a due diverse strategie. Il primo metodo prevede l'esecuzione di una spinta che consenta di rispettare una determinata soglia sulla PoC al TCA, imponendo poi che il satellite rientri in sicurezza in un punto appartenente alla sua orbita nominale. A questo scopo, la dinamica di congiunzione dei due oggetti è presentata in un sistema di riferimento cartesiano e poi proiettata sul B-plane, centrato sull'oggetto secondario. Il secondo metodo obbliga semplicemente che, al fine manovra, il satellite abbia gli stessi parametri kepleriani dell'orbita originale, trascurando l'anomalia vera.

Nella seconda parte, la tesi tratta in modo più specifico collisioni in regime geostazionario. In questo regime orbitale particolare, gli oggetti subiscono perturbazioni gravitazionali che possono causare un cambiamento nel moto del satellite, tale da violare lo slot a lui assegnato caratterizzato da precisi confini di latitudine e longitudine. Per poter far fronte a questo, è necessario adottare strategie ad-hoc in modo da mantenere il satellite confinato all'interno del box attraverso manovre di Station-Keeping (SK). L'obiettivo è formulare una procedura che consenta di realizzare una manovra di SK e allo stesso tempo

evitare una possibile collisione. A differenza dei primi due metodi previsti, modellati considerando un moto kepleriano, l'incorporazione di CAM e SK richiede l'aggiunta di una perturbazione geopotenziale nel modello dinamico.

In ognuno dei casi analizzati sono stati sviluppati metodi completalmente analitici, basati sull'approssimazione del moto orbitale grazie alla STM. L'effetto delle non linearità nel caso LEO viene indagato confrontando la soluzione ottenuta con una procedura semi-analitica capace di calcolare la manovra ottima attraverso più linearizzazioni successive. Al fine di soddisfare i requisiti operativi, viene inoltre presentato un metodo iterativo in grado di trovare la soluzione Bang-Bang a partire dalla soluzione analitica del problema di controllo per manovre a spinta continua. Successivamente, viene esaminata l'applicazione del metodo iterativo precedente per approssimare una manovra impulsiva ed infine, è stata trovata una soluzione puramente bang-bang che non utilizza tecniche di smoothing. I diversi algoritmi sono confrontati in termini di efficienza e robustezza computazionale.

Parole chiave: GEO, CAM, station-keeping, PoC, TCA, ottimizzazione

Contents

1 | Introduction

This first chapter provides a general introduction to the space debris problem and the purpose of the thesis. After presenting the framework, a brief review about the state of the art of collision avoidance maneuvers adopting low-thrust propulsion is reported. Finally, the last part of the chapter focuses on a dissertation about the thesis work.

1.1. Space Debris

Space debris is human-generated junk left around the Earth. The number of artificial objects no longer functional for operative applications has gradually increased since the start of space activity.
In 2013 NASA reported that more than 210 000 pieces at least the size of a softball were being tracked, ad an estimate of 500 000 pieces at least the size of marble is thought to exist. More than 100 million even smaller objects, ranging down to the size of a tiny fleck of paint, are too small to be detected or tracked [13].

Figure 1.1: Space debris distribution around Earth source [7](ESA).

Fig. 1.1 is a computer-generated picture that represents the space debris population located in two main regions. The first is the ring of objects in Geostationary Earth Orbit (GEO), at 36 000 km, and the second cloud is in Low Earth Orbit (LEO), between 400 and 2000 km of altitude.

During the early years of space exploration, scientists and astronomers feared that the missions might be threatened by the presence of natural debris around our home planet. However, no mission was hindered by the object of this type. The real problem is represented by artificial debris generated as time goes by.

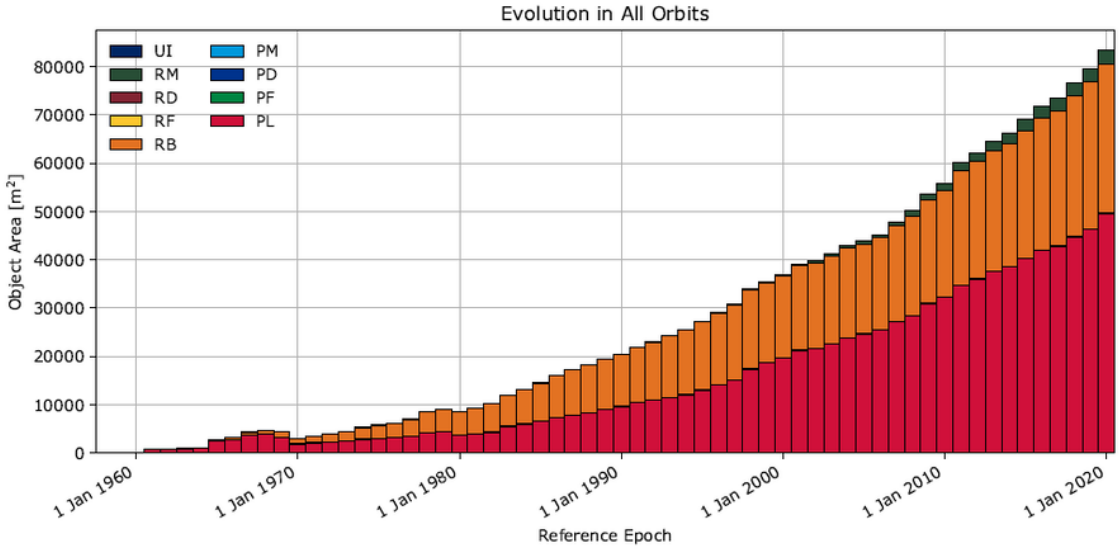

Figure 1.2: Space debris object area evolution in all orbits source [7](ESA).

Classification	Description
PL	Payload
PF	Payload Fragmentation Debris
PD	Payload Debris
PM	Payload Mission related Object
RB	Rocket Body
RF	Rocket Fragmentation Debris
RD	Rocket Debris
RM	Rocket Mission Related Object
UI	Unidentified

Table 1.1: Object Classification.

Fig. 1.2 shows the steadily increasing of artificial debris since the beginning of the space age. This cloud of objects is generated mainly from spacecraft and rocker stages break ups, and it needs to be constantly monitored to predict and avoid future collisions. Considering things stand, impacts between debris and working satellites seem to grow relentlessly.

Starting from 2009 the European Space Agency (ESA) has implemented the Space Situational Awareness (SSA) Program, which allows Europe to acquire the independent capability to watch objects and natural phenomena that could harm both on-ground and on-orbit facilities. In particular, the program focuses on: Space Weather and solar activity prediction, Near-Earth Object (NEO) monitoring for detecting natural objects such as asteroids that can impact Earth, and Space Surveillance and Tracking (SST) to watch active and inactive satellites. Under SSA, SST constantly updates a data catalog for all orbiting objects to send alerts to the stakeholders and command dedicated maneuvers if a collision is likely to occur. Further information is reported in [8].

The objective of sustainable use of space environment can be achieved by following the existing guidelines and standards:

- Design rockets and spacecraft to minimize the amount of shedding, and material becoming detached during launch and operation, due to the harsh conditions of space.
- Prevent explosions by releasing stored energy, "passivating" spacecraft once at the end of their lives.
- Design end-of-life disposal of satellites, moving them out of the way of working satellites.
- Prevent in-space impacts through careful choice of orbits placement and by performing Collision Avoidance Maneuvers.

This thesis focuses on the last measure, i.e., Collision Avoidance Maneuver (CAM) design both in LEO and GEO regimes.

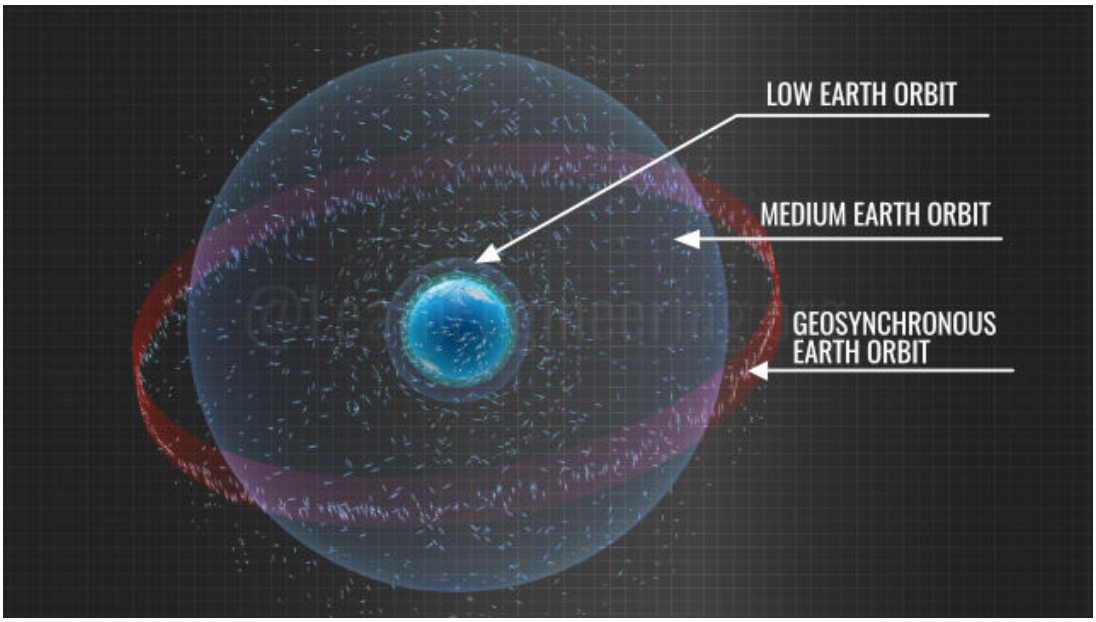

Figure 1.3: Different orbital regimes around Earth source [16].

LEO represents the most adopted region for remote sensing, imaging, and commercial applications due to its close proximity to the Earth. The intensive usage of this space sector has transformed it into a bullets depository. Furthermore, the proliferation of space junk continues essentially unabated owing to rocket bodies, paint flecks, mission-related payloads, and fragments resulting from previous collisions.

The situation in the GEO ring is widely different because, as far as it is known, the debris spatial density is lower than in some LEO altitudes. The reason relies on the lower number of space missions that interest this region and on the higher distance that gives a higher resident volume. However, the total number of operating objects is overwhelming [27].

The objects which constitute the GEO region are upper stages, apogee boost motors, and mission-related tools like deployment hardware and instrument covers. The above list is enlarged by each non-operational satellite that represents a potential hazard to other active satellites once it reaches its end of life. Regrettably, only the largest objects are regularly observed and cataloged. However, there are several potential sources of small-size debris, such as explosion fragments that cannot be detected, and becomes an even more alarming threat for other assets [7].

When, at TCA, a threshold on the Miss Distance (MD), or on the PoC, is exceeded, a collision avoidance maneuver is performed.

The onboard thrusters are fired to generate the change in trajectory planned and perform CAMs. The cost of the maneuver can be evaluated by looking at the Δv given from the propulsion system.
The time interval between the encounter and the prediction time, the trajectory constraints, and the onboard propulsion system affect the fuel consumption. A CAM executes depending on the available engine technology. An impulsive strategy is preferable with a high thrust propulsion system. Conversely, low-thrust firings are typically associated to high specific impulse engines.

Moving on to CAM planning, it is possible to adopt long-term and short-term strategies. In the former, the maneuver is commanded a certain number of revolutions before the closest approach. It consists on an along-track separation between the spacecraft and the debris object. The collision is avoided by reaching the encounter point at a new arrival time. The second strategy requires a larger Δv. CAM counts on the radial separation between the spacecraft and the debris, which is achieved with an altitude increase at the encounter point [26]. At the end of each maneuver, the spacecraft shall return to its nominal orbit. There are two different ways to accomplish this objective i.e. including the position constraint in the optimization problem or combining the station-keeping maneuver with the CAM execution.

Since 2009, Conjunction Messages have been sent by Joint Space Operations Center (JSpOC) to all spacecraft owners and operators, concerning approximately 48000 objects listed in the Two-Line Element set (TLE) provided by US Strategic Command (USSTRATCOM).
JSpOC provides a Conjunction Assessment Report about a proximity event between a primary satellite and another satellite or space object; it also includes the TCA, the miss distance, relative position and velocity, observation statistics, the satellite covariance matrices and the time of last acceptable observation. The standard format Conjunction Summary Message (CSM)/Conjunction Data Message (CDM) is prepared by the Consultative Committee for Space Data Systems (CCSDS). Detailed information about CDM can be found in [9].

Every week hundreds of alerts are issued for spacecraft in LEO. In most cases, the collision risk decreases during the weeks thanks to the new information obtained on the debris orbit. However, sometimes an operative action is demanded to prevent the impact.
Nowadays, CAMs are planned on-ground, with the support of specific tools. If the predefined threshold on the probability or the miss distance is exceeded, a maneuver is designed by mission planners. The Space Debris Office (SDO) is the department of the ESA in charge of all the activities concerning space debris; a complete description of the

SDO current collision avoidance service can be found in [19].
Due to the increasing number of satellites launched into orbit, current "manual" methods for avoiding in-space collisions and the creation of new debris will not be enough. For this reason, it is fundamental an onboard autonomous solution.

1.2. State of the Art

To consider a CAM optimal, the collision probability of a satellite with one, or more, space objects reduces below a prescribed threshold while minimizing a cost function.
The literature regarding the optimization of impulsive collision avoidance practices is the most thorough; however, in the last years, researches have deepened the theory behind low-thrust CAM.
Rasotto et al. in [23] found an impulsive fuel-optimal maneuver through the implementation of a genetic algorithm. Multi-objective particle swarm optimizers are employed by Morselli et al. [21] to design optimal CAMs. Both the methods involve an high computational effort due to the fully numerical procedure. Research on low-thrust optimization methods includes the semi-analytical method developed by Reiter et al. [24] for rapid collision avoidance, based on the hypothesis that the optimal thrust is always radial.

In 2021 Palermo [22] developed an analytic solution for the Energy Optimal Problem (EOP) using PoC at TCA as final constraint, both in cartesian coordinates and B-plane dynamics formulation. The analytic solution is then used to find, using a smoothing technique, the bang-bang acceleration profile of the Fuel Optimal Problem (FOP). More semi-analytical methods were proposed in [12]; this approach harnesses average dynamics maximizing the miss distance with the assumption of continuous tangential thrust.

Bombardelli and Hernando-Ayuso [14] investigated the problem of optimum low-thrust collision avoidance between two objects in circular orbits; the thrust vector of the maneuvered satellite, applied continuously for a given time span, is held constant in magnitude. The optimal control is written in B-plane coordinates in order to reduce significantly the dimension of the resulting Two Point Boundary Value Problem (TwPBVP) to only two with a constant costate vector.

Martinez Chamarro et al. [18] present two approaches to computing low-thrust CAM; the first is based on the reconstruction of a bang-bang structure by applying a smoothing approach to an EOP continuous solution in the second method, the maneuver design is formulated as a convex optimization problem.

The literature about the combination of low-thrust CAM and GEO Station Keeping (SK)

is almost nonexistent. In 2017 Gazzino resumes the principal aspect of the linearized state space representation of the dynamics of a Geostationary orbit [10]. Two years later he used this dynamical model to define and solve the FOP for geostationary SK using low-Thrust electric propulsion [11].

In 2012 Lee developed a collision avoidance maneuver for low Earth orbit (LEO) and geostationary Earth orbit (GEO) satellites maintained in a keeping area [15]. A Genetic Algorithm (GA) is used to obtain both the maneuver start time and the delta-V to reduce the probability of collision with uncontrolled space objects or debris. The limitation of using GA as optimization algorithm is represented by the numerical effort.

Finally, Cantoni in 2021 during her thesis work [4] developed a numerically efficient strategy to solve the EOP for an SK maneuver that includes the possibility to execute a CAM. The principal limitation is the continuous acceleration profile not capable to reproduce a bang-bang structure and the choice of the final state selected only by imposing a target on the Geostationary box.

1.3. Dissertation

This thesis strives to complete the work of Palermo adjoining CAM and the re-entry to the original orbital regime. It fixes the terminal state or the final desired orbital elements with a Three Point Boundary Value Problem (ThPBVP).

The second part of the research is a procedure capable to solve the EOP associated to SK and to an eventual CAM. Differently from the work developed by Cantoni, the dynamic leverages is modeled using the Equinoctial Orbital Element (EOE) presented in Gazzino's works [10]. It is more computationally efficient compared to the Cartesian one and it makes the bang-bang adaption straightforward.
Another improvement of this research consists in the choice of the target state at the end of the maneuver; the terminal state is tailored to maximize. This is achieved both with an analytical approximation and with an optimization procedure.

Summing all, the scope is to provide numerically efficient and robust methods to perform an optimized CAM for different orbital regimes; the thesis is divided into 5 chapters.

Chapter 2 introduces the baseline to work on conjunction analysis. In particular, the collision framework, the B-Plane reference, the concepts of Probability of Collision, and Squared Mahalanobis Distance. Moreover, it presents the derivation of the state transition matrix and showcases a brief description of the adopted dynamical models and the fundamentals of the GEO SK routines.

Chapter 3 presents the CAM optimal control problem. In the first part, the solution of the EOP and the associated FOP transformation fixing the terminal state is presented. In the second part, a similar procedure is applied to solve the problem of fixing the final orbit; this variation leads to a problem farming in keplerian elements. The state variation allows to express easily the terminal constraints and simply to leave free the final true anomaly.

Chapter 4 focuses the combination of a CAM and a SK maneuver. The developed algorithm is capable to understand if SK alone is sufficient to respect the PoC constraints, and it is combined with CAM if not.

Chapter 5 is the final part of this thesis work, it summarizes the conclusions and suggestions for further developments.

2 | Fundamentals

This chapter contains the necessary mathematical background to get the insights on the work presented in this master thesis. It begins with the fundamentals of conjunction dynamics and the formulation in B-plane coordinates. Then, the focus shifts to the collision probability, with the assumption of short-term encounters. Right after, dynamical models used in this master thesis are presented, followed by the basic notions on optimal control theory. The chapter concludes with the introduction of the STM.

2.1. Conjunction Analysis

To analyze a possible collision consider two objects experiencing a conjunction event with an expected relative position $\vec{r}_e$. The manoeuvrable spacecraft is called "primary object", and is indicated with the symbol O_p, while the uncooperative debris is the "secondary object" , O_s.
The state vectors (position and velocity) of the primary and secondary center of mass are in a generic (inertial or a local) reference frame (r.f.) $\hat{\Re}$, as $\vec{x}_p = (\vec{r}_p, \vec{v}_p)$ and $\vec{x}_s = (\vec{r}_s, \vec{v}_s)$. Each object, at a generic time t, has a dynamics evolution expressed by $\vec{f}_p$ and $\vec{f}_s$.

$$\begin{aligned} \frac{d\,\vec{v}_p(t)}{dt} &= \vec{f}_p(t, \vec{x}_p), \\ \frac{d\,\vec{v}_s(t)}{dt} &= \vec{f}_s(t, \vec{x}_s). \end{aligned} \tag{2.1}$$

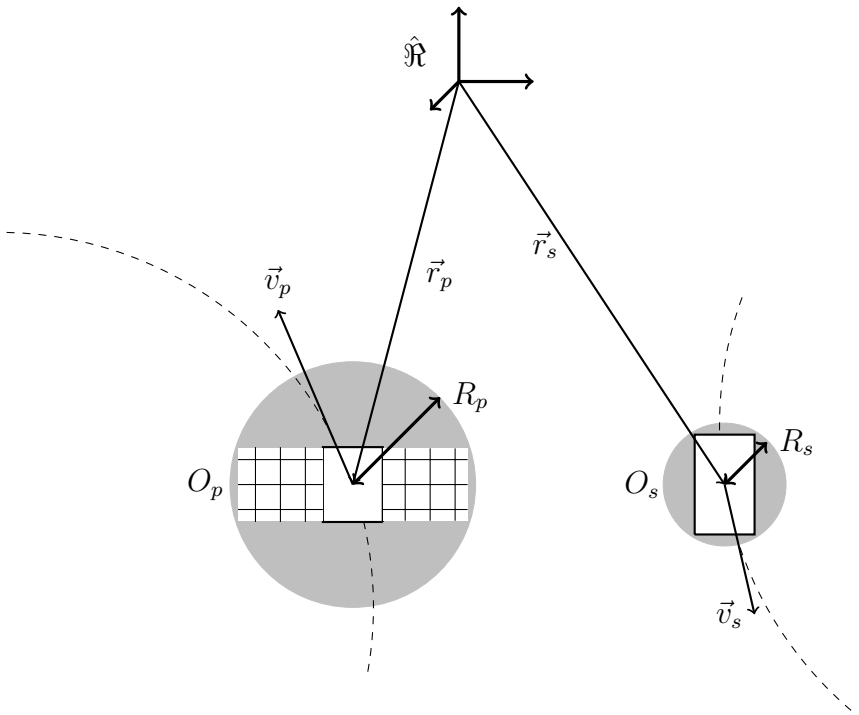

Figure 2.1: Encounter between two objects.

The collision domain simplifies with the Spherical geometry hypothesis: O_p and O_s are modeled as spheres of radii R_p and R_s respectively.
Figure 2.1 represents the space configuration of an encounter between two objects modeled in such a way. The approximation allows to neglect the objects geometry and attitude a priori knowledge.

2.2. B-plane Definition

Let $\{x, y, z\}$ represent an inertial r.f. centred at $O_p - O_s$ and with axes directions defined as:

$$\vec{u}_x = \frac{\vec{v}_p}{||\vec{v}_p||}, \qquad \vec{u}_z = \frac{\vec{v}_p \times \vec{v}_s}{||\vec{v}_p \times \vec{v}_s||}, \qquad \vec{u}_y = \vec{u}_z \times \vec{u}_x. \tag{2.2}$$

Within a small time interval $\Delta t \ll 1$, the motion of both the objects can be approximated as uniform and rectilinear.
The collision avoidance dynamics is set in B-plane coordinates (see Fig 2.2. The B-plane comes handy to describe the position vector $\vec{b}_{3D} = [\xi, \eta, \zeta]^\top$ in such reference system is defined as follows:

- $\vec{u}_\xi = \frac{\vec{v}_s \times \vec{v}_p}{||\vec{v}_s \times \vec{v}_p||}$ direction of the Minimum Orbit Intersection Distance (MOID)

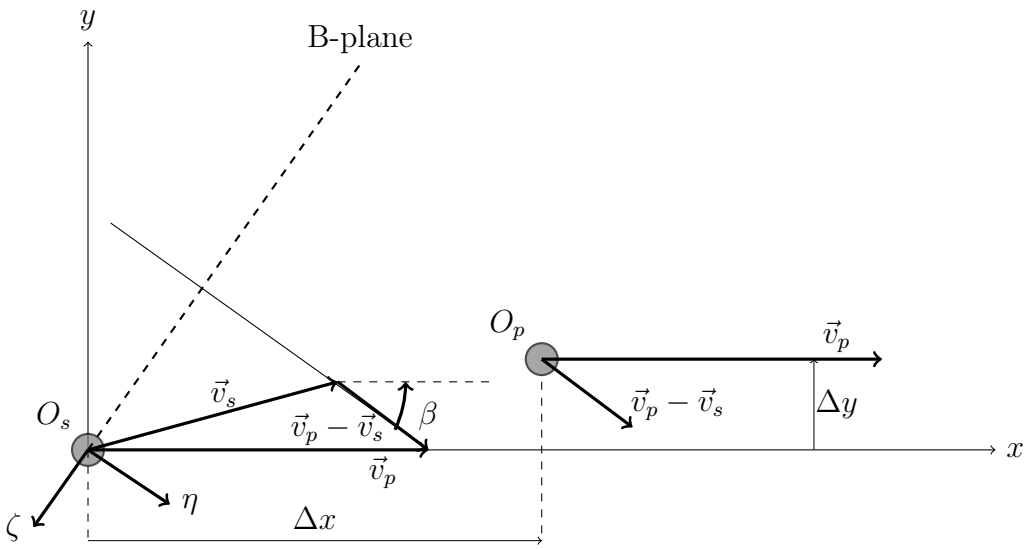

Figure 2.2: Encounter frame and B-plane: snapshot of $O_p - O_s$ encounter geometry ($x-y$ plane) after the manoeuvre.

orthogonal to the geocentric velocity vectors $\vec{v}_p$ and $\vec{v}_s$;

- $\vec{u}_\eta = \dfrac{\vec{v}_p - \vec{v}_s}{||\vec{v}_p - \vec{v}_s||}$ direction of the velocity of O_p relative to O_s;
- $\vec{u}_\zeta = \vec{u}_\xi \times \vec{u}_\eta$ direction opposite to B-plane velocity projection of O_s.

The unit vectors define the rotation matrix from the inertial reference frame to the B-plane

$$\vec{R}_{b,3\mathrm{D}} = [\vec{u}_\xi,\ \vec{u}_\eta,\ \vec{u}_\zeta]^\top, \tag{2.3}$$

while the projection in the η-axis is achieved by

$$\vec{R}_{b,2\mathrm{D}} = [\vec{u}_\xi,\ \vec{u}_\zeta]^\top. \tag{2.4}$$

At TCA, the orbital elements of O_p are defined as: a_0 semi-major axis, e_0 eccentricity, R_c radial orbital distance, θ_c true anomaly.

Additionally, for the ease of notation, the 2D position vector in the B-plane is defined as $\vec{b} = [\xi, \zeta]^\top$, constructed from the first and third components of the $\vec{b}_{3\mathrm{D}}$ vector.

2.3. Short-term Encounter Characteristics

The short-term encounter hypothesis lowers the problem complexity. It holds every time that the encounter is almost instantaneous. As it is stated in [1]:

- The primary and the secondary object nominal trajectories can be approximated to straight lines, with constant velocities during the encounter since it lasts just few seconds.
- There is no velocity uncertainty during the encounter. This is valid because typical velocity errors are of the order of few meters/second, and the encounter does not last that much to condition PoC.
- The position uncertainty during the encounter is constant and equal to the value at the estimated conjunction. This comes directly from the previous point.
- The positions uncertainties of the primary and the secondary objects are represented by Gaussian distributions, exploited for the collision probability estimation.

2.4. Collision Probability and Squared Mahalanobis Distance

Considering again the hypothesis of spherical geometry, a collision is assumed to occur in a time interval I if and only if a date $\bar{t}\,\epsilon\, I$ exists such that:

$$||\vec{r}(\bar{t})|| = ||\vec{r}_p(\bar{t}) - \vec{r}_s(\bar{t})|| \leq R_p + R_s. \tag{2.5}$$

To simplify the PoC evaluation, the collision assembly at an instant $\bar{t}$ can be substituted with the combined sphere of radius $s_A = R_p + R_s$: it is the hard body radius, shown in Figure 2.3.

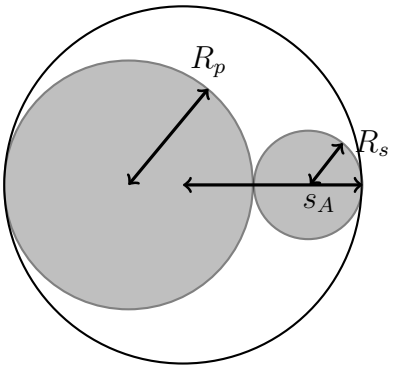

Figure 2.3: Combined body representation.

PoC can be written, in general terms, as the triple integral of the probability distribution function $f_r(\vec{r})$ of the primary relative position with respect to the second over the volume V swept by a sphere of radius s_A centred at secondary body:

$$\text{PoC} = \int_V f_r(\vec{r})\mathrm{d}\vec{r}. \tag{2.6}$$

Where the Gaussian Probability density function (PDF) of this relative position $f_r(\vec{r})$ is given by:

$$f_r(\vec{r}) = \frac{1}{\sqrt{2\pi^3 \det \vec{C}_r}} \exp\left[-\frac{1}{2}(\vec{r}-\vec{r}_e)^\top \vec{C}_r^{-1}(\vec{r}-\vec{r}_e)\right], \tag{2.7}$$

$\vec{C}_r$ is the combined covariance matrix of $\vec{r}$, obtained summing the individual covariance matrices of the two objects, and expressed in the same orthonormal base, when the two (Gaussian) quantities are statistically independent.
Considering the short-term encounter hypothesis, as said in paragraph 2.3, one can assume the motion of the two objects as uniform rectilinear with deterministically known velocities, and compute the collision probability as a two-dimensional integral on the collision B-plane.
Thanks to this approximation, the integration volume is reduced over a disk centred in the origin (see [20] for a detailed derivation), and Eq. 2.6 can be rewritten as a 2D integral:

$$\text{PoC} = \int_A \frac{1}{2\pi\sigma_\xi\sigma_\zeta\sqrt{1-\rho_{\xi\zeta}^2}} \exp\Bigg\{ -\frac{1}{2(1-\rho_{\xi\zeta}^2)}\Bigg[\left(\frac{\xi-\xi_e}{\sigma_\xi}\right)^2 + \left(\frac{\zeta-\zeta_e}{\sigma_\zeta}\right)^2 + \\ - 2\rho_{\xi\zeta}\left(\frac{\xi-\xi_e}{\sigma_\xi}\right)\left(\frac{\zeta-\zeta_e}{\sigma_\zeta}\right)\Bigg]\Bigg\}\mathrm{d}\xi\mathrm{d}\zeta, \tag{2.8}$$

where $r_e = [\xi_e, 0, \zeta_e]^\top$ is the expected closest approach relative position in the B-plane; A is a circular area of radius s_A; σ_ξ, σ_ζ, and $\rho_{\xi\zeta}$ can be extracted from the relative position covariance matrix in B-plane axes whose $\{\xi, \zeta\}$ submatrix reads:

$$\vec{C}_{\xi\zeta} = \begin{bmatrix} \sigma_\xi^2 & \rho_{\xi\zeta}\sigma_\xi\sigma_\zeta \\ \rho_{\xi\zeta}\sigma_\xi\sigma_\zeta & \sigma_\zeta^2 \end{bmatrix}. \tag{2.9}$$

There are several methods for calculating the 2D collision probability, many of which are collected and compared in [20]. In this thesis, it has been chosen to follow the PoC definition by Chan in [5] truncated at $m = 3$. Eq. 2.8 represents the equivalent of integrating a properly scaled isotropic Gaussian distribution function over an elliptical cross section. The final collision probability reduces to a Rician integral if the elliptical area is approximated as a circular cross-section of equal surface. The integral boils down to the following convergent series:

$$\mathrm{PoC}(u, v) = e^{-\frac{v}{2}} \sum_{m=0}^{\infty} \frac{v^m}{2^m m!} \left[1 - e^{-\frac{u}{2}} \sum_{k=0}^{m} \frac{u^k}{2^k k!} \right], \tag{2.10}$$

where u is the ratio of the impact cross-sectional area to the area of the 1σ covariance ellipse in the B-plane:

$$u = \frac{s_A^2}{\sigma_\xi \sigma_\zeta \sqrt{1 - \rho_{\xi\zeta}^2}}, \tag{2.11}$$

and v is the squared Mahalanobis distance (Squared Mahalanobis Distance (SMD)):

$$v = \mathrm{SMD} = \left[\left(\frac{\xi_e}{\sigma_\xi} \right)^2 + \left(\frac{\zeta_e}{\sigma_\zeta} \right)^2 - 2\rho_{\xi\zeta}^2 \frac{\xi_e \zeta_e}{\sigma_\xi \sigma_\zeta} \right] / (1 - \rho_{\xi\zeta}^2), \tag{2.12}$$

$$= (\vec{r}_f - \vec{r}_s)^\top \vec{R}_{b,2\mathrm{D}}^\top \vec{C}^{-1} \vec{R}_{b,2\mathrm{D}} (\vec{r}_f - \vec{r}_s), \tag{2.13}$$

$$= \vec{b}_f^\top \vec{C}^{-1} \vec{b}_f. \tag{2.14}$$

Two functions for the assessment of PoC and SMD, following Eqs. 2.10 and 2.13 are implemented: $poc\_chan(\Delta\vec{r}, \mathrm{CDM})$, $squared\_mahalanobis\_distance(\Delta\vec{r}, \mathrm{CDM})$ and the function $poc2smd(\mathrm{PoC}, \mathrm{CDM})$ allows to calculate the SMD corresponding to a given value of PoC.

2.5. Dynamical Models

In this section, the three different dynamical models adopted in the thesis work are presented. In Chapter 3, the keplerian unperturbed motion is modeled in cartesian coordinates and classical orbital elements. In Chapter 4, the orbital motion is simulated using the EOE linearized state-space model that encompasses the tesseral harmonic perturbation for the Earth's gravity field.

2.5.1. Cartesian Model: Restricted Two Body Problem

Consider a system of celestial bodies, like the solar system, each of them is characterized by a motion relative to the others described by the n-body problem. If the number system narrows to only two bodies, and one has a much larger mass, the relative acceleration vector can be stated as:

$$\ddot{\mathbf{r}} = -\frac{\mu}{r^3}\mathbf{r} \tag{2.15}$$

In particular, the two-body dynamics is:

$$\begin{cases} \dot{\mathbf{r}} = \mathbf{v} \\ \dot{\mathbf{v}} = -\dfrac{\mu}{r^3}\mathbf{r} + \mathbf{a}_c \end{cases} \tag{2.16}$$

where $\mathbf{a}_c$ is the contribution of the control acceleration.

The two-body dynamics is suitable for a preliminary design of any maneuver around the Earth.

2.5.2. Gauss Planetary Equations

These equations serve for deriving a numerically efficient propagator for a keplerian motion incorporating a non-conservative perturbing acceleration. In the case analyzed, the perturbations are composed of the control acceleration only stemming from a CAM:

$$\mathbf{x} = \begin{bmatrix} a := Semimajor\,axis \\ e := Eccentricity \\ i := Inclination \\ \Omega := RAAN \\ \omega := Argument\,of\,perigee \\ \theta := Trueanomaly \end{bmatrix} \qquad \mathbf{a_c} = \begin{bmatrix} a_n := Radial\,component \\ a_t := Tangential\,component \\ a_h := Out\,of\,plane\,component \end{bmatrix} \tag{2.17}$$

$$\mathbf{f} = \begin{cases} \dot{a} = 2\sqrt{\dfrac{a^3}{\mu}\left(\dfrac{1+e\cos\theta+e^2}{1-e^2}\right)}a_t \\ \dot{e} = \sqrt{\dfrac{a}{\mu}\left(\dfrac{1-e^2}{1+e\cos\theta+e^2}\right)}\left[2(e+\cos\theta)a_t - \dfrac{(1-e)^2}{1+e\cos\theta}\sin\theta u_n\right] \\ \dfrac{di}{dt} = \sqrt{\dfrac{a}{\mu}(1-e^2)}\sin\theta + \omega a_h \\ \dot{\Omega} = \sqrt{\dfrac{a}{\mu}(1-e^2)}\dfrac{\sin\theta+\omega}{\sin i}a_h \\ \dot{\omega} = \sqrt{\dfrac{a}{\mu}\left(\dfrac{1-e^2}{1+e\cos\theta+e^2}\right)}\left[2\sin\theta a_t - \left(2e + \dfrac{(1-e)^2}{1+e\cos\theta}\cos\theta\right)a_n\right] + \\ \qquad\qquad - \sqrt{\dfrac{a}{\mu}(1-e^2)}\dfrac{\sin\theta+\omega\cos i}{\sin i}a_h \\ \dot{\theta} = \sqrt{\dfrac{\mu}{a^3(1-e^2)^3}}(1+e\cos\theta^2) + \dot{\omega} \end{cases} \tag{2.18}$$

2.6. Dynamics of Geostationary satellite

The EOE entails a motion linearization about the station keeping position. A detailed analysis of this model is presented by Gazzino in [10]. The EOE are defined as follows:

$$\mathbf{x_{eoe}} = \begin{bmatrix} a \\ e_x = e\cos\omega + \Omega \\ e_y = e\sin\omega + \Omega \\ i_x = \tan\frac{i}{2}\cos\Omega \\ i_y = \tan\frac{i}{2}\sin\Omega \\ l_{M\Theta} = \Omega + \omega + M - \Theta \end{bmatrix} \qquad \mathbf{a_c} = \begin{bmatrix} a_n \\ a_t \\ a_h \end{bmatrix} \tag{2.19}$$

Where $\Theta(t)$ represents Greenwich right ascension.

The correspondent non-linear dynamics is expressed as:

$$\frac{d\mathbf{x_{eoe}}}{dt} = \mathbf{f_l}(\mathbf{x_{eoe}}, t) + \mathbf{f_g}(\mathbf{x_{eoe}}, t)\mathbf{a_c} \tag{2.20}$$

Introducing the nominal keeping position:

$$\begin{aligned} \mathbf{x_{sk}} &= \left[a_{sk}, 0, 0, 0, 0, l_{M\Theta,sk}\right]^T \\ \frac{d\mathbf{x_{sk}}}{dt} &= \left[0, 0, 0, 0, 0, \sqrt{\tfrac{\mu}{a_{sk}^3}} - \omega_T\right]^T = \mathbf{0} \end{aligned} \tag{2.21}$$

It is now possible to define a dynamical model based on the relative state:

$$\begin{aligned} \mathbf{x} &= \mathbf{x_{eoe}} - \mathbf{x_{sk}} \\ \frac{d\mathbf{x}}{dt} &= \mathbf{f_l}(\mathbf{x_{eoe}}, t) + \mathbf{f_g}(\mathbf{x_{eoe}}, t)\mathbf{u} - \mathbf{0} \end{aligned} \tag{2.22}$$

The dynamical system linearizes through a first-order Taylor power series expansion:

$$\begin{aligned} \mathbf{x} &= \mathbf{x_{eoe}} - \mathbf{x_{sk}} \\ \frac{d\mathbf{x}}{dt} &= \mathbf{f_l}(\mathbf{x_{eoe}}, t) + \mathbf{f_g}(\mathbf{x_{eoe}}, t)\mathbf{a_c} - \mathbf{0} \end{aligned} \tag{2.23}$$

The previous therms can be represented by the following state matrices:

$$\mathbf{A}(t) = \left.\frac{\partial \mathbf{f_l}}{\partial \mathbf{x}}\right|_{\mathbf{x_{sk}}} \qquad \mathbf{D}(t) = \mathbf{f_l}(\mathbf{x_{sk}}, t) \qquad \mathbf{B}(t) = \mathbf{f_g}(\mathbf{x_{sk}}, t)$$

The control matrix $\mathbf{B}$ can be found in [17]. The equations of motion are then:

$$\dot{\mathbf{x}} = \mathbf{A}(t)\mathbf{x} + \mathbf{D}(t) + \mathbf{B}(t)\mathbf{u} \tag{2.24}$$

Perturbations

Regarding the GEO region, the most relevant perturbation originates from the Non-spherical Earth Geopotential.
The gravity potential of the Earth, labelled with W, is a function of the geocentric radial

distance (r), geocentric latitude (ψ), and the geocentric longitude (λ) [6]. In particular:

$$W(r,\psi,\lambda) = V_W(r,\psi,\lambda) + R(r,\psi) \tag{2.25}$$

where V_W is the gravitational potential and R is the rotational potential of the Earth that have the following shapes:

$$V_W(r,\psi,\lambda) = \frac{GM}{r}\left[1 + \sum_{n=2}^{N}\left(\frac{a}{r}\right)^n \sum_{m=0}^{n}(C_n^m cos(m\lambda) + S_n^m sin(m\lambda))P_n^m(t)\right] \tag{2.26}$$

$$W(r,\psi) = \frac{\omega^2}{2}(rcos\psi)^2 \tag{2.27}$$

where: r, ψ, λ are polar coordinates, $t = sin\psi$, GM is the product between the Earth's gravitational constants and the Earth's mass, a is the semi-major axis of the reference orbit, n and m are positive integeres or zero, C_n^m and S_n^m are geopotential coefficients of n^{th} degree and m^{th} order, $P_n^m(t)$ are the associated Legendre functions and N is the maximum degree and order of the available coefficients.

In the analysis performed in Chapter 4 the geopotential contribution is extended up to the second-order ($N = 2$), because responsible for the violation of the allocated geostationary longitude slot. The effect of the perturbation in the dynamics is translated in a modification of the state matrix $\mathbf{A}$ and the vector $\mathbf{D}$. Therefore, in the case analyzed the linear elements can be decomposed into two parts:

$$\begin{aligned}\mathbf{A}(t) &= \mathbf{A_{kep}}(t) + \mathbf{A_{J2}}(t)\\ \mathbf{D}(t) &= \mathbf{D_{kep}}(t) + \mathbf{D_{J2}}(t)\end{aligned} \tag{2.28}$$

An accurate description of how these matrices are computed can be found in [10].

2.7. Optimal Control Theory

The principal aspect of this thesis work is the analytical resolution of various optimal control problems. In this sense, a brief description of the optimal control theory explained in [3] is mandatory. Let's suppose to define the general EOP.

$$J := \int_{t_i}^{t_f} \frac{1}{2}\mathbf{a_c}^T\mathbf{a_c}dt \tag{2.29}$$

Introducing the Hamiltonian expression:

$$H := \frac{1}{2}\mathbf{a_c}^T\mathbf{a_c} + \boldsymbol{\lambda}^T\mathbf{f}(\mathbf{x}, \mathbf{a_c}) \tag{2.30}$$

It is possible to modify the functional as follow:

$$J := \int_{t_i}^{t_f} \frac{1}{2}\mathbf{a_c}^T\mathbf{a_c} + \boldsymbol{\lambda}^T \left[\mathbf{f}(\mathbf{x}, \mathbf{a_c}) - \dot{\mathbf{x}}\right] dt \tag{2.31}$$

Where: $\boldsymbol{\lambda}^T\dot{\mathbf{x}} = -\dot{\boldsymbol{\lambda}}^T\mathbf{x} + \frac{d(\boldsymbol{\lambda}^T\mathbf{x})}{dt}$

The necessary conditions to reach the minimization of the previous functional consist in setting to 0 its first variation:

$$\delta J = \boldsymbol{\lambda}^T\delta\mathbf{x}\Big|_{t_0}^{t_f} + \int_{t_i}^{t_f} \frac{\partial H}{\partial \mathbf{a_c}}\delta\mathbf{a_c} + \frac{\partial H}{\partial \mathbf{x}}\delta\mathbf{x} + \dot{\boldsymbol{\lambda}}^T\delta\mathbf{x}dt = 0 \tag{2.32}$$

2.7.1. Interior Point Constraints

The threshold on PoC at TCA determines an interior point constraints. The boundary condition can be represented as:

$$N\left(\mathbf{x}(\mathbf{t_1})\right) = 0 \qquad [t_i < t_1, t_f] \tag{2.33}$$

As explained in [3] the Interior-point constraint has to be adjoined to the performance index introducing a multiplier ν.

$$J := \nu N(\mathbf{x}(t_1)) + \int_{t_i}^{t_f} \frac{1}{2}\mathbf{a_c}^T\mathbf{a_c}dt \tag{2.34}$$

The necessary condition can be obtained splitting the integral at t_1 and imposing null the first variation:

$$\delta J = \boldsymbol{\lambda}^T\delta\mathbf{x}\Big|_{t_0}^{t_{1^-}} + \boldsymbol{\lambda}^T\delta\mathbf{x}\Big|_{t_{1^+}}^{t_0} + \nu\frac{\partial N}{\partial \mathbf{x}(t_1)}d\mathbf{x}(t_1) + \int_{t_i}^{t_f} \frac{\partial H}{\partial \mathbf{a_c}}\delta\mathbf{a_c} + \frac{\partial H}{\partial \mathbf{x}}\delta\mathbf{x} + \dot{\boldsymbol{\lambda}}^T\delta\mathbf{x}dt = 0 \tag{2.35}$$

Summarizing the procedure, the interior boundary condition generate a discontinuity in

the co-state variables that can be expressed as follow:

$$\nu \frac{\partial N}{\partial \mathbf{x}(t_1)} - \boldsymbol{\lambda}^T(t_1^-) + \boldsymbol{\lambda}^T(t_1^+) = 0 \tag{2.36}$$

2.8. State Transition Matrix

Analogously to what is reported in [25], the state transition matrix (STM), labeled as $\boldsymbol{\Phi}(t, t_0)$, maps the variation of the state of a non-linear system at an arbitrary initial time t_0 into the variation of the state at an arbitrary final time t_f. For time-varying systems, the STM is found by integrating:

$$\dot{\boldsymbol{\Phi}}(t, t_0) = \mathbf{A}(t)\boldsymbol{\Phi}(t, t_0) \tag{2.37}$$

with initial condition $\boldsymbol{\Phi}(t_0, t_0) = \mathbf{I}$, and $\mathbf{A}(t)$ is the state matrix of the linear system:

$$\dot{\mathbf{x}}(t) = \mathbf{A}(t)\mathbf{x} \tag{2.38}$$

To obtain an analytical solution for an EOP CAM, the general procedure requires to linearize the motion around the nominal trajectory represented by the state $\mathbf{x}_n$, with no control term.

Therefore, the resulting state matrix normalized with respect to the nominal states has the following expression:

$$\mathbf{A} = \left. \frac{\partial \boldsymbol{f}(\mathbf{x}, t)}{\partial \mathbf{x}} \right|_{\mathbf{x}_n} \tag{2.39}$$

Consequently, the resulting STM is:

$$\delta \mathbf{x}_f = \boldsymbol{\Phi}(\mathbf{x}_n, t_0, t_f)\delta \mathbf{x}_0 \tag{2.40}$$

3 | Low-Thrust CAM EOP and FOP Design

This chapter covers the approach to address the collision avoidance problem. The dissertation is subdivided into two main segments, one for the Point To Point Maneuver (PTPM) and one for the Point To Orbit Maneuver (PTOM). Each part reports the analytical resolution of the EOP and the correspondent transformation to obtain the FOP solution. Then, for the first transfer, the semi-analytic solution adopting successive linearization is presented. Moreover, the bang-bang transformation is computed with an increasing level of thrust to attribute the maneuver to an impulsive one. At the end of the sections, more relevant results are reported.

3.1. Low-Thrust Point to Point EOP CAM Formulation

The objective is to reduce the PoC below a threshold value. In doing this it is necessary to minimize the fuel consumption considering the additional constraint to return to the unmaneuvered point of the initial orbit. The full mathematical description of the resolution procedure can be found in Appendix A, while in this section, only the most important passages, necessary to understand the applied methodology, are presented.

3.1.1. Problem Formulation

Assuming a Keplerian orbit, known: $\mathbf{x}(t_0) = \mathbf{x_0}$ initial state, t_0 initial time, t_{ca} time of closest approach, t_f final time, and $\mathbf{x}(t_f) = \mathbf{x_f}$ the final state obtained by a Keplerian motion between t_0 and t_f.

The problem is envisioned as an EOP CAM with an interior point constraint on the SMD.

This leads to the definition of the following functional:

$$J := \nu\Psi(t_{ca}, \mathbf{x}(t_{ca})) + \int_{t_i}^{t_f} \frac{1}{2}\mathbf{a_c}^T\mathbf{a_c}dt \tag{3.1}$$

Where:

$$\Psi(t_{ca}, \mathbf{x}(t_{ca})) = SMD(\mathbf{r}(t_{ca})) - \overline{SMD} \geq 0 \tag{3.2}$$

The objective function can be rewritten by introducing the Hamiltonian, substituted inside the cost function:

$$H := \frac{1}{2}\mathbf{a_c}^T\mathbf{a_c} + \boldsymbol{\lambda}^T\mathbf{f}(\mathbf{x}, \mathbf{a_c}) \tag{3.3}$$

$$J := \nu\Psi(t_{ca}, \mathbf{x}(t_{ca})) + \int_{t_i}^{t_f} \frac{1}{2}\mathbf{a_c}^T\mathbf{a_c} + \boldsymbol{\lambda}^T\left[\mathbf{f}(\mathbf{x}, \mathbf{a_c}) - \dot{\mathbf{x}}\right] dt \tag{3.4}$$

In which: $\boldsymbol{\lambda}^T\dot{\mathbf{x}} = -\dot{\boldsymbol{\lambda}}^T\mathbf{x} + \frac{d(\boldsymbol{\lambda}^T\mathbf{x})}{dt}$

The optimal control solves by imposing the first variation of the functional. This leads to a system of differential and algebraic equations:

$$\begin{cases} \nu\dfrac{\partial\Psi}{\partial\mathbf{x}(t_{ca})} - \boldsymbol{\lambda}^T(t_{ca}^-) + \boldsymbol{\lambda}^T(t_{ca}^+) = 0 \\ \left.\dfrac{\partial\mathbf{x}}{\partial\eta}\right|_{t_i} = 0 \\ \left.\dfrac{\partial\mathbf{x}}{\partial\eta}\right|_{t_f} = 0 \\ \dfrac{\partial H}{\partial\mathbf{a_c}} = \mathbf{a_c} + \boldsymbol{\lambda_v} = 0 \Longrightarrow \mathbf{a_c} = -\boldsymbol{\lambda_v} \\ \dfrac{\partial H}{\partial\mathbf{x}} + \dot{\boldsymbol{\lambda}}^T = 0 \Longrightarrow \dot{\boldsymbol{\lambda}} = -\left[\dfrac{\partial H}{\partial\mathbf{x}}\right]^T = -\left[\dfrac{\partial\mathbf{f}}{\partial\mathbf{x}}\right]^T\boldsymbol{\lambda} \\ \dfrac{\partial H}{\partial\boldsymbol{\lambda}} = \dot{\mathbf{x}} = \mathbf{f}(\mathbf{x}, \mathbf{a_c}) \\ \nu \geq 0 \\ \nu\Psi = 0 \end{cases} \tag{3.5}$$

Where:

$$\left[\frac{\partial\mathbf{f}}{\partial\tilde{\mathbf{x}}}\right] = \begin{bmatrix} \mathbf{0_{3\times3}} & \mathbf{I_{3\times3}} \\ \frac{3\mu}{r^5}\mathbf{r}\mathbf{r}^T - \frac{\mu}{r^3}\mathbf{I_{3\times3}} & \mathbf{0_{3\times3}} \end{bmatrix} \tag{3.6}$$

Solving the algebraic equation of the control acceleration as a function of the co-state the

following ThPBVP it is obtained:

$$\begin{cases} \dot{\mathbf{r}} = \mathbf{v} \\ \dot{\mathbf{v}} = -\dfrac{mu}{r^3}\mathbf{r} - \boldsymbol{\lambda}_v \\ \dot{\boldsymbol{\lambda}}_r = \dfrac{\mu}{r^3}\boldsymbol{\lambda}_v - \dfrac{3\mu \mathbf{r}^T \boldsymbol{\lambda}_v}{r^5}\mathbf{r} \\ \dot{\boldsymbol{\lambda}}_v = -\boldsymbol{\lambda}_r \end{cases} \qquad BCs: \begin{cases} \mathbf{x}(t_0) = \mathbf{x_0} \\ \mathbf{x}(t_{ca^-}) = \mathbf{x}(t_{ca^+}) \\ \nu \dfrac{\partial \Psi}{\partial \tilde{\mathbf{x}}(t_{ca})} - \boldsymbol{\lambda}^T(t_{ca}^-) + \boldsymbol{\lambda}^T(t_{ca}^+) = 0 \\ \mathbf{x}(t_f) = \mathbf{x_f} \\ \Psi(t_{ca}) = 0 \end{cases} \tag{3.7}$$

3.1.2. EOP Solution: Single Linearization

In Sec. 3.1.1, the Optimal Control Problem (OCP) turns into finding the initial costate and the adjoined multiplicator. The resolution procedure requires to subdivide the trajectory in two segments in the intervals $[t_1; t_{ca}]$ and $[t_{ca}; t_f]$. This step applies the interior point constraint. To obtain an analytical solution the two trajectories have to be linearized with respect to the Keplerian unperturbed motion by virtue of the STM.

$$\begin{cases} \dot{\boldsymbol{\Phi}}(t) = \mathbf{A}(t)\boldsymbol{\Phi}(\mathbf{x}(t_0), t) \\ \boldsymbol{\Phi}(\mathbf{x}(t_0), t_0) = \mathbf{I} \end{cases} \tag{3.8}$$

Where:

$$\mathbf{A} = \begin{bmatrix} \mathbf{0_{3\times3}} & \mathbf{I_{3\times3}} & \mathbf{0_{3\times3}} & \mathbf{0_{3\times3}} \\ \frac{3\mu}{r^5}\mathbf{r}\mathbf{r}^T - \frac{\mu}{r^3}\mathbf{I_{3\times3}} & \mathbf{0_{3\times3}} & \mathbf{0_{3\times3}} & -\mathbf{I_{3\times3}} \\ \mathbf{0_{3\times3}} & \mathbf{0_{3\times3}} & \mathbf{0_{3\times3}} & \frac{\mu}{r^3}\mathbf{I_{3\times3}} - \frac{3\mu}{r^5}\mathbf{r}\mathbf{r}^T \\ \mathbf{0_{3\times3}} & \mathbf{0_{3\times3}} & -\mathbf{I_{3\times3}} & \mathbf{0_{3\times3}} \end{bmatrix}$$

First Trajectory Arc

The linearization of the first arc brings to the following system of equations:

$$\begin{bmatrix} \boldsymbol{\delta}\mathbf{r_{ca}} \\ \boldsymbol{\delta}\mathbf{v_{ca}} \\ \boldsymbol{\delta\lambda}_{r_{ca}}^- \\ \boldsymbol{\delta\lambda}_{v_{ca}}^- \end{bmatrix} = \begin{bmatrix} \boldsymbol{\Phi_{11}} & \boldsymbol{\Phi_{12}} & \boldsymbol{\Phi_{13}} & \boldsymbol{\Phi_{14}} \\ \boldsymbol{\Phi_{21}} & \boldsymbol{\Phi_{22}} & \boldsymbol{\Phi_{23}} & \boldsymbol{\Phi_{24}} \\ \boldsymbol{\Phi_{31}} & \boldsymbol{\Phi_{32}} & \boldsymbol{\Phi_{33}} & \boldsymbol{\Phi_{34}} \\ \boldsymbol{\Phi_{41}} & \boldsymbol{\Phi_{42}} & \boldsymbol{\Phi_{43}} & \boldsymbol{\Phi_{44}} \end{bmatrix} \begin{bmatrix} \boldsymbol{\delta}\mathbf{r_0} \\ \boldsymbol{\delta}\mathbf{v_0} \\ \boldsymbol{\delta\lambda}_{r_0} \\ \boldsymbol{\delta\lambda}_{v_0} \end{bmatrix} \tag{3.9}$$

Working on the first two vectorial equations; starting from the initial conditions $\boldsymbol{\delta}\mathbf{r_0} = \boldsymbol{\delta}\mathbf{v_0} = 0$, it is possible to express the initial co-state as a function of the perturbation of

the state at TCA.

$$\begin{cases} \boldsymbol{\delta\lambda}_{r_0} = \mathbf{D}\boldsymbol{\delta}\mathbf{r_{ca}} + \mathbf{E}\boldsymbol{\delta}\mathbf{v_{ca}} \\ \boldsymbol{\delta\lambda}_{v_0} = \mathbf{M}\boldsymbol{\delta}\mathbf{r_{ca}} + \mathbf{B}\boldsymbol{\delta}\mathbf{v_{ca}} \end{cases} \tag{3.10a}$$

$$\mathbf{D} = [\boldsymbol{\Phi}_{\mathbf{13}}^{-1} - \boldsymbol{\Phi}_{\mathbf{13}}^{-1}\boldsymbol{\Phi}_{\mathbf{14}}\mathbf{M}] \qquad \mathbf{E} = -\boldsymbol{\Phi}_{\mathbf{13}}^{-1}\boldsymbol{\Phi}_{\mathbf{14}}\mathbf{B} \tag{3.10b}$$

$$\mathbf{D} = [\boldsymbol{\Phi}_{\mathbf{13}}^{-1} - \boldsymbol{\Phi}_{\mathbf{13}}^{-1}\boldsymbol{\Phi}_{\mathbf{14}}\mathbf{M}] \qquad \mathbf{E} = -\boldsymbol{\Phi}_{\mathbf{13}}^{-1}\boldsymbol{\Phi}_{\mathbf{14}}\mathbf{B} \tag{3.10c}$$

The symbol δ for the co-state variables is redundant because the variation is null along the un-maneuvered trajectory they assume the null value. Consequently, this symbol is now on omitted for these variables.

The two Eqs. 3.10a come handy to make the costates at TCA- dependent on the state at conjunction:

$$\begin{cases} \boldsymbol{\lambda}_{r_{ca}}^{-} = [\boldsymbol{\Phi}_{\mathbf{33}}\mathbf{D} + \boldsymbol{\Phi}_{\mathbf{34}}\mathbf{M}]\boldsymbol{\delta}\mathbf{r_{ca}} + [\boldsymbol{\Phi}_{\mathbf{34}}\mathbf{B} + \boldsymbol{\Phi}_{\mathbf{33}}\mathbf{E}]\boldsymbol{\delta}\mathbf{v_{ca}} \\ \boldsymbol{\lambda}_{v_{ca}}^{-} = [\boldsymbol{\Phi}_{\mathbf{43}}\mathbf{D} + \boldsymbol{\Phi}_{\mathbf{44}}\mathbf{M}]\boldsymbol{\delta}\mathbf{r_{ca}} + [\boldsymbol{\Phi}_{\mathbf{44}}\mathbf{B} + \boldsymbol{\Phi}_{\mathbf{43}}\mathbf{E}]\boldsymbol{\delta}\mathbf{v_{ca}} \end{cases} \Longrightarrow \begin{cases} \boldsymbol{\lambda}_{r_{ca}}^{-} = \mathbf{F}\boldsymbol{\delta}\mathbf{r_{ca}} + \mathbf{G}\boldsymbol{\delta}\mathbf{v_{ca}} \\ \boldsymbol{\lambda}_{v_{ca}}^{-} = \mathbf{H}\boldsymbol{\delta}\mathbf{r_{ca}} + \mathbf{L}\boldsymbol{\delta}\mathbf{v_{ca}} \end{cases} \tag{3.11a}$$

$$\mathbf{F} = [\boldsymbol{\Phi}_{\mathbf{33}}\mathbf{D} + \boldsymbol{\Phi}_{\mathbf{34}}\mathbf{M}] \qquad \mathbf{G} = [\boldsymbol{\Phi}_{\mathbf{34}}\mathbf{B} + \boldsymbol{\Phi}_{\mathbf{33}}\mathbf{E}] \tag{3.11b}$$

$$\mathbf{H} = [\boldsymbol{\Phi}_{\mathbf{43}}\mathbf{D} + \boldsymbol{\Phi}_{\mathbf{44}}\mathbf{M}] \qquad \mathbf{L} = [\boldsymbol{\Phi}_{\mathbf{44}}\mathbf{B} + \boldsymbol{\Phi}_{\mathbf{43}}\mathbf{E}] \tag{3.11c}$$

Second Trajectory Arc

For the secondary arc, the state variables and the velocity co-state are continuous at TCA; while the interior point constraint imposes a discontinuity on the position co-state. The final target point lies on the unmaneuvered Keplerin orbit. For this reason, the perturbation of the final state needs to be assumed as: $\boldsymbol{\delta}\mathbf{r_f} = \boldsymbol{\delta}\mathbf{v_f} = 0$

$$\begin{bmatrix} \boldsymbol{\delta}\mathbf{r_f} \\ \boldsymbol{\delta}\mathbf{v_f} \\ \boldsymbol{\lambda}_{r_f} \\ \boldsymbol{\lambda}_{v_f} \end{bmatrix} = \begin{bmatrix} \boldsymbol{\Phi}_{\mathbf{11}} & \boldsymbol{\Phi}_{\mathbf{12}} & \boldsymbol{\Phi}_{\mathbf{13}} & \boldsymbol{\Phi}_{\mathbf{14}} \\ \boldsymbol{\Phi}_{\mathbf{21}} & \boldsymbol{\Phi}_{\mathbf{22}} & \boldsymbol{\Phi}_{\mathbf{23}} & \boldsymbol{\Phi}_{\mathbf{24}} \\ \boldsymbol{\Phi}_{\mathbf{31}} & \boldsymbol{\Phi}_{\mathbf{32}} & \boldsymbol{\Phi}_{\mathbf{33}} & \boldsymbol{\Phi}_{\mathbf{34}} \\ \boldsymbol{\Phi}_{\mathbf{41}} & \boldsymbol{\Phi}_{\mathbf{42}} & \boldsymbol{\Phi}_{\mathbf{43}} & \boldsymbol{\Phi}_{\mathbf{44}} \end{bmatrix} \begin{bmatrix} \boldsymbol{\delta}\mathbf{r_{ca}} \\ \boldsymbol{\delta}\mathbf{v_{ca}} \\ \boldsymbol{\lambda}_{r_{ca}}^{+} \\ \boldsymbol{\lambda}_{v_{ca}} \end{bmatrix} \tag{3.12}$$

Recalling the co-state discontinuity expressed in the boundary conditions of Eq. 3.7, and

substituting the expression of the SMD constraint derivative:

$$\boldsymbol{\lambda}_{r_{ca}}^{+} = \boldsymbol{\lambda}_{r_{ca}}^{-} - 2\nu \mathbf{R_{2b}}^{T}\mathbf{C}^{-1}\mathbf{R_{2b}}\boldsymbol{\delta}\mathbf{r}_{\mathbf{imp}}^{\mathbf{m}} \tag{3.13}$$

Where $\boldsymbol{\delta}\mathbf{r}_{\mathbf{imp}}^{\mathbf{m}} = \mathbf{r}_{\mathbf{ca}}^{\mathbf{m}} - \mathbf{r_s}$ is the position vector from the secondary object at TCA to the primary in cartesian coordinates.

Working on the first two vectorial equations of system 3.12 and substituting Eq. 3.11a and Eq. 3.13 it is possible to obtain:

$$\mathbf{N}\boldsymbol{\delta}\mathbf{r_{ca}} + \mathbf{P}\boldsymbol{\delta}\mathbf{v_{ca}} - \nu\mathbf{Q}\mathbf{R_{2b}}\boldsymbol{\delta}\mathbf{r}_{\mathbf{imp}}^{\mathbf{m}} = 0 \tag{3.14a}$$

$$\begin{aligned} \mathbf{N} &= [\boldsymbol{\Phi_{21}} + \boldsymbol{\Phi_{24}}\mathbf{H} + \boldsymbol{\Phi_{23}}\mathbf{F}]; \\ \mathbf{P} &= [\boldsymbol{\Phi_{22}} + \boldsymbol{\Phi_{24}}\mathbf{L} + \boldsymbol{\Phi_{23}}\mathbf{G}]; \\ \mathbf{Q} &= 2\boldsymbol{\Phi_{23}}\mathbf{R_{2b}}^{T}\mathbf{C}^{-1} \end{aligned} \tag{3.14b}$$

And:

$$\tilde{\mathbf{N}}\boldsymbol{\delta}\mathbf{r_{ca}} + \tilde{\mathbf{P}}\boldsymbol{\delta}\mathbf{v_{ca}} - \nu\tilde{\mathbf{Q}}\mathbf{R_{2b}}\boldsymbol{\delta}\mathbf{r}_{\mathbf{imp}}^{\mathbf{m}} = 0 \tag{3.15a}$$

$$\begin{aligned} \tilde{\mathbf{N}} &= [\boldsymbol{\Phi_{11}} + \boldsymbol{\Phi_{14}}\mathbf{H} + \boldsymbol{\Phi_{13}}\mathbf{F}] \\ \tilde{\mathbf{P}} &= [\boldsymbol{\Phi_{12}} + \boldsymbol{\Phi_{14}}\mathbf{L} + \boldsymbol{\Phi_{13}}\mathbf{G}] \\ \tilde{\mathbf{Q}} &= 2\boldsymbol{\Phi_{13}}\mathbf{R_{2b}}^{T}\mathbf{C}^{-1} \end{aligned} \tag{3.15b}$$

Eq. 3.14a can be solved for $\boldsymbol{\delta}\mathbf{v_{ca}}$ and substituted in Eq. 3.15 in order to find the expression of $\boldsymbol{\delta}\mathbf{r_{ca}}$ as a function of the position vector $\boldsymbol{\delta}\mathbf{r}_{\mathbf{imp}}^{\mathbf{m}}$ and the multiplier ν:

$$\boldsymbol{\delta}\mathbf{r_{ca}} = \nu\mathbf{S}^{-1}\mathbf{T}\mathbf{R_{2b}}\boldsymbol{\delta}\mathbf{r}_{\mathbf{imp}}^{\mathbf{m}} \tag{3.16a}$$

$$\mathbf{S} = [\tilde{\mathbf{N}} - \tilde{\mathbf{P}}\mathbf{P}^{-1}\mathbf{N}] \qquad \mathbf{T} = [\tilde{\mathbf{Q}} - \tilde{\mathbf{P}}\mathbf{P}^{-1}\mathbf{Q}] \tag{3.16b}$$

SMD Constraint

To find an analytic solution to the problem, it demands combining the preceding relations with the SMD constraint at TCA. This can be done by adding and subtracting $\mathbf{r_s}$ on the left term and then premultipling Eq. 3.16a by $\mathbf{R_{2b}}$. This operation transfers the problem in B-plane reducing the dimension of the equation.

$$\mathbf{R_{2b}}[\mathbf{r}_{\mathbf{ca}}^{\mathbf{m}} - \mathbf{r_s} - \mathbf{r_{ca}} + \mathbf{r_s}] = \nu\mathbf{R_{2b}}\mathbf{S}^{-1}\mathbf{T}\mathbf{R_{2b}}\boldsymbol{\delta}\mathbf{r}_{\mathbf{imp}}^{\mathbf{m}} \tag{3.17a}$$

$$\mathbf{R_{2b}}[\boldsymbol{\delta}\mathbf{r}^{\mathbf{m}}_{\mathbf{imp}} - \boldsymbol{\delta}\mathbf{r}_{\mathbf{imp}}] = \nu\mathbf{R_{2b}}\mathbf{S}^{-1}\mathbf{T}\mathbf{R_{2b}}\boldsymbol{\delta}\mathbf{r}^{\mathbf{m}}_{\mathbf{imp}} \tag{3.17b}$$

$$\mathbf{b}^{\mathbf{m}}_{\mathbf{imp}} - \mathbf{b}_{\mathbf{imp}} = \nu\mathbf{R_{2b}}\mathbf{S}^{-1}\mathbf{T}\mathbf{b}^{\mathbf{m}}_{\mathbf{imp}} \tag{3.17c}$$

The previous equation can be inverted to obtain the expression of the maneuvered position vector in B-plane.

$$\mathbf{b}^{\mathbf{m}}_{\mathbf{imp}} = [\mathbf{I} - \nu\mathbf{U}]^{-1}\mathbf{b}_{\mathbf{imp}} \tag{3.18a}$$

$$\mathbf{U} = \mathbf{R_{2b}}\mathbf{S}^{-1}\mathbf{T} \tag{3.18b}$$

Finally, by using the following relation of linear algebra:

$$[\mathbf{I} - \nu\mathbf{U}]^{-1} = \frac{1}{det(\mathbf{I} - \nu\mathbf{U})}[\mathbf{I} - \nu det(\mathbf{U})\mathbf{U}^{-1}] \tag{3.19}$$

And applying the constraint on the SMD; it is possible to obtain a fourth-degree-equation that can be solved analytically as a function of ν:

$$\begin{aligned}\nu^2{\mathbf{b}_{\mathbf{imp}}}^T\mathbf{Z}^T\mathbf{C}^{-1}\mathbf{Z}\mathbf{b}_{\mathbf{imp}} - \nu{\mathbf{b}_{\mathbf{imp}}}^T[\mathbf{Z}^T\mathbf{C}^{-1} + \mathbf{C}^{-1}\mathbf{Z}]\mathbf{b}_{\mathbf{imp}} = \\ \alpha^2\overline{SMD} - {\mathbf{b}_{\mathbf{imp}}}^T\mathbf{C}^{-1}\mathbf{b}_{\mathbf{imp}}\end{aligned} \tag{3.20a}$$

$$\alpha = det(\mathbf{I} - \nu\mathbf{U}) \qquad \mathbf{Z} = det(\mathbf{U})\mathbf{U}^{-1} \tag{3.20b}$$

Once the value of ν is known, the initial costates come strightfoward by following backwards the algorithm. The overall procedure can be resumed in the following pseudo-algorithm.

Algorithm 3.1 EOP Point to Point. Part 1

Input: $\mathbf{r}_{p_{TCA}}$, $\mathbf{v}_{p_{TCA}}$, $\mathbf{r}_{s_{TCA}}$, $\overline{\text{SMD}}$, $\Delta\theta_1$,$\Delta\theta_2$, t_{ca}
Output: SMD, $\mathbf{a}_c$, $\boldsymbol{\Delta}\mathbf{v}$
for i = length($\Delta\theta_1$) **do**
    T_1 time interval corresponding to the selected $\Delta\theta_1$
    Keplerian backward propagation
    tspan_backward = $[0, -T_1]$
    $\mathbf{x_{pTCA}} = [\mathbf{r_{pTCA}}, \mathbf{v_{pTCA}}]$
    $[\mathbf{r}_0, \mathbf{v}_0] = keplerian\_backpropagation(\mathbf{x_{pTCA}}, \mathbf{tspan\_backward})$

Algorithm 3.1 EOP Point to Point. Part 2

for j = length($\Delta\theta_2$) **do**
  T_2 time interval corresponding to the selected $\Delta\theta_2$
  Keplerian forward propagation
  tspan_forward = $[0, T_2]$
  $[\mathbf{r}_f, \mathbf{v}_f]$ = *keplerian_forward_propagation*($\mathbf{x_{pTCA}}$, **tspan_forward**)
  STM_1 computation
  $tspan_1$ =$[0, T_1]$
  $\mathbf{x}_0 = [\mathbf{r}_0, \mathbf{v}_0]$
  $[\mathbf{STM_1}]$ = *stateTrans*($\mathbf{tspan_1}$, $\mathbf{x}_0$)
  STM_2 computation
  $tspan_2$ =$[0, T_2]$
  $[\mathbf{STM_2}]$ = *stateTrans*($\mathbf{tspan_2}$, $\mathbf{x}_{pTCA}$)
  Solve the non-linear system
  find ν from eq. (3.20a)
  compute $\boldsymbol{\delta}\mathbf{r}_{ca}$ from Eq. 3.18a
  compute $\boldsymbol{\delta}\mathbf{v}_{ca}$ from Eq. 3.14a
  compute $[\boldsymbol{\lambda}_{r_0}, \boldsymbol{\lambda}_{v_0}]$ from Eq. 3.10a
  Controlled forward propagation
  $tspan$=$[0, T_1 + T_2]$
  $\mathbf{y}_0 = [\mathbf{r}_0, \mathbf{v}_0, \boldsymbol{\lambda}_{r_0}, \boldsymbol{\lambda}_{v_0}]$
  $[\mathbf{r}_{man}, \mathbf{v}_{man}, \boldsymbol{\lambda}_{r_{man}}, \boldsymbol{\lambda}_{v_{man}}, \mathbf{r_{ca}}]$ = *control_propagator*($\mathbf{y}_0$, **tspan_forward**)
  $\Delta\mathbf{r} = \mathbf{r}_{ca} - \mathbf{r}_s$
  [SMD] = *squared_mahalanobis_distance*($\Delta\mathbf{r}$)
  $\mathbf{a}_c$ = -$\boldsymbol{\lambda}_{v_{man}}$
  Δv = *trapz*($\mathbf{a}_c$, Δt)
end for
end for

3.1.3. EOP Solution: Iterative Linearizations

To reduce the error due to non-linear effects, a semi-analytic solution based on iterative linearizations is developed. The first iteration follows the one presented in Sect. 3.1.2, while from the second linearization on, it requires a different procedure. In fact, they are performed with respect to maneuvered trajectories; this implies including some additional food for thoughts detailed in this section.

First Trajectory Arc

The analysis of the first trajectory arc is the same of the first linearization and brings to an analogous system of equations:

$$\begin{bmatrix} \boldsymbol{\delta \mathbf{r}_{ca}} \\ \boldsymbol{\delta \mathbf{v}_{ca}} \\ \boldsymbol{\delta \lambda}_{r_{ca^-}} \\ \boldsymbol{\delta \lambda}_{v_{ca^-}} \end{bmatrix} = \begin{bmatrix} \boldsymbol{\Phi_{11}} & \boldsymbol{\Phi_{12}} & \boldsymbol{\Phi_{13}} & \boldsymbol{\Phi_{14}} \\ \boldsymbol{\Phi_{21}} & \boldsymbol{\Phi_{22}} & \boldsymbol{\Phi_{23}} & \boldsymbol{\Phi_{24}} \\ \boldsymbol{\Phi_{31}} & \boldsymbol{\Phi_{32}} & \boldsymbol{\Phi_{33}} & \boldsymbol{\Phi_{34}} \\ \boldsymbol{\Phi_{41}} & \boldsymbol{\Phi_{42}} & \boldsymbol{\Phi_{43}} & \boldsymbol{\Phi_{44}} \end{bmatrix} \begin{bmatrix} \boldsymbol{\delta \mathbf{r}_0} \\ \boldsymbol{\delta \mathbf{v}_0} \\ \boldsymbol{\delta \lambda}_{r_0} \\ \boldsymbol{\delta \lambda}_{v_0} \end{bmatrix} \tag{3.21}$$

$$\begin{cases} \boldsymbol{\delta \lambda}_{r_0} = \mathbf{D} \boldsymbol{\delta \mathbf{r}_{ca}} + \mathbf{E} \boldsymbol{\delta \mathbf{v}_{ca}} \\ \boldsymbol{\delta \lambda}_{v_0} = \mathbf{M} \boldsymbol{\delta \mathbf{r}_{ca}} + \mathbf{B} \boldsymbol{\delta \mathbf{v}_{ca}} \end{cases} \tag{3.22}$$

$$\begin{cases} \boldsymbol{\delta \lambda}_{r_{ca^-}} = \mathbf{F} \boldsymbol{\delta \mathbf{r}_{ca}} + \mathbf{G} \boldsymbol{\delta \mathbf{v}_{ca}} \\ \boldsymbol{\delta \lambda}_{v_{ca^-}} = \mathbf{H} \boldsymbol{\delta \mathbf{r}_{ca}} + \mathbf{L} \boldsymbol{\delta \mathbf{v}_{ca}} \end{cases} \tag{3.23}$$

It is relevant to notice that the symbol δ for the co-state variables must not be omitted. In fact, the successive linearizations are performed with regard to the maneuvered trajectory which has a non-null co-state.

Second Trajectory Arc

The linearization produces rather different results. The principal modification is due to two reasons. To start off, the perturbation on the final state is here comprised to correct the state error obtained at the end of the previous iteration. Following, the costates discontinuity relation tweaks due to interior point constraint.
If we consider the discontinuity expression in the general iteration:

$$\boldsymbol{\delta \lambda}_{r_{ca^+}} = \boldsymbol{\lambda}^{k+1}_{r_{ca^+}} - \boldsymbol{\lambda}^{k}_{r_{ca^+}} \tag{3.24}$$

Where k indicates the number of iterations already executed. Recalling Eq. 3.13:

$$\boldsymbol{\lambda}^{\mathbf{k+1}}_{r_{ca^+}} - \boldsymbol{\lambda}^{\mathbf{k}}_{r_{ca^+}} = \boldsymbol{\lambda}^{\mathbf{k+1}}_{r_{ca^-}} - \boldsymbol{\lambda}^{\mathbf{k}}_{r_{ca^-}} - 2\nu \mathbf{R_{2b}}^T \mathbf{C}^{,-1} \mathbf{R_{2b}} (\mathbf{r}^{\mathbf{m\,k+1}}_{\mathbf{ca}} - \mathbf{r_s} - \mathbf{r}^{\mathbf{m\,k}}_{\mathbf{ca}} + \mathbf{r_s}) \tag{3.25}$$

That can be expressed as:

$$\boldsymbol{\delta \lambda}^{+}_{r_{ca}} = \boldsymbol{\delta \lambda}^{-}_{r_{ca}} - 2\nu \mathbf{R_{2b}}^T \mathbf{C}^{-1} \mathbf{R_{2b}} \boldsymbol{\delta \mathbf{r}^{m}_{ca}} \tag{3.26}$$

The constraint deviation is no longer expressed as a function of the position of the secondary object at TCA. Then, the resolution proceeds as in the previous case with the only difference of the non-null final state perturbation. From STM it is possible to obtain the expression of the perturbation on the state at TCA:

$$\boldsymbol{\delta}\mathbf{v_{ca}} = -\mathbf{P}^{-1}\mathbf{N}\boldsymbol{\delta}\mathbf{r_{ca}} + \nu\mathbf{P}^{-1}\mathbf{Q}\mathbf{R_{2b}}\boldsymbol{\delta}\mathbf{r_{ca}} + \mathbf{P^{-1}}\boldsymbol{\delta}\mathbf{v_f} \tag{3.27a}$$

$$\boldsymbol{\delta}\mathbf{r_{ca}} = \nu\mathbf{S}^{-1}\mathbf{T}\mathbf{R_{2b}}\boldsymbol{\delta}\mathbf{r_{ca}} + \mathbf{S^{-1}}(\boldsymbol{\delta}\mathbf{r_f} - \tilde{\mathbf{P}}\mathbf{P}^{-1}\boldsymbol{\delta}\mathbf{v_f}) \tag{3.27b}$$

For the complete explanation of the mathematical resolutions see Appendix A.

SMD Constraint

Transforming the problem in B-plane by a pre-multiplication of $\mathbf{R_{2b}}$ the equation obtained is similar to Eq. 3.18a:

$$\mathbf{b_{imp}}^{k+1} = [\mathbf{I} - \nu\mathbf{U}]^{-1}\mathbf{k} + \mathbf{b_{imp}}^{k} \tag{3.28}$$

Where $\mathbf{k}$ is a known vector containing the state offset at the final time.

Finally, to update the multiplier requires to plug the SMD relation in the resolution scheme. Again, the result obtained is a fourth-degree equation that can be solved as a function of ν:

$$\begin{aligned} \nu^2\mathbf{k}^T\mathbf{Z}^T\mathbf{C}^{-1}\mathbf{Z}\mathbf{k} - \nu\mathbf{k}^T[\mathbf{Z}^T\mathbf{C}^{-1} + \mathbf{C}^{-1}\mathbf{Z}]\mathbf{k} = \\ \alpha^2\overline{SMD} - (\mathbf{b_{imp}^k} + \mathbf{k})^T\mathbf{C}^{-1}(\mathbf{b_{imp}^k} + \mathbf{k}) \end{aligned} \tag{3.29a}$$

$$\alpha = det(\mathbf{I} - \nu\mathbf{U}) \qquad \mathbf{Z} = det(\mathbf{U})\mathbf{U}^{-1} \tag{3.29b}$$

As before value of ν can be used to retrieve all the previous quantity needed, including the initial co-state. The resulting procedure is an expansion of algorithm 3.1 that can be presented as follow.

Algorithm 3.2 EOP Point to Point with successive linearization. Part 1

Input: $\mathbf{r}_{p_{TCA}}$, $\mathbf{v}_{p_{TCA}}$, $\mathbf{r}_{s_{TCA}}$, $\overline{\text{SMD}}$, $\Delta\theta_1$,$\Delta\theta_2$, t_{ca},n_{lin}
Output: SMD, $\mathbf{a}_c$, $\boldsymbol{\Delta}\mathbf{v}$
for i = length($\Delta\theta_1$) **do**
  T_1 time interval corresponding to the selected $\Delta\theta_1$
  Keplerian backward propagation
  tspan_backward = $[0, -T_1]$
  $\mathbf{x_{pTCA}} = [\mathbf{r_{pTCA}}, \mathbf{v_{pTCA}}]$
  $[\mathbf{r}_0, \mathbf{v}_0] = keplerian\_backpropagation(\mathbf{x_{pTCA}}, \mathbf{tspan\_backward})$
  $\mathbf{x}_0 = [\mathbf{r}_0, \mathbf{v}_0]$
  for j = length($\Delta\theta_2$) **do**
    T_2 time interval corresponding to the selected $\Delta\theta_2$
    Keplerian forward propagation
    tspan_forward = $[0, T_2]$
    $[\mathbf{r}_{f2b}, \mathbf{v}_{f2b}] = keplerian\_forward\_propagation(\mathbf{x_{pTCA}}, \mathbf{tspan\_forward})$
    for k=n_{lin} **do**
      if k=1 **then**
        $\mathbf{STM_1}$ **computation**
        $tspan_1 = [0, T_1]$
        $[\mathbf{STM_1}] = stateTrans(\mathbf{tspan_1}, \mathbf{x}_0)$
        $\mathbf{STM_2}$ **computation**
        $tspan_2 = [0, T_2]$
        $[\mathbf{STM_2}] = stateTrans(\mathbf{tspan_2}, \mathbf{x}_{pTCA})$
        Solve the non-linear system
        find ν from Eq.3.20a
        compute $\boldsymbol{\delta}\mathbf{r}_{ca}$ from Eq. 3.27b
        compute $\boldsymbol{\delta}\mathbf{v}_{ca}$ from Eq. 3.27a
        update $\boldsymbol{\lambda_0}=\boldsymbol{\lambda_0} + \boldsymbol{\delta\lambda_0}$ from Eq. 3.22
        compute $\boldsymbol{\lambda}^+_{ca}=[\boldsymbol{\lambda}_{r^+_{ca}}, \boldsymbol{\lambda}_{v^+_{ca}}]$ from Eq. 3.13

Algorithm 3.2 EOP Point to Point with successive linearization. Part 2

else
  STM$_1$ computation
  $tspan_1$ =[0, T_1]
  [**STM$_1$**] = *stateTransMod*(**tspan$_1$**, [$\mathbf{x}_0$; $\boldsymbol{\lambda}_0$])
  STM$_2$ computation
  $tspan_2$ =[0, T_2]
  $\mathbf{x}_{\mathbf{pTCA}}$ = [$\mathbf{r}_{\mathbf{pTCA}}$, $\mathbf{v}_{\mathbf{pTCA}}$]
  [**STM$_2$**] = *stateTransMod*(**tspan$_2$**, [$\mathbf{x}_{pTCA}$; $\boldsymbol{\lambda}_{ca}^{+}$])
  find ν from Eq.3.29a
end if
Controlled forward propagation
$tspan$=[0, $T_1 + T_2$]
$\mathbf{y}_0$ = [$\mathbf{r}_0$, $\mathbf{v}_0$, $\boldsymbol{\lambda}_{r_0}$, $\boldsymbol{\lambda}_{v_0}$]
[$\mathbf{r}_{man}$, $\mathbf{v}_{man}$, $\boldsymbol{\lambda}_{\boldsymbol{man}}$, $\mathbf{r}_{\mathbf{ca}}$] = *control_propagator*($\mathbf{y}_0$, **tspan_forward**)
$\Delta\mathbf{r} = \mathbf{r}_{ca} - \mathbf{r}_s$
$\Delta\mathbf{r_f} = \mathbf{r}_f - \mathbf{r}_{f2b}$
$\Delta\mathbf{v_f} = \mathbf{v}_f - \mathbf{v}_{f2b}$
end for
[SMD] = *squared_mahalanobis_distance*($\Delta\mathbf{r}$)
$\mathbf{a}_c$ = -$\boldsymbol{\lambda}_{\boldsymbol{man}}$
Δv = *trapz*($\mathbf{a}_c$, Δt)
end for
end for

3.2. Low-Thrust Point to Point FOCP CAM Transformation

Despite being analytical, the solution of the EOP proposed in the previous section provides a continuous unbounded control acceleration profile that can exceed the thrusters' capabilities. In addition, the EOP does not provide the solution with minimum propellant consumption. All limitations are overcome by facing the FOP with bounds on the thrust magnitude. The resulting bang-bang control profile is easier to implement in an operative mission scenario limiting the propellant consumption. Consequently, this section introduces a numerical procedure to establish a fuel-optimal solution from an energy-optimal one.

3.2.1. Problem Definition

The resolution procedure starts by defining the FOP cost function :

$$J := \nu\Psi(t_{ca}, \mathbf{x}(t_{ca})) + \lambda_{v,th} \int_{t_i}^{t_f} a_{max}\epsilon dt \tag{3.30}$$

Where $\lambda_{v,th}$ is a positive scaling factor whose purpose will be clarified afterwards. Thanks to Pontryagin's maximum principle, the optimal control law (ϵ^*, α^*), providing $\mathbf{a_c} = a_{max}\epsilon^*\alpha^*$, is

$$\begin{cases} \alpha^* = -\dfrac{\boldsymbol{\lambda_v}}{\lambda_v} \\ \epsilon^* = 1 \; if \; \lambda_v > \lambda_{v,th} \Longrightarrow \epsilon = \dfrac{1}{2}\left[1 - \tanh\left(\dfrac{\lambda_v - \lambda_{v,th}}{\rho}\right)\right] \\ \epsilon^* = 0 \; if \; \lambda_v < \lambda_{v,th} \end{cases} \tag{3.31}$$

This formulation captures the discontinuous bang-bang profile with a hyperbolic tangent function. This Smooth Finite Difference (SFD) method is based on [29], and it is adopted to ease the numerical solver convergence. ρ is a scaling parameter that governs the transition from continuous to step functions.

The problem is traduced in the following ThPBVP

$$\begin{cases} \dot{\mathbf{r}} = \mathbf{v} \\ \dot{\mathbf{v}} = -\dfrac{mu}{r^3}\mathbf{r} - \dfrac{1}{2}a_{max}\left[1 - \tanh\left(\dfrac{\lambda_v - \lambda_{v,th}}{\rho}\right)\right]\dfrac{\boldsymbol{\lambda_v}}{\lambda_v} \\ \dot{\boldsymbol{\lambda}}_{\boldsymbol{r}} = \dfrac{\mu}{r^3}\boldsymbol{\lambda_v} - \dfrac{3\mu\mathbf{r}^T\boldsymbol{\lambda_v}}{r^5}\mathbf{r} \\ \dot{\boldsymbol{\lambda}}_{\boldsymbol{v}} = -\boldsymbol{\lambda_r} \end{cases} \tag{3.32a}$$

$$BCs : \begin{cases} \mathbf{x}(t_0) = \mathbf{x_0} \\ \mathbf{x}(t_{ca^-}) = \mathbf{x}(t_{ca^+}) \\ \nu\dfrac{\partial\Psi}{\partial\tilde{\mathbf{x}}(t_{ca})} - \boldsymbol{\lambda}^T(t_{ca}^-) + \boldsymbol{\lambda}^T(t_{ca}^+) = 0 \\ \mathbf{x}(t_f) = \mathbf{x_f} \\ \Psi(t_{ca}) = 0 \end{cases} \tag{3.32b}$$

The control acceleration term is, undoubtedly, an approximation of a bang-bang policy. However, this continuous formulation gives comparable results with respect to the optimal

bang-bang one when ρ takes sufficiently small values. There is no closed-form solution for this Multi-Point Boundary Value Problem (MPBVP). Yet, the EOP solution is a suited first guess, and a threshold value for $\lambda_{v,th}$ is crucial to start the procedure. To this aim, $\Delta v = \int_{t_0}^{t_f} a_{max}\lambda_v dt$ of the energy-optimal solution is computed, as well as the equivalent burning time t_b, i.e., the time needed to obtain the same Δv by the thrusting with the maximum affordable acceleration:

$$t_b = \frac{\Delta v}{a_{max}} = \int_{t_0}^{t_f} \lambda_v dt \tag{3.33}$$

The main idea is to define $\lambda_{v,th}$ so that the thruster fires up for $\lambda_v > \lambda_{v,th}$ (λ_v still belonging to the EOP) and switched off otherwise. The equivalent bang-bang burning time should be equal to t_b. The procedure to get $\lambda_{v,th}$ is based on the bisection method:

1. Set two initial boundary values for $\lambda_{v,th}$ for the first bisection iteration, namely $\lambda_{v,th1} = max(\lambda_v)$ and $\lambda_{v,th2} = min(\lambda_v)$.
2. Evaluate the burning time t_b^c for $\lambda_v > \lambda_{v,th1}$ and for $\lambda_v > \lambda_{v,th2}$.
3. Iteratively update $\lambda_{v,th1}$ or $\lambda_{v,th2}$ with the bisection method taking as cost function $J = t_b^c - t_b$
4. Do step 3 until $|t_b^c - t_b| < \Delta t_{tol}$ with Δt_{tol} prescribed tolerance.

Using the resulting $\lambda_{v,th}$, and the EOP sates and co-states profiles from t_0 to t_f, the ThPBVP is solved numerically with the four-stage Lobatto IIIa formula embedded in the *bvp5c* MATLAB function with dynamics of Eq. 3.32a.

3.2.2. Numerical Algorithm

The value of ρ has a twofold role: it is responsible for shaping a quasi discontinuous accelleration profile to the detriment of finding a solution with *bvp5c* in one single step. In addition, the numerical complexity of the problem is enhanced by the presence of the interior point constraint.
To overcome this limitation, an iterative procedure changes the value of ρ at each step. Starting from a predefined value, until the solver does not find a solution, ρ is incremented. Once the convergence is reached, the solution is used as the initial guess for the successive iteration with a lower value of ρ. The algorithm of this procedure is represented in Fig. 3.1.

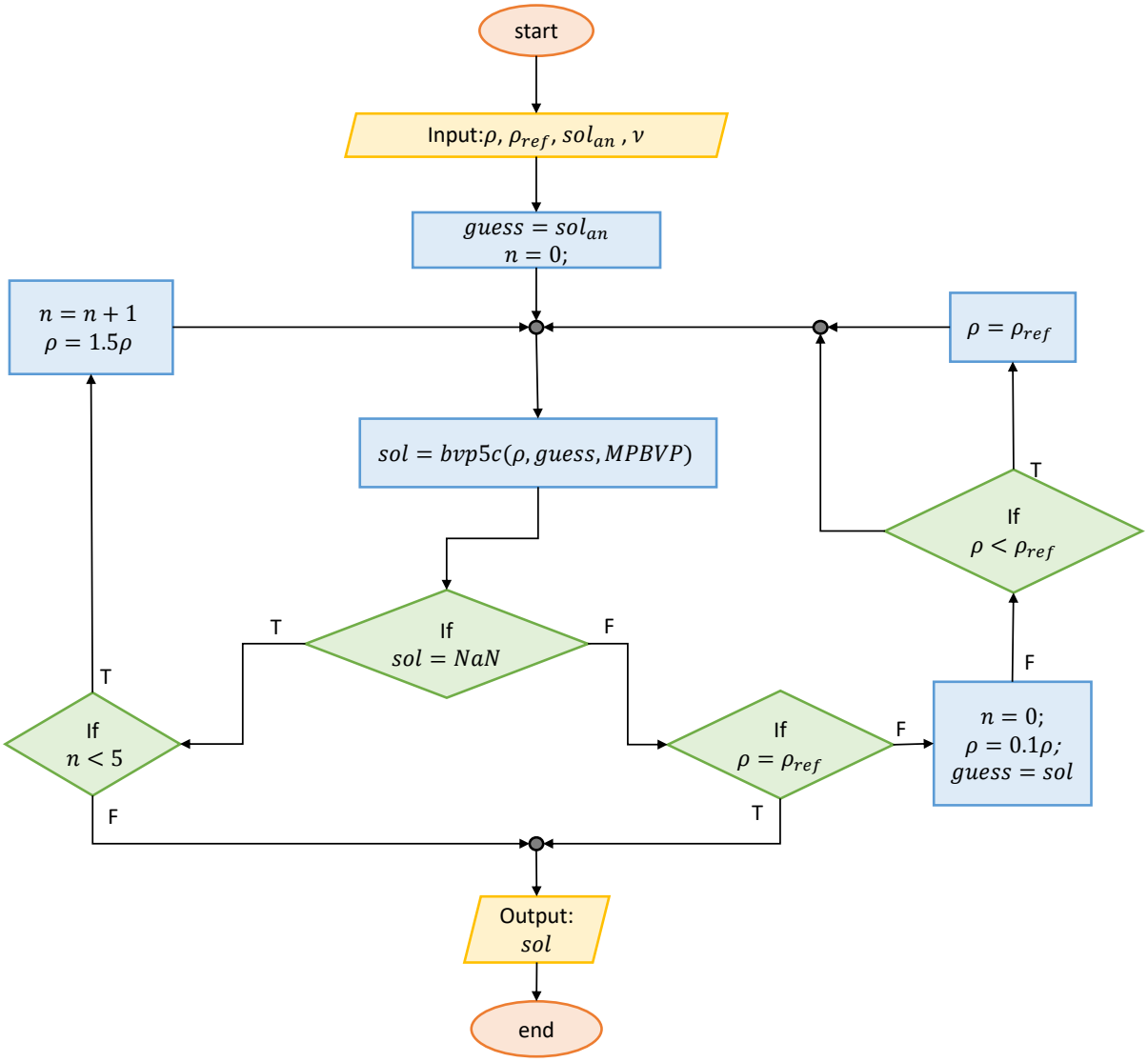

Figure 3.1: Point to Point FOP algorithm.

3.3. Results

3.3.1. Test Case

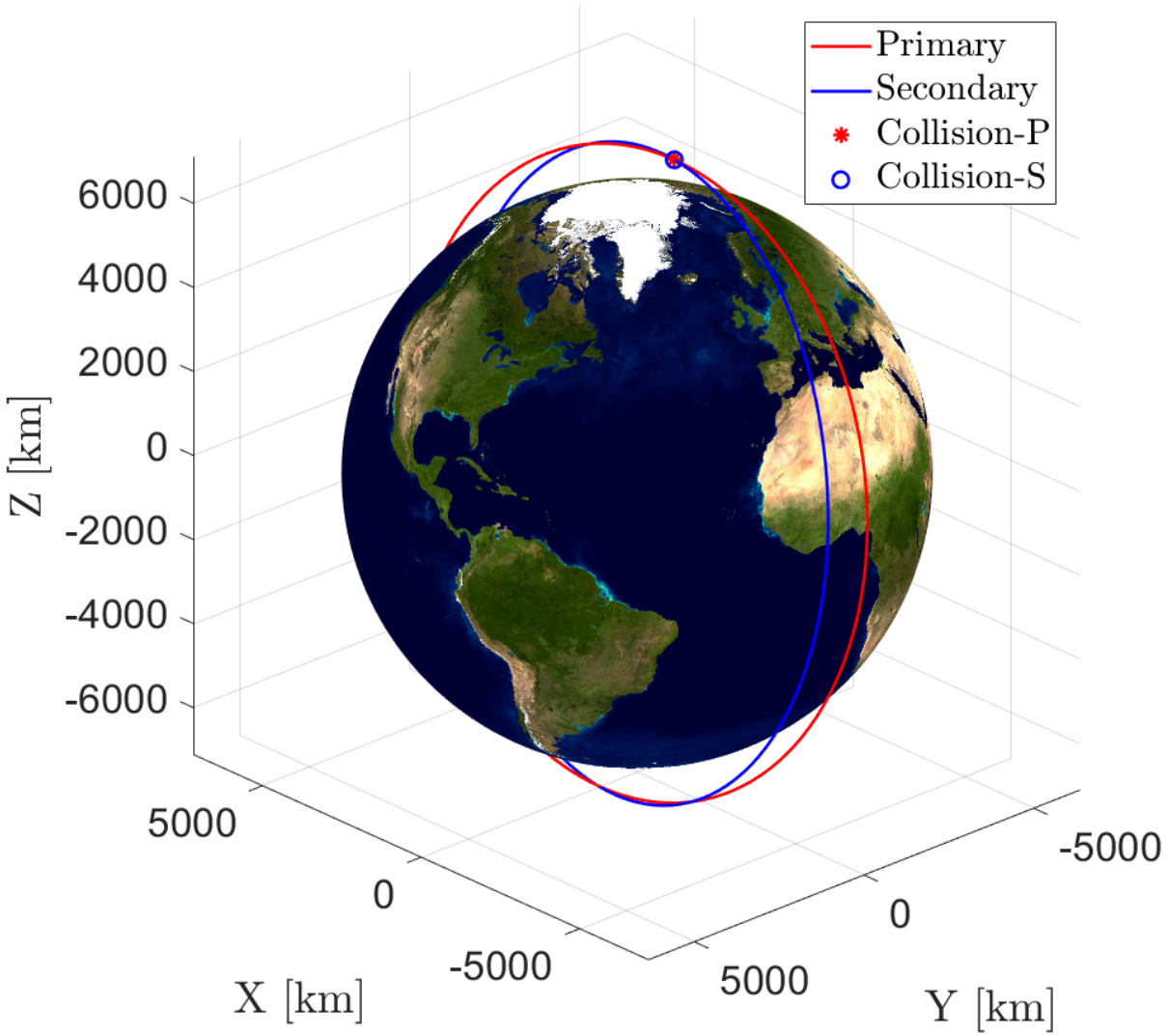

Figure 3.2: Test case collision representation.

The methods presented so far are applied to a test case extracted from [2], a database of 2,170 conjunction cases taken from the ESA Collision Avoidance Challenge [30]. A representation of the collision can be found in Figure 3.2. Table 3.1 reports the position and velocity vectors of the primary and secondary spacecraft at the conjunction in Earth Centered Inertial (ECI) frame, the PoC, the SMD and the miss distance d. The combined cross-sectional radius of the spacecraft is $s_A = 29.7$ m. The Keplerian elements of the two orbits are computed and displayed in Table 3.2.

Table 3.1: Test case conjunction data.

$\vec{r}_p$[km]	[2.3305, -1103.7, 7105.9]$^\top$
$\vec{r}_s$[km]	[2.3335, -1103.7, 7105.9]$^\top$
$\vec{v}_p$ [km/s]	[-7.4429, -6.1373e-04, 3.9514e-03]$^\top$
$\vec{v}_s$ [km/s]	[7.3537, -1.1428, -0.19825]$^\top$
PoC	1.3604e-01
SMD	0.87166
d [km]	0.0432

Table 3.2: Test case orbital elements, in order: semi-major axis, eccentricity, inclination, Right Ascension of the Ascending Node (RAAN), argument of the periapsis, true anomaly.

	a	e	i	Ω	ω	θ
O_p	7186.7 km	0.00064	98.83 °	0 °	289.38 °	160.60 °
O_s	7190.2 km	0.0024	81.28 °	170.93 °	184.41 °	266.99 °

The position covariance matrices of the two satellites, expressed in their respective ECI reference frame, are:

$$\vec{C}_p = \begin{bmatrix} 0.9317 & -2.6234 & 0.2360 \\ -2.6234 & 1778.0 & -0.9331 \\ 0.2360 & -0.9331 & 0.1917 \end{bmatrix} \cdot 10^{-4}\ \text{km}^2 \tag{3.34}$$

$$\vec{C}_s = \begin{bmatrix} 6.3466 & -19.6229 & 0.7077 \\ -19.6229 & 0.0820 & 11.3982 \\ 0.7077 & 11.3982 & 2.5103 \end{bmatrix} \cdot 10^{-4}\ \text{km}^2 \tag{3.35}$$

The corresponding combined covariance matrix in B-plane coordinates is:

$$\vec{C} = \begin{bmatrix} 7.21756 & -0.7580 \\ -0.7580 & 51.9201 \end{bmatrix} \cdot 10^{-4}\ \text{km}^2 \tag{3.36}$$

In the following section, the methods are compared using a dynamical model which only considers Keplerian motion, as expressed in Eq. 3.7.

All the simulations presented in this dissertation are run with a processor "AMD RYZEN9 3900x" and 32 GB Ram Memory.

The results reported in this section are obtained from the application of the algorithms presented in 3.1, 3.2, and Fig. 3.7. The collision probability is imposed as $PoC = 10^{-6}$ that leads to a threshold of $SMD = 26.9016$. The FOP is solved considering a level of acceleration of $a_{max} = 1.5 \cdot 10^{-5} \frac{m}{s^2}$

3.3.2. Linearized Solution

The results are obtained by applying algorithms 3.1, 3.2. To verify the validity of the solutions; the position of the primary object at TCA can be represented in B-plane.

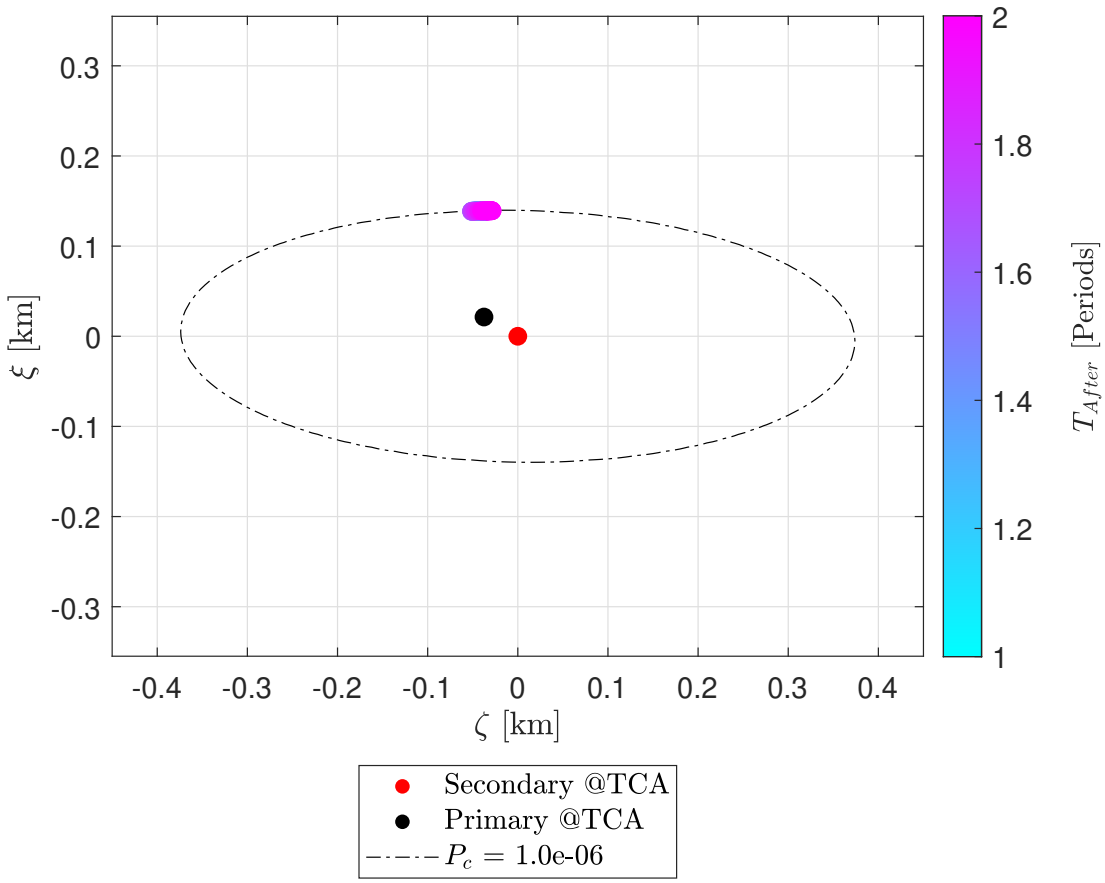

Figure 3.3: Position of the primary object, achieved with the optimal maneuver, and represented in b-plane for one linearizations.

In Fig. 3.3, the object position at TCA always belongs to the ellipse that represents the PoC threshold. The same results are obtained with an higher number of linearizations.

Looking at Fig. 3.4 the Δv values of the maneuvers obtained are reported in a surf plot. For various linearizations, there is no significant change in the cost of the operation.

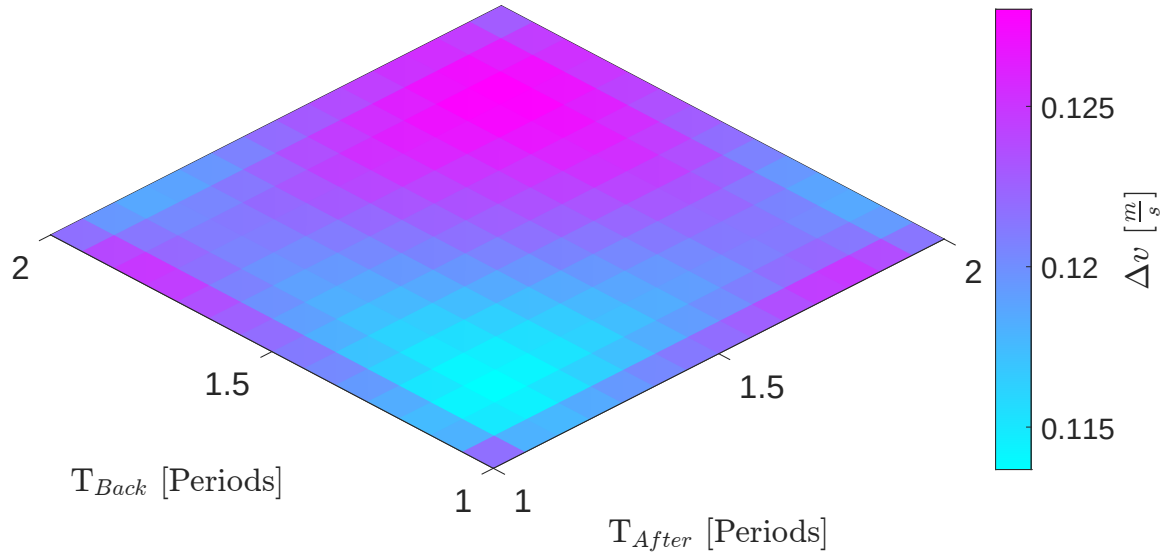

Figure 3.4: Maneuver cost computed with analytic procedure with one linearization, and analyzing multiple propagation time span for each trajectory arc.

The most important parameter for comparing the solution with different levels of linearizations is represented by the position error at the reentry point. Fig. 3.5 depicts the error due to the non-linear effects is low in all the cases analyzed. The solution accuracy slightly decreases passing from the first to the second iteration, while it strongly diminishes at the third consecutive linearization.

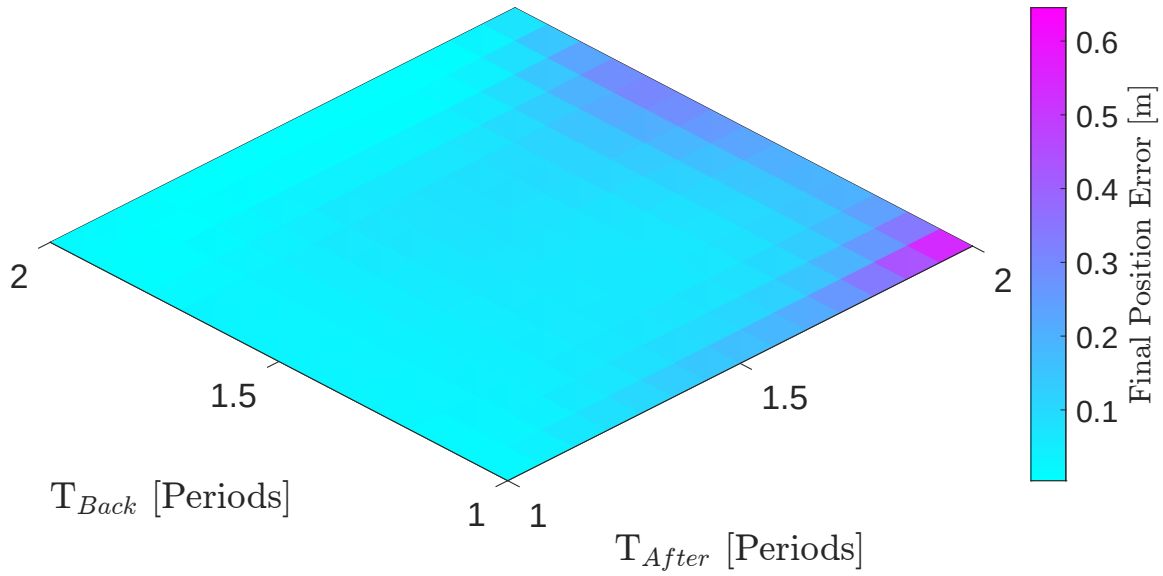

(a) 1 Linearization.

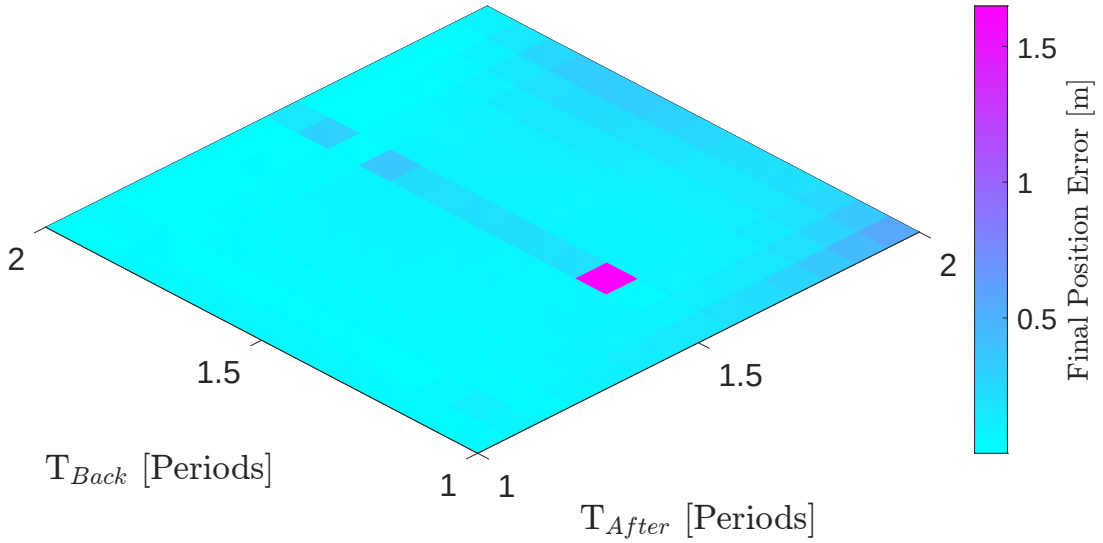

(b) 2 Linearizations.

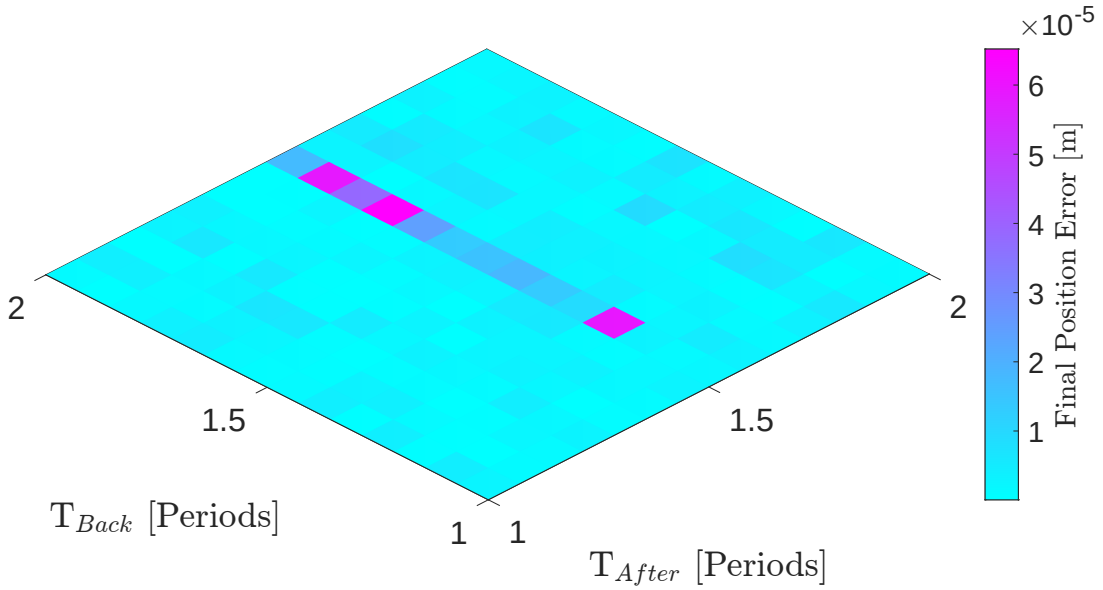

(c) 3 Linearizations.

Figure 3.5: Position error at the end of the maneuver computed with analytic procedure with different numbers of linearizations, and analyzing multiple propagation time span for each trajectory arc.

From high accuracy, it comes a greater computational burden with successive linearizations as shown in Fig. 3.6. In addition, increasing the maneuvering time, even the computational time becomes higher.

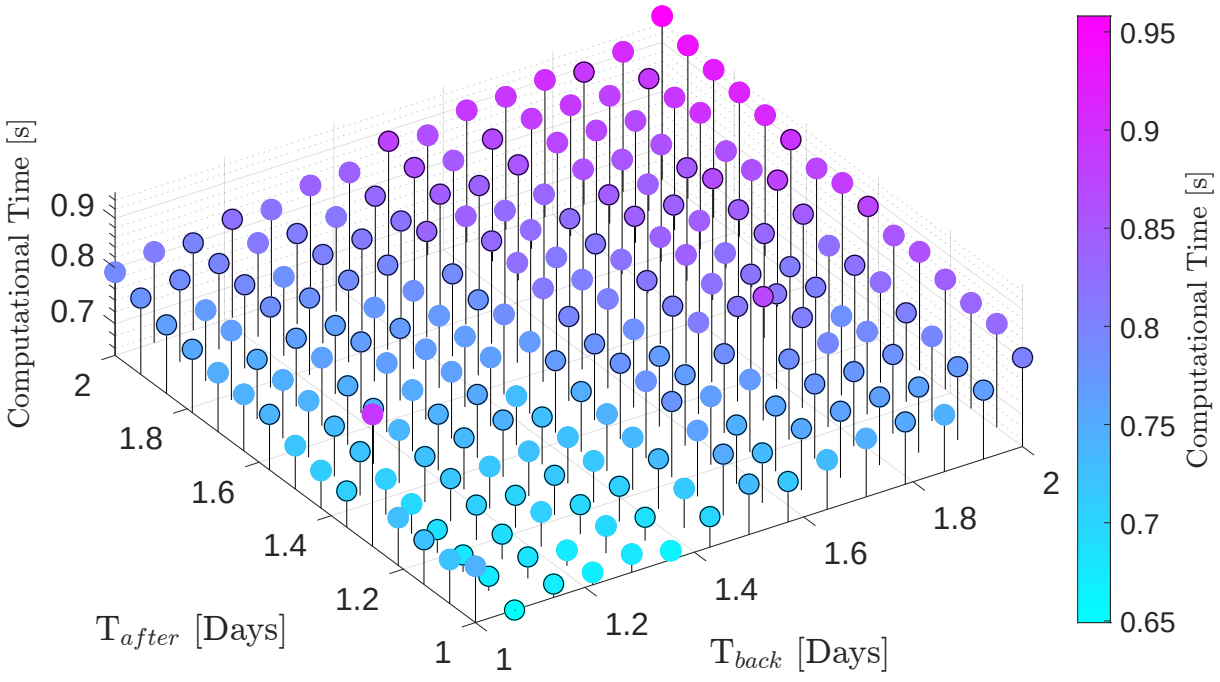

(a) 1 Linearization.

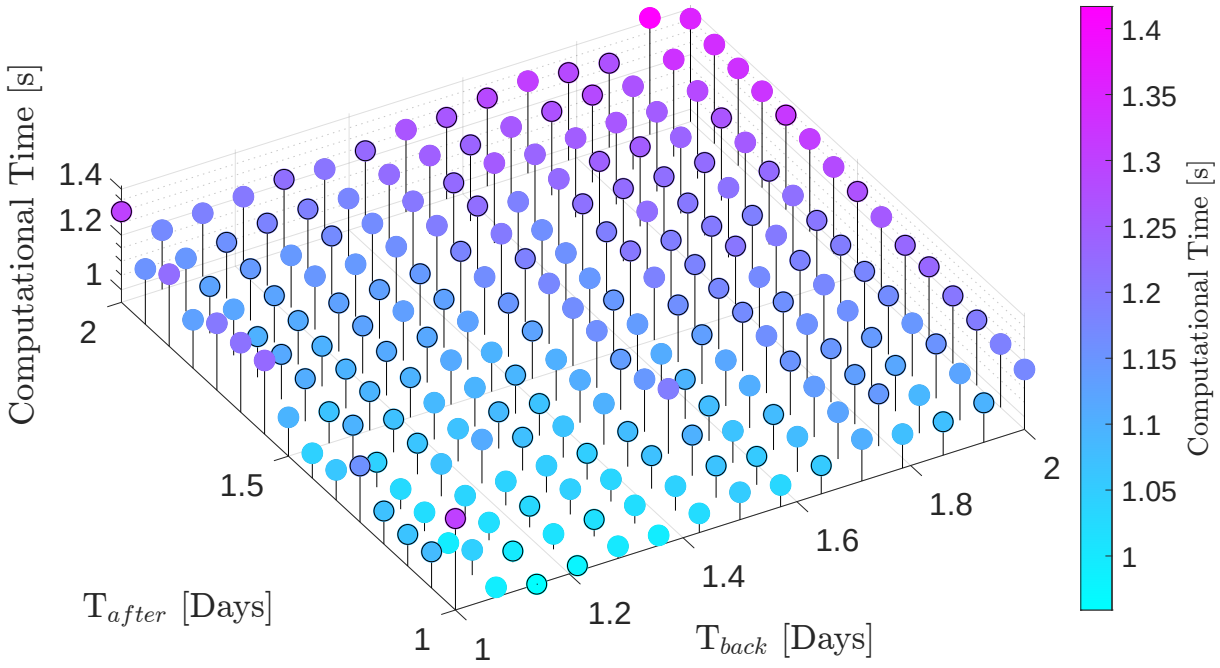

(b) 2 Linearizations.

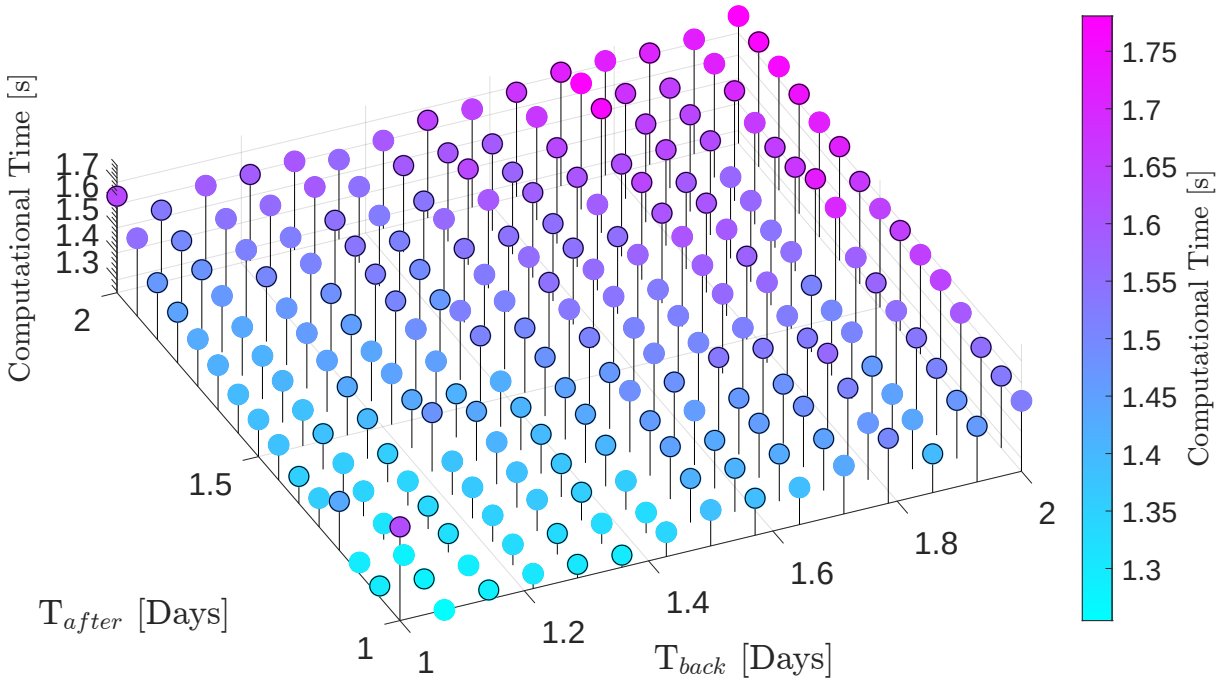

(c) 3 Linearizations.

Figure 3.6: Computational time spent to find the maneuver solution for each number of linearization. The time is computed for each CAM analyzed.

3.3.3. FOP Transformation

The results obtained applying the algorithm shown in Fig. 3.1 to transform the EOP solution in the FOP one are reported in this section. The outcome compares with the one achieved with one linearization.

To begin with, Fig. 3.7 pictures the final position of the primary landing on the iso-probability curve at TCA.

The effectiveness of the FOP procedure can be verified by comparing the Δv obtained from the two optimal control problems. Notably, in Fig. 3.9 each grid point of the FOP scheme claims a less expensive maneuver in fuel consumption perspective when likened to the EOP counterpart.

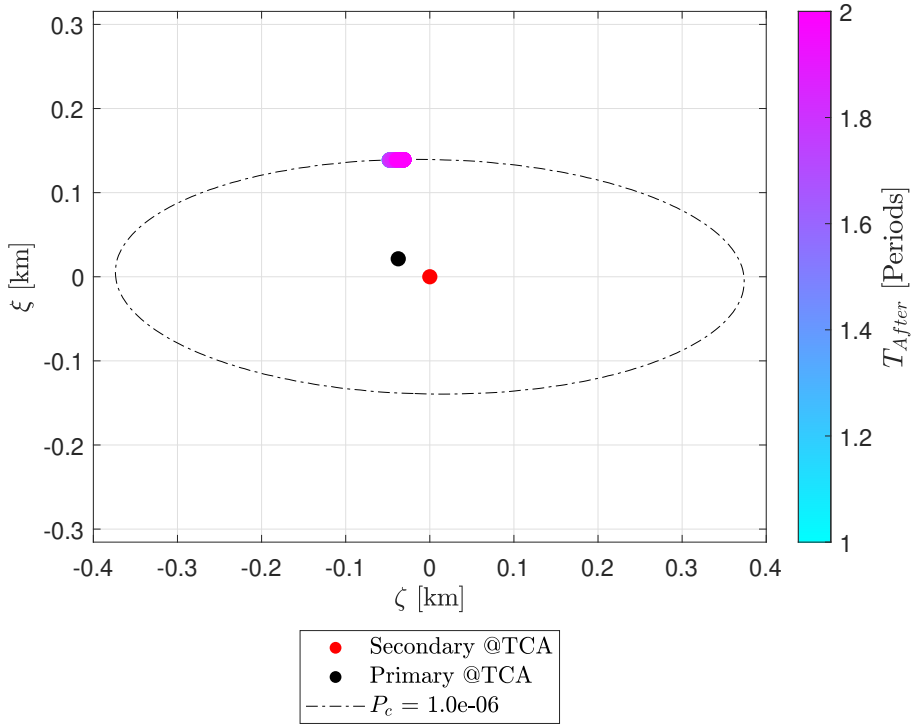

Figure 3.7: Position at TCA obtained from the FOP solution of the primary object in b-plane for the various value of the second trajectory arc.

Moreover, Fig. 3.8bis subject to a Δv flattening because of the constant acceleration level adopted across the simulation. In the EOP solution, each transfer has a periodic-like shape in which each peak has its own magnitude.

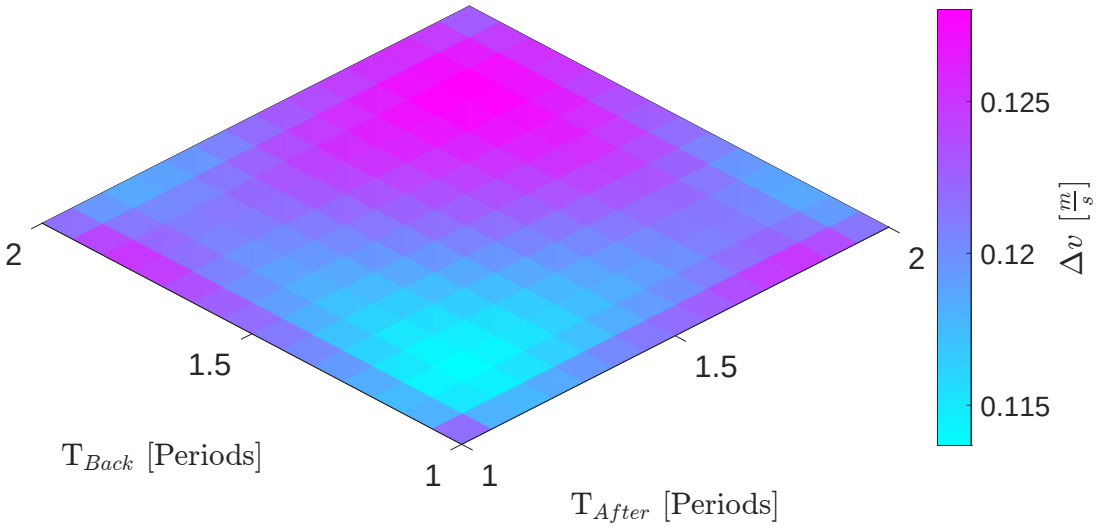

(a) Analytic Δv magnitude.

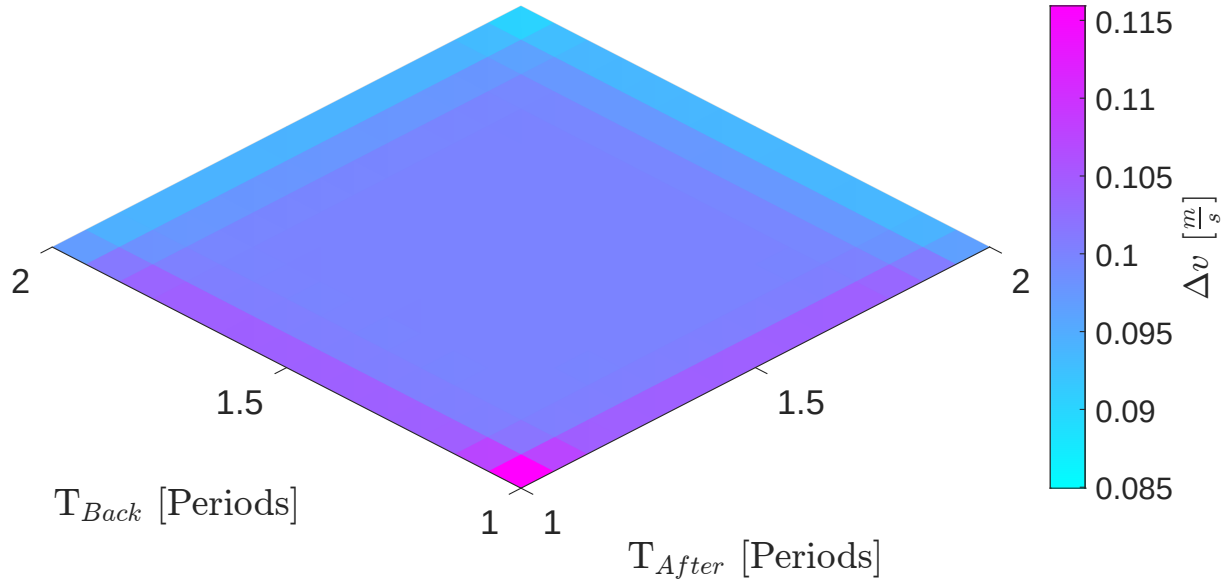

(b) Bang-bang Δv magnitude.

Figure 3.8: Δv results from FOP and EOP solutions.

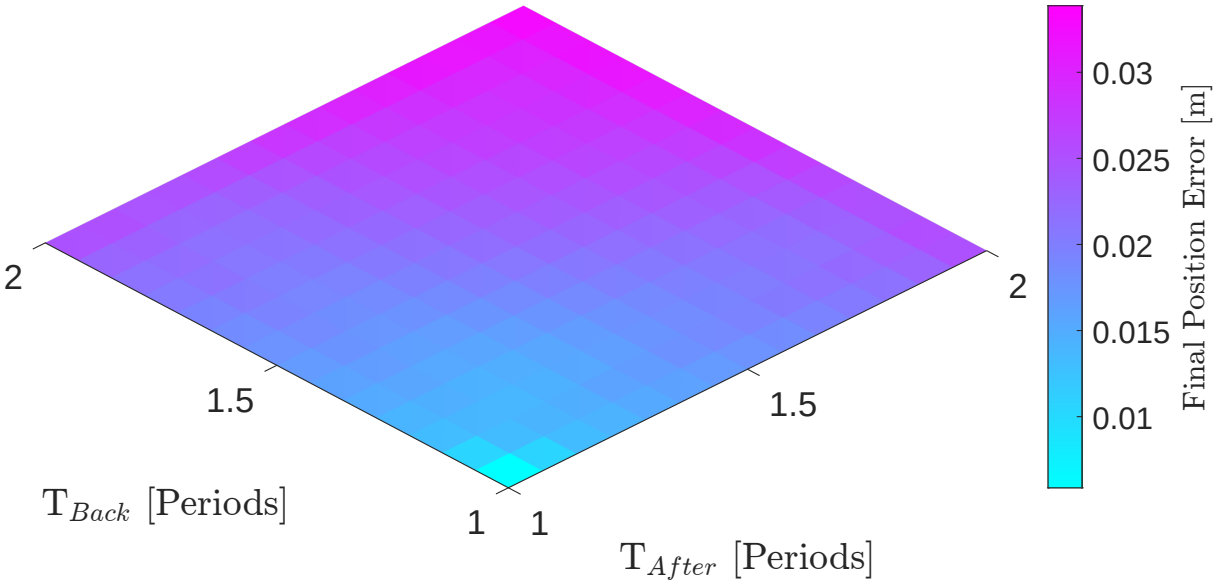

Figure 3.9: Δv difference.

The computational effort in Fig. 3.10 is at least one or two orders of magnitude greater than the analytical to resolve the EOP CAM planning. The discrepancy arises from the devised iterative procedure for ρ to comply with the stringent boundary conditions and solver convergence.

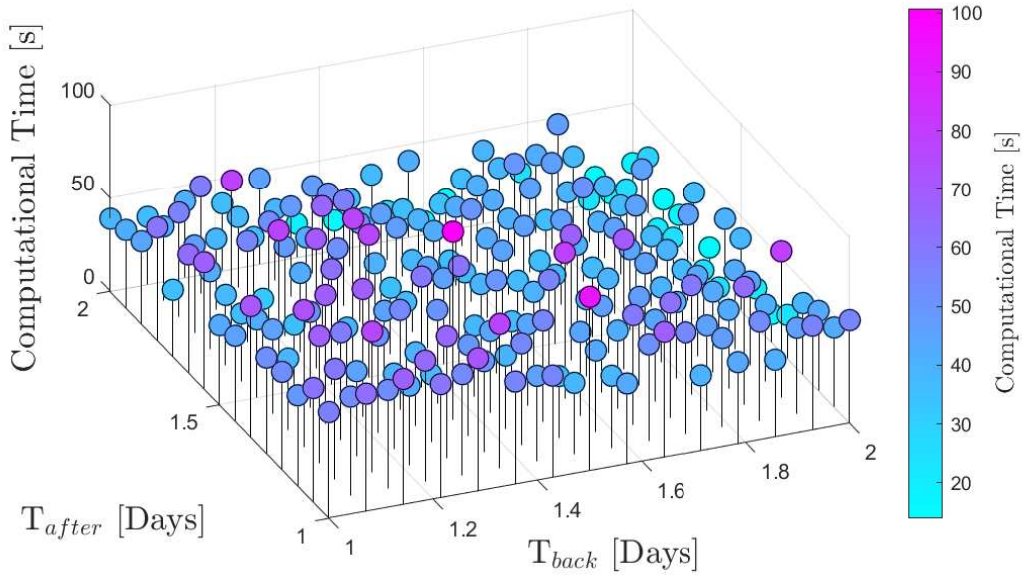

Figure 3.10: Computational time for the bang-bang transformation.

3.3.4. Minimum Δv

Analyzing the case of minimum Δv obtained from the analytic solution, it is possible to show the comparison between the continuous and the bang-bang acceleration profiles. Figure 3.11 reports the EOP solution and the acceleration obtained in each iteration of algorithm 3.1.

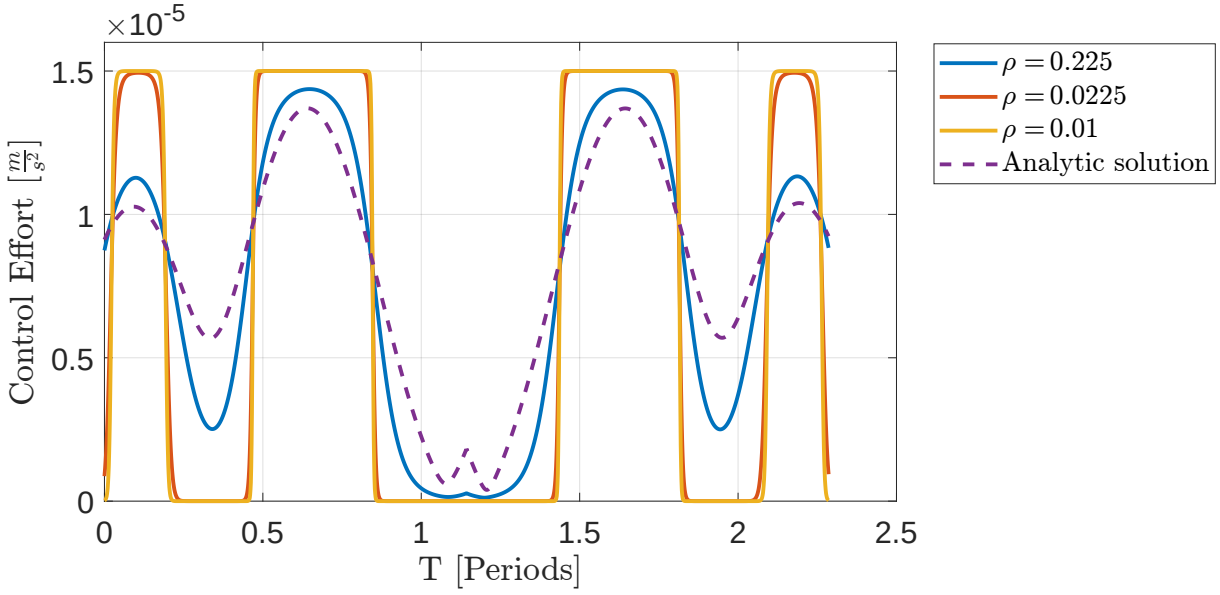

Figure 3.11: Comparison of analytic acceleration profile and FOP solution obtained with different values of ρ for the optimal EOP problem.

Figure 3.12 report the result of the minimum Δv FOP. Note that for the two maneuver the minimum Δv condition achieved in the two CAM policies does not match in magnitude and overall maneuvering time.

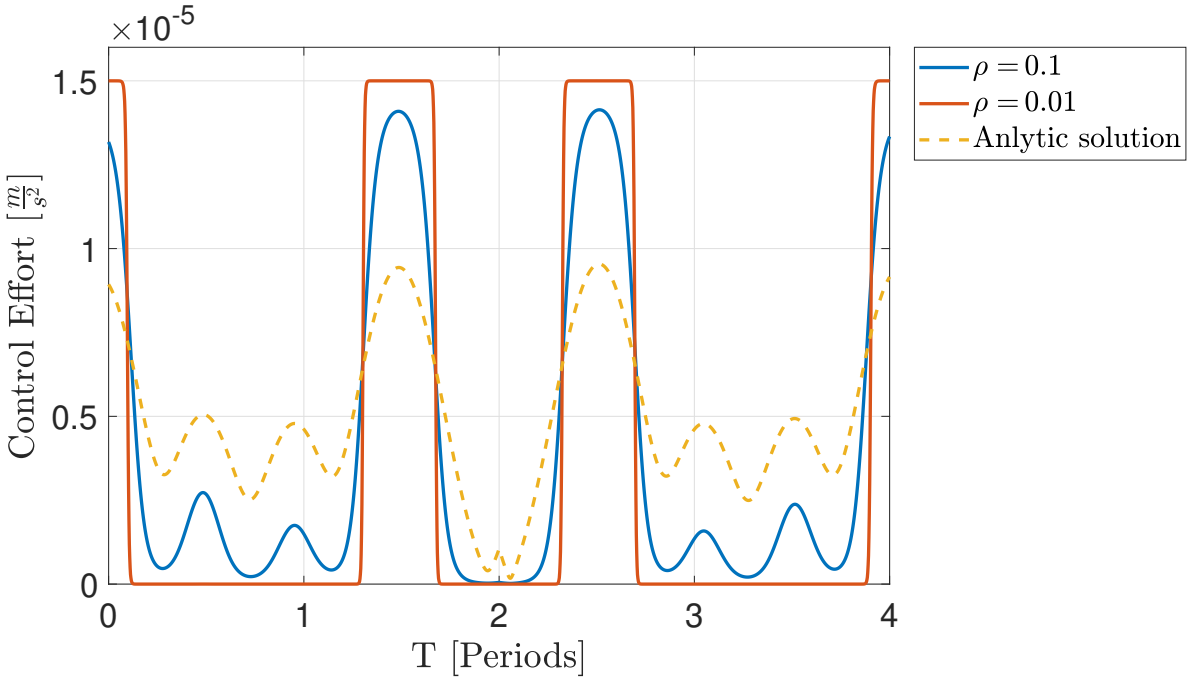

Figure 3.12: Comparison of analytic acceleration profile and FOP solution obtained with different values of ρ for the optimal FOP problem.

The explanation behind this phenomenon lies in the shape of the analytic control action. As can be seen in the optimal bang-bang maneuver the EOP acceleration demands a low-level continuous thrust. For this reason, Algorithm 3.1 results particularly effectively in maneuver cost reduction. For what concerns the optimal EOP solution, the obtained shape is already near to the bang-bang one dealing with a lower cost reduction.

Non-approximated Discontinue Dynamics

In the previous paragraph, the solution of the FOP results from the approximated dynamics of Sect. 3.2.1. The resolution of the ThPBVP is here proposed by adopting the MATLAB function *fsolve* modeling a non-continue dynamics without using approximation techniques. For convergence purposes the initial guess must lie nearby the exact solution; thus, the reference trajectory originates from the SFD FOP solution.

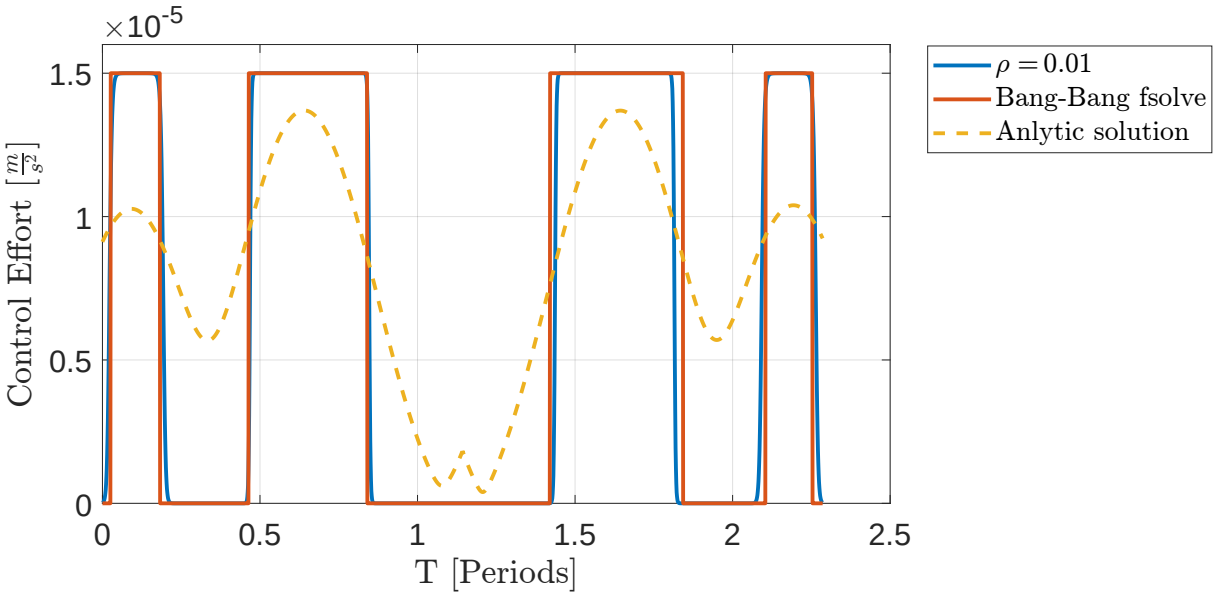

Figure 3.13: Comparison of analytic acceleration profile and FOP solution obtained with and without smoothing approximation.

In Fig. 3.13 the two acceleration profiles are shown, while Tab. 3.3 displays the final position error obtained by propagating the SFD solution with the non-continue dynamics and the computational time to compute the Discontinue Finite Difference (DFD) maneuver.

Table 3.3: Smothing error and *fsolve* computational time.

Smoothing error [km]	1.94
fsolve time [s]	15.17

Approximated impulsive maneuver

Algorithm 3.1 is suited to estimate an impulsive maneuver. By increasing the level of the maximum acceleration available onboard, the firing time lessens. This effect can be appreciated in Fig. 3.14.

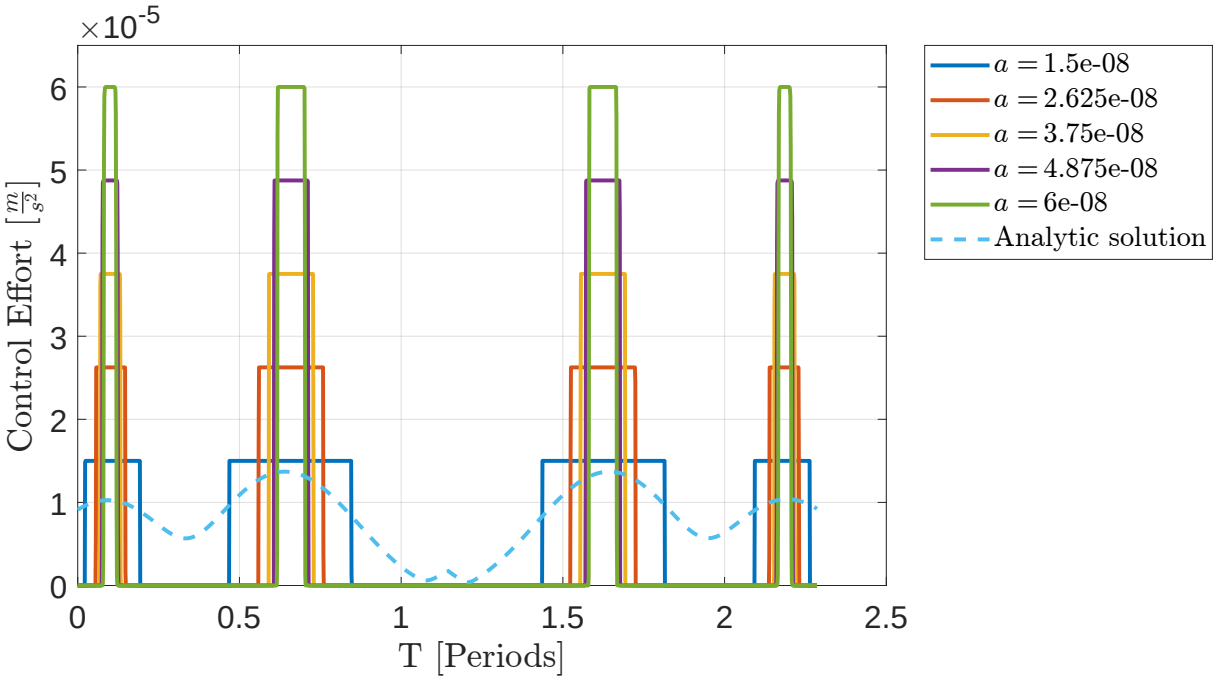

Figure 3.14: FOP acceleration profile for different values of maximum acceleration obtained with $\rho = 10^{-4}$ as smoothing parameter.

As indicated in Fig. 3.14 the smoothing parameter lowers as the acceleration grows implying a higher computational time as can be seen in Fig. 3.15.

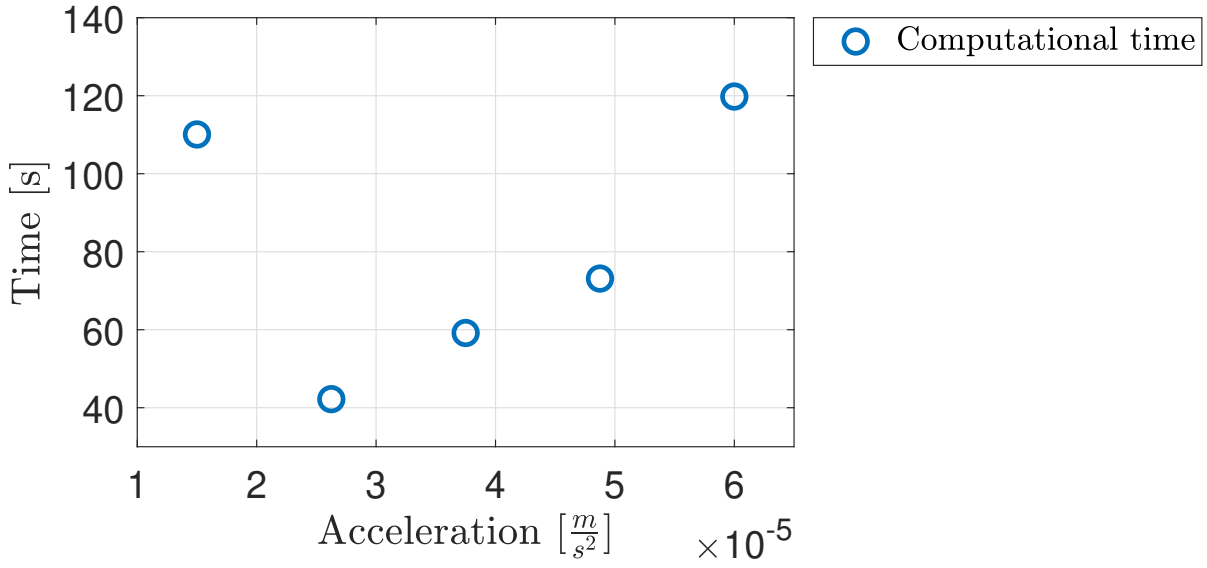

Figure 3.15: FOP computational for different values of maximum acceleration obtained with $\rho = 10^{-4}$ as smoothing parameter.

3.4. Low-Thrust Point to Orbit EOP CAM Formulation

In the previous problem, the final state is constrained. For some applications it is maybe beneficial returning to the initial orbit only. This would lead to a more efficient transfer with slightly different results in terms of final state. The solution presented can be particularly useful when there are no restrictive time limitations in station keeping.

3.4.1. Problem Formulation

The dynamics still feature a purely Keplerian motion but with a slight difference: the final target is a set of five orbital elements leaving out the true anomaly. The principal drawback of this approach belongs to the SMD boundary condition identified in ECI/B-plane frames.

The functional defined has the same structure as the previous one. The only difference is the expression of the constraint on the SMD at TCA:

$$J := \nu\Pi(t_{ca}, \mathbf{x}(t_{ca})) + \int_{t_i}^{t_f} \frac{1}{2}\mathbf{a_c}^T\mathbf{a_c}dt \tag{3.37a}$$

$$\Pi(t_{ca}, \mathbf{x}(t_{ca})) = SMD(\mathbf{r}(t_{ca})) - \overline{SMD} \geq 0 \tag{3.37b}$$

The functional morphs into:

$$H := \frac{1}{2}\mathbf{a_c}^T\mathbf{a_c} + \boldsymbol{\lambda}^T\mathbf{f}(\mathbf{x}, \mathbf{a_c}) \tag{3.38a}$$

$$J := \nu\Pi(t_{ca}, \mathbf{x}(t_{ca})) + \int_{t_i}^{t_f} \frac{1}{2}\mathbf{a_c}^T\mathbf{a_c} + \boldsymbol{\lambda}^T\left[\mathbf{f}(\mathbf{x}, \mathbf{a_c}) - \dot{\mathbf{x}}\right] dt \tag{3.38b}$$

Then imposing again the necessary condition by assuming null the first variation of the

objective function. The following system of algebraic and differential equations reads:

$$\begin{cases} \nu \dfrac{\partial \Pi}{\partial \mathbf{x}(t_{ca})} - \boldsymbol{\lambda}^T(t_{ca}^-) + \boldsymbol{\lambda}^T(t_{ca}^+) = 0 \\ \left.\dfrac{\partial \mathbf{x}}{\partial \eta}\right|_{t_i} = 0 \\ \left.\dfrac{\partial \mathbf{x}'}{\partial \eta}\right|_{t_f} = 0 \\ \lambda_\theta(t_f) = 0 \\ \dfrac{\partial H}{\partial \mathbf{a_c}} = 0 \Longrightarrow \mathbf{a_c} = \mathbf{a_c}(\boldsymbol{\lambda}) \\ \dfrac{\partial H}{\partial \mathbf{x}} + \dot{\boldsymbol{\lambda}}^T = 0 \Longrightarrow \dot{\boldsymbol{\lambda}} = -\left[\dfrac{\partial H}{\partial \mathbf{x}}\right]^T = -\left[\dfrac{\partial \mathbf{f}}{\partial \mathbf{x}}\right]^T \boldsymbol{\lambda} \\ \dfrac{\partial H}{\partial \boldsymbol{\lambda}} = \dot{\mathbf{x}} = \mathbf{f}(\mathbf{x}, \mathbf{a_c}(\boldsymbol{\lambda}) \\ \nu \geq 0 \\ \nu \Pi = 0 \end{cases} \tag{3.39}$$

Where:

$$\mathbf{x}' = \begin{bmatrix} a \\ e \\ i \\ \Omega \\ \omega \end{bmatrix} \tag{3.40}$$

Once the algebraic control solution is obtained, the problem is again translated in a ThPBVP:

$$\begin{cases} \dot{\mathbf{x}} = \mathbf{f}(\mathbf{x}, \mathbf{a_c}) \\ \dot{\boldsymbol{\lambda}} = -\left[\dfrac{\partial \mathbf{f}}{\partial \mathbf{x}}\right]^T \boldsymbol{\lambda} \end{cases} \qquad BCs: \begin{cases} \mathbf{x}(t_0) = \mathbf{x_0} \\ \mathbf{x}(t_{ca^-}) = \mathbf{x}(t_{ca^+}) \\ \nu \dfrac{\partial \Pi}{\partial \tilde{\mathbf{x}}(t_{ca})} - \boldsymbol{\lambda}^T(t_{ca}^-) + \boldsymbol{\lambda}^T(t_{ca}^+) = 0 \\ \mathbf{x}'(t_f) = \mathbf{x}'_\mathbf{f} \\ \boldsymbol{\lambda_\theta}(t_f) = 0 \\ \Pi(t_{ca}) = 0 \end{cases} \tag{3.41}$$

The complete mathematical development of Sect. 3.4 is reported in Appendix B.

3.4.2. EOP Solution

Once the ThPBVP is obtained, the resolution procedure follows the one described in Sec 3.1.2. It passes through the linearizations of the two trajectory arcs and the application of the SMD constraint to find the multiplier.

First Trajectory Arc

The objective is to find the expression of the co-state at TCA as function of the state perturbation at the same instant:

$$\begin{bmatrix} \boldsymbol{\delta}\mathbf{x}_{\mathbf{ca}^-} \\ \boldsymbol{\lambda}_{ca^-} \end{bmatrix} = \begin{bmatrix} \boldsymbol{\Phi}_{xx} & \boldsymbol{\Phi}_{x\lambda} \\ \boldsymbol{\Phi}_{\lambda x} & \boldsymbol{\Phi}_{\lambda\lambda} \end{bmatrix} \begin{bmatrix} \boldsymbol{\delta}\mathbf{x}_0 \\ \boldsymbol{\lambda}_0 \end{bmatrix} \tag{3.42a}$$

$$\boldsymbol{\lambda}_{ca^-} = \boldsymbol{\Phi}_{\lambda\lambda}\boldsymbol{\Phi}_{x\lambda}^{-1}\boldsymbol{\delta}\mathbf{x}_{\mathbf{ca}^-} \tag{3.42b}$$

In view of the second part, it will be useful decompose Eq. 3.42b as done with the state vector in Eq. 3.41:

$$\boldsymbol{\lambda}'_{ca^-} = \mathbf{E}\boldsymbol{\delta}\mathbf{x}'_{\mathbf{ca}^-} + \mathbf{w}\theta_{ca^-} \tag{3.43a}$$

$$\lambda_{\theta_{ca^-}} = \mathbf{g}\boldsymbol{\delta}\mathbf{x}'_{\mathbf{ca}^-} + P\theta_{ca^-} \tag{3.43b}$$

Where:

$$\boldsymbol{\lambda}' = \begin{bmatrix} \lambda_a \\ \lambda_e \\ \lambda_i \\ \lambda_\Omega \\ \lambda_\omega \end{bmatrix} \qquad \boldsymbol{\Phi}_{\lambda\lambda}\boldsymbol{\Phi}_{x\lambda}^{-1} = \begin{bmatrix} \mathbf{E} & \mathbf{w} \\ \mathbf{g} & P \end{bmatrix} \tag{3.44}$$

Co-state Discontinuity

For this particular problem, the analytic solution needs to introduce a zero-order Taylor expansion linked to the co-state discontinuity equation.

$$\frac{\partial \Pi}{\partial \mathbf{x}(t_{ca})} = \boldsymbol{\varphi}(\mathbf{x}_{\mathbf{ca}}) \approx \boldsymbol{\varphi}(\mathbf{x}_{\mathbf{ref}}(t_{ca})) = \boldsymbol{\varphi} \tag{3.45}$$

The discontinuity equation can be split as:

$$\begin{aligned} \boldsymbol{\lambda}'_{\boldsymbol{ca}^+} &= \boldsymbol{\lambda}'_{\boldsymbol{ca}^-} - \nu\boldsymbol{\varphi}' \\ \lambda_{\theta_{ca^+}} &= \lambda_{\theta_{ca^-}} - \nu\varphi_\theta \end{aligned} \tag{3.46}$$

Second Trajectory Arc

The previous decomposition on the first five orbital elements and the last co-state variable is crucial for the terminal boundary conditions.

$$\begin{bmatrix} \boldsymbol{\delta}\mathbf{x}'_{\mathbf{f}} \\ \delta\theta_f \\ \boldsymbol{\lambda}'_{\boldsymbol{f}} \\ \lambda_{\theta_f} \end{bmatrix} = \begin{bmatrix} \boldsymbol{\Phi}_{x'x'} & \boldsymbol{\Phi}_{x'\theta} & \boldsymbol{\Phi}_{x'\lambda'} & \boldsymbol{\Phi}_{x'\lambda_\theta} \\ \boldsymbol{\Phi}_{\theta x'} & \boldsymbol{\Phi}_{\theta\theta} & \boldsymbol{\Phi}_{\theta\lambda'} & \boldsymbol{\Phi}_{\theta\lambda_\theta} \\ \boldsymbol{\Phi}_{\lambda' x'} & \boldsymbol{\Phi}_{\lambda'\theta} & \boldsymbol{\Phi}_{\lambda'\lambda'} & \boldsymbol{\Phi}_{\lambda'\lambda_\theta} \\ \boldsymbol{\Phi}_{\lambda_\theta x'} & \boldsymbol{\Phi}_{\lambda_\theta\theta} & \boldsymbol{\Phi}_{\lambda_\theta\lambda'} & \boldsymbol{\Phi}_{\lambda_\theta\lambda_\theta} \end{bmatrix} \begin{bmatrix} \boldsymbol{\delta}\mathbf{x}'_{\mathbf{ca}} \\ \delta\theta_{ca} \\ \boldsymbol{\lambda}'_{\boldsymbol{ca}^+} \\ \lambda_{\theta_{ca^+}} \end{bmatrix} \tag{3.47}$$

The STM and the co-state discontinuity is to reframe the state perturbation at TCA.

$$\delta\theta_{ca} = \nu\frac{M}{L} \tag{3.48a}$$

$$\boldsymbol{\delta}\mathbf{x}'_{\mathbf{ca}} = \nu\mathbf{B}^{-1}\mathbf{n} \tag{3.48b}$$

The two equations can be coupled to obtain:

$$\boldsymbol{\delta}\mathbf{x}_{\mathbf{ca}} = \nu\mathbf{h} \qquad \mathbf{h} = \begin{bmatrix} \mathbf{B}^{-1}\mathbf{n} \\ \frac{M}{L} \end{bmatrix} \tag{3.49}$$

3.4.3. SMD Constraint Application

Solving for ν is all about imposing the SMD condition and reformulating the state at the closest approach:

$$\mathbf{x}(t_{ca}) = \mathbf{x}_{\mathbf{ref}}(t_{ca}) + \nu\mathbf{h} \tag{3.50}$$

Defining $\boldsymbol{\rho}(\mathbf{x})$ as the function to pass from keplerian elements to position vector in ECI coordinates; the constraint expression results:

$$\left[\boldsymbol{\rho}(\mathbf{x}_{\mathbf{ca}}) - \mathbf{r}_{\mathbf{s}}(t_{ca})\right]^T \mathbf{Q} \left[\boldsymbol{\rho}(\mathbf{x}_{\mathbf{ca}}) - \mathbf{r}_{\mathbf{s}}(t_{ca})\right] = \overline{SMD} \tag{3.51}$$

Where:

$$\mathbf{Q} = \mathbf{R_{2b}}^T \mathbf{C}^{-1} \mathbf{R_{2b}} \tag{3.52}$$

This equation has no closed-form solution. For this reason a first-order Taylor expansion of $\boldsymbol{\rho}(\mathbf{x})$ is used:

$$\boldsymbol{\rho}(\mathbf{x_{ca}}) \approx \mathbf{r_p}(t_{ca}) + \nu \mathbf{Jh} \tag{3.53}$$

The polynomial in ν is then:

$$[\mathbf{r_p}(t_{ca}) + \nu \mathbf{Jh} - \mathbf{r_s}(t_{ca})]^T \, \mathbf{Q} \, [\mathbf{r_p}(t_{ca}) + \nu \mathbf{Jh} - \mathbf{r_s}(t_{ca})] = \overline{SMD} \tag{3.54}$$

As usual from the value of the multiplier, it is possible to obtain the initial co-state. The numerical algorithm that corresponds to this procedure is represented in 3.3

Algorithm 3.3 EOP Point to orbit. Part 1

Input: $\mathbf{x}_{p_{TCA}}$, $\mathbf{r}_{s_{TCA}}$, $\overline{\text{SMD}}$, $\Delta\theta_1$,$\Delta\theta_2$, t_{ca}
Output: SMD, $\mathbf{a}_c$, $\mathbf{\Delta v}$
for i = length($\Delta\theta_1$) **do**
  T_1 time interval corresponding to the selected $\Delta\theta_1$
  Gauss Keplerian backward propagation
  tspan_backward = $[0 \; -T_1]$
  $\mathbf{x}_0 = keplerian\_gauss\_back\_propagation(\mathbf{x}_{p_{TCA}}, \mathbf{tspan\_backward})$
  for j = length($\Delta\theta_2$) **do**
    T_2 time interval corresponding to the selected $\Delta\theta_2$
    Keplerian forward propagation
    tspan_forward = $[0 \; T_2]$
    $\mathbf{x}_f = keplerian\_gauss\_forward\_propagation(\mathbf{x}_{p_{TCA}}, \mathbf{tspan\_forward})$
    STM_1 computation
    $tspan_1 = [0 \; T_1]$
    $[\mathbf{STM_1}] = stateTrans\_gauss(\mathbf{tspan_1}, \mathbf{x}_0)$
    STM_2 computation
    $tspan_2 = [0 \; T_2]$
    $[\mathbf{STM_2}] = stateTrans\_gauss(\mathbf{tspan_2}, \mathbf{x}_{pTCA})$

Algorithm 3.3 EOP Point to orbit. Part 2

Solve the non-linear system
find ν from eq. (3.54)
compute $\boldsymbol{\delta}\mathbf{x}_{ca}$ from Eq. 3.49
compute $\boldsymbol{\lambda}_0$
Controlled forward propagation
$tspan$=[0 $T_1 + T_2$]
$\mathbf{y}_0 = [\mathbf{x}_0, \boldsymbol{\lambda}_0]$
$[\mathbf{x}_{man}, \boldsymbol{\lambda}_{man}, \mathbf{x_{ca}}] = control\_propagator\_gauss(\mathbf{y}_0, \mathbf{tspan\_forward})$
$\mathbf{r_{ca}}$=$par2rv(\mathbf{x_{ca}})$
$\Delta\mathbf{r} = \mathbf{r}_{ca} - \mathbf{r}_s$
[SMD] = $squared\_mahalanobis\_distance(\Delta\mathbf{r})$
$\mathbf{a}_c = f(\boldsymbol{\lambda}_{man})$
$\Delta v = trapz(\mathbf{a}_c, \Delta t)$
end for
end for

3.5. Low-Thrust Point to Orbit FOP Transformation

The limitations described in Sec. 3.2 are present even in the analytical solution of the point-to-orbit maneuver. A similar procedure of the point-to-point algorithm is adopted to transform the EOP in a FOP considering a bang-bang profile with bound on the thrust magnitude.

3.5.1. Problem Definition

With orbital elements, the relation between control acceleration and co-state variables is more complex than the one computed in Eq. 3.7. However, this leads only to a trickly algebraic derivation, which does not affect the procedure presented in Sect. 3.2.1. The cost function reads:

$$J := \nu\Pi(t_{ca}, \mathbf{x}(t_{ca})) + u_{th} \int_{t_i}^{t_f} a_{max}\epsilon dt \tag{3.55}$$

Again it is possible to apply the Pontryagin's maximum principle in order to find the optimal control law (ϵ^*, α^*), providing $\mathbf{a_c} = a_{max}\epsilon^*\alpha^*$.

$$\begin{cases} \alpha^* = \dfrac{\mathbf{u}(\boldsymbol{\lambda})}{u(\boldsymbol{\lambda})} \\ \epsilon^* = 1 \; if \; u(\boldsymbol{\lambda}) > u_{th} \Longrightarrow \epsilon = \dfrac{1}{2}\left[1 - \tanh\left(\dfrac{u(\boldsymbol{\lambda}) - u_{th}}{\rho}\right)\right] \\ \epsilon^* = 0 \; if \; u(\boldsymbol{\lambda}) < u_{th} \end{cases} \tag{3.56}$$

Putting side by side Eq. 3.31 and Eq. 3.56, it is easy to notice that $\mathbf{u}(\boldsymbol{\lambda})$ is an involved expression in $\boldsymbol{\lambda_v}$ variable.
The parameter u_{th} assumes the same role as $\lambda_{v,th}$. It represents the threshold acceleration on the continuous profile over which the thrusters switch on. It comes with the same iterative procedure described in Sec. 3.2.1, giving rise to ThPBVP:

$$\begin{cases} \dot{\mathbf{x}} = \mathbf{f}(\mathbf{x}, a_{max}, \mathbf{u}(\boldsymbol{\lambda}), u_{th}) \\ \dot{\boldsymbol{\lambda}} = -\left[\dfrac{\partial \mathbf{f}}{\partial \mathbf{x}}\right]^T \boldsymbol{\lambda} \end{cases} \qquad BCs: \begin{cases} \mathbf{x}(t_0) = \mathbf{x_0} \\ \mathbf{x}(t_{ca^-}) = \mathbf{x}(t_{ca^+}) \\ \nu \dfrac{\partial \Pi}{\partial \tilde{\mathbf{x}}(t_{ca})} - \boldsymbol{\lambda}^T(t_{ca}^-) + \boldsymbol{\lambda}^T(t_{ca}^+) = 0 \\ \mathbf{x}'(t_f) = \mathbf{x}'_\mathbf{f} \\ \boldsymbol{\lambda_\theta}(t_f) = 0 \\ \Pi(t_{ca}) = 0 \end{cases} \tag{3.57}$$

The correspondent numerical algorithm is analogous to the one reported in Fig. 3.1, However, it consider the MPBVP presented in Eq. 3.57

3.6. Results

In this section, the results of the PTOM are analyzed. The second and test bench are the same of Sect. 3.3.1.

3.6.1. EOP and FOP Solutions

As reported in Sect. 3.3.3 the EOP and FOP routines are likened. In Fig. 3.15 the position in B-plane at TCA of the primary object is presented. The spacecraft correctly matches the PoC ellipse for all targeted points. This result is achieved both for the analytic solution and for the FOP transformation.

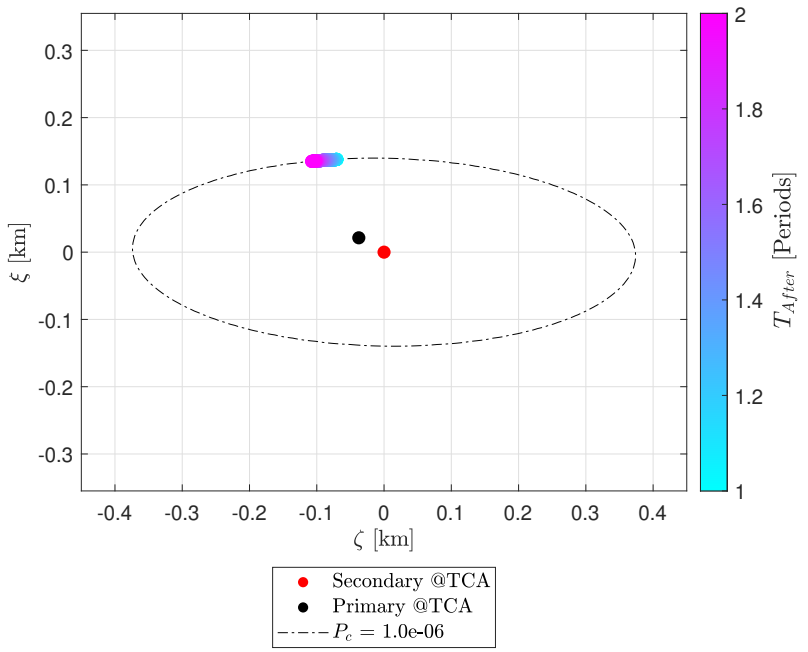

(a) EOP.

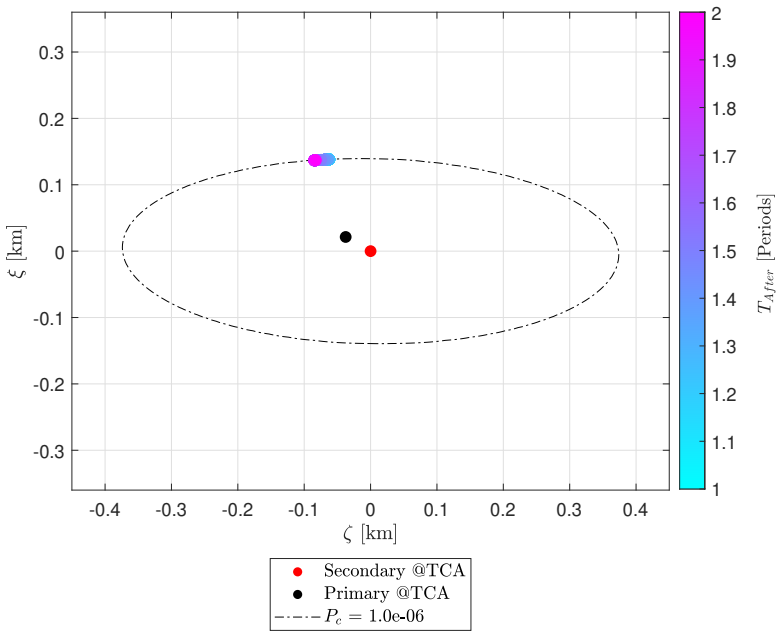

(b) FOP.

Figure 3.15: Position of the primary object in b-plane at TCA obtained from the EOP and FOP solutions. All the maneuvers are represented and the color of the object change varying the length of the second arc.

Then, in Fig. 3.16 the comparison goes on for what concerns the total Δv. Predictably, FOP is less expensive than the EOP transfer.

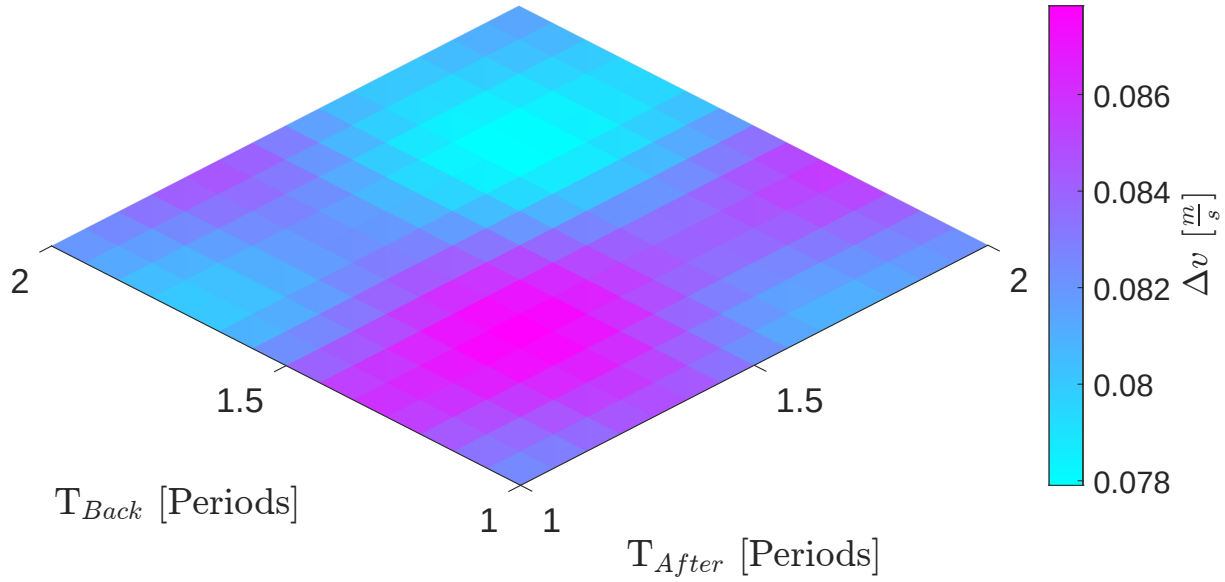

(c) Analytic Δv magnitude.

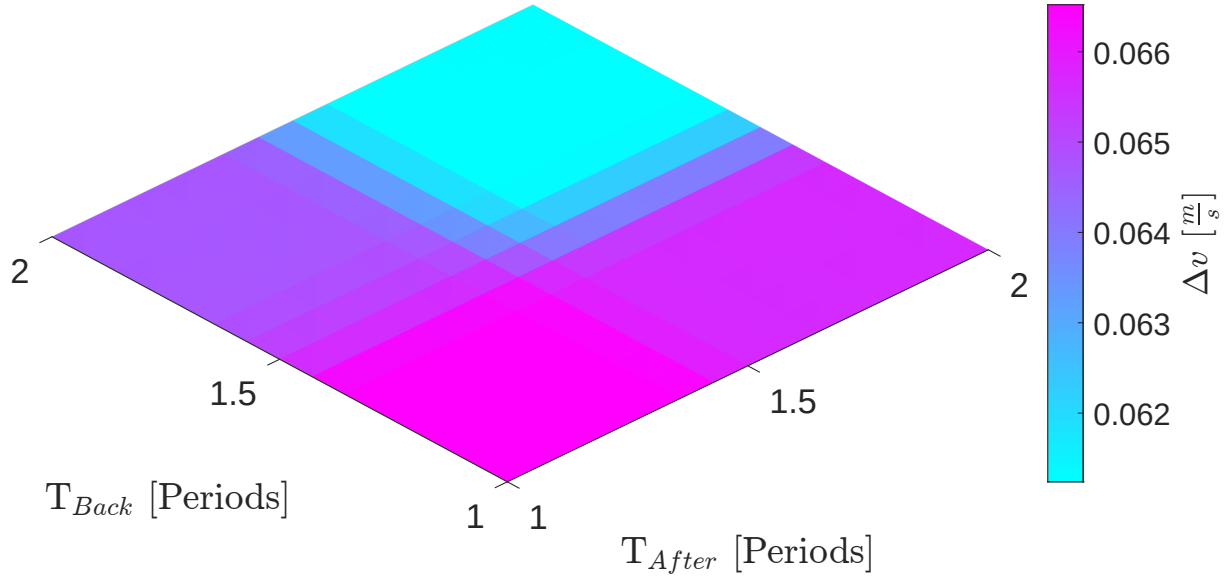

(d) Bang-bang Δv magnitude.

Figure 3.16: Δv obtained from analytic and FOP solution.

The difference in the maneuvers cost can be appreciated in detail in Fig. 3.17.

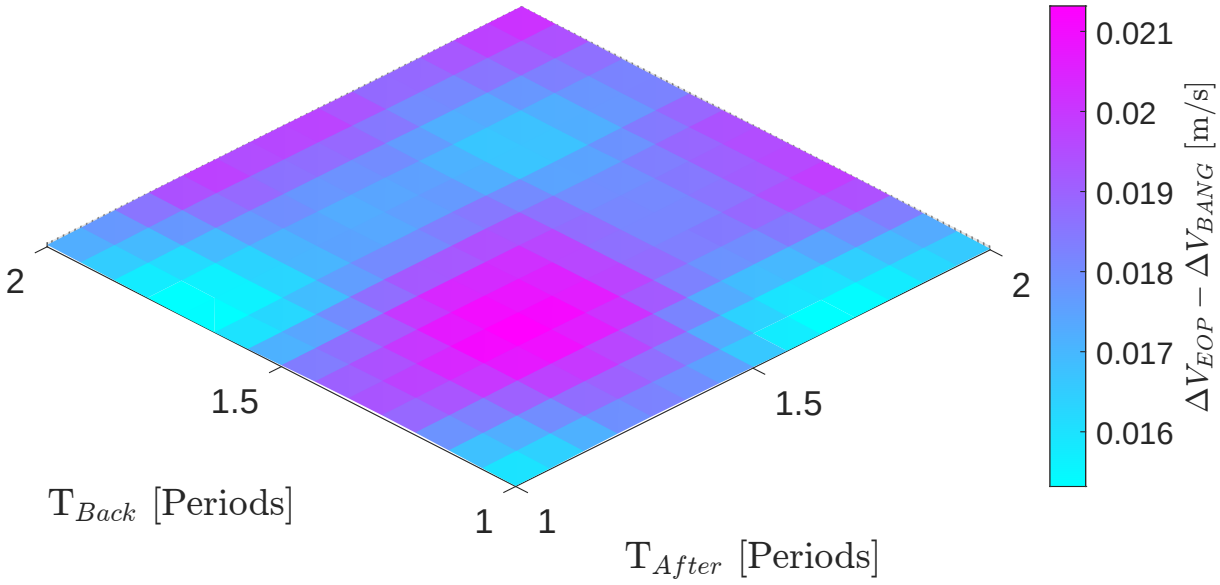

Figure 3.17: Δv difference between EOP and FOP solutions.

The computational time spent to find the EOP and FOP solution with algorithms 3.3 and 3.1 is presented in Fig. 3.18. Once again, the numerical effort of the analytic solution is strongly affected by the propagation time span, while the FOP computational time does not have an evident dependency on the latter.

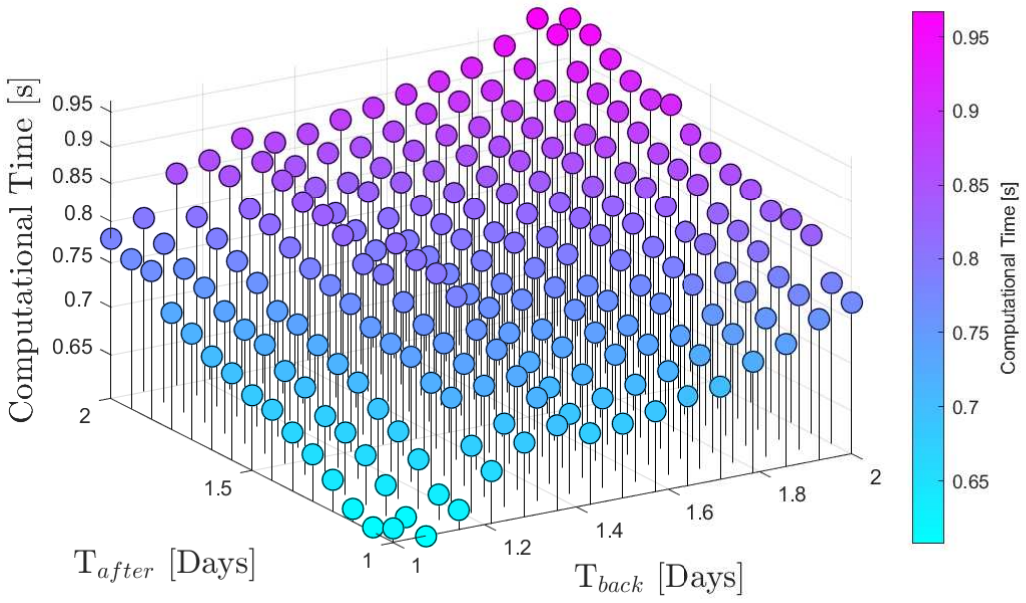

(a) EOP computational time.

Figure 3.18: Computational time for EOP and FOP solution.

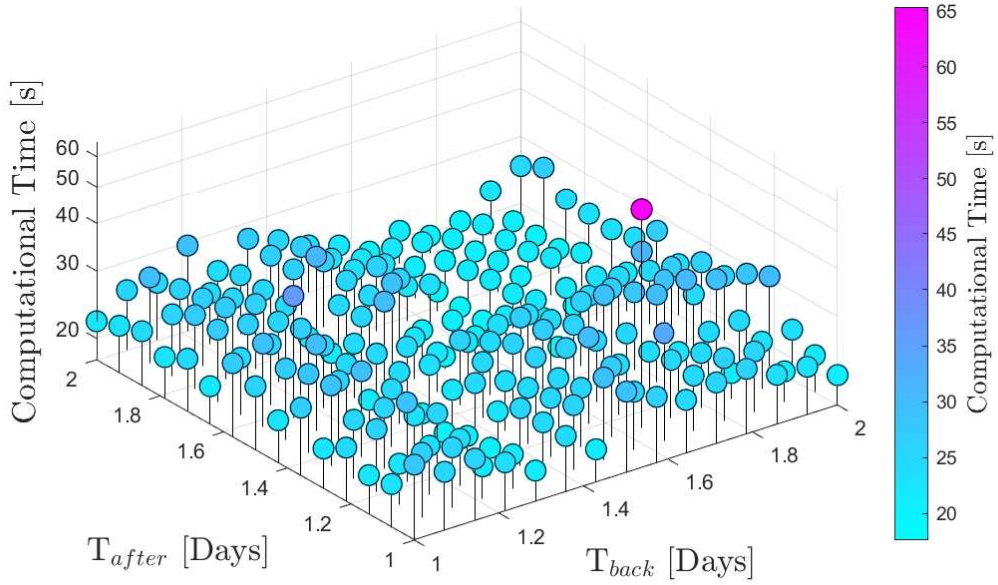

(b) FOP computational time.

Figure 3.18: Computational time for EOP and FOP solution.

Minimum Δv Maneuver

The acceleration profile achieved for the analytic minimum cost maneuver is presented in Fig. 3.19.

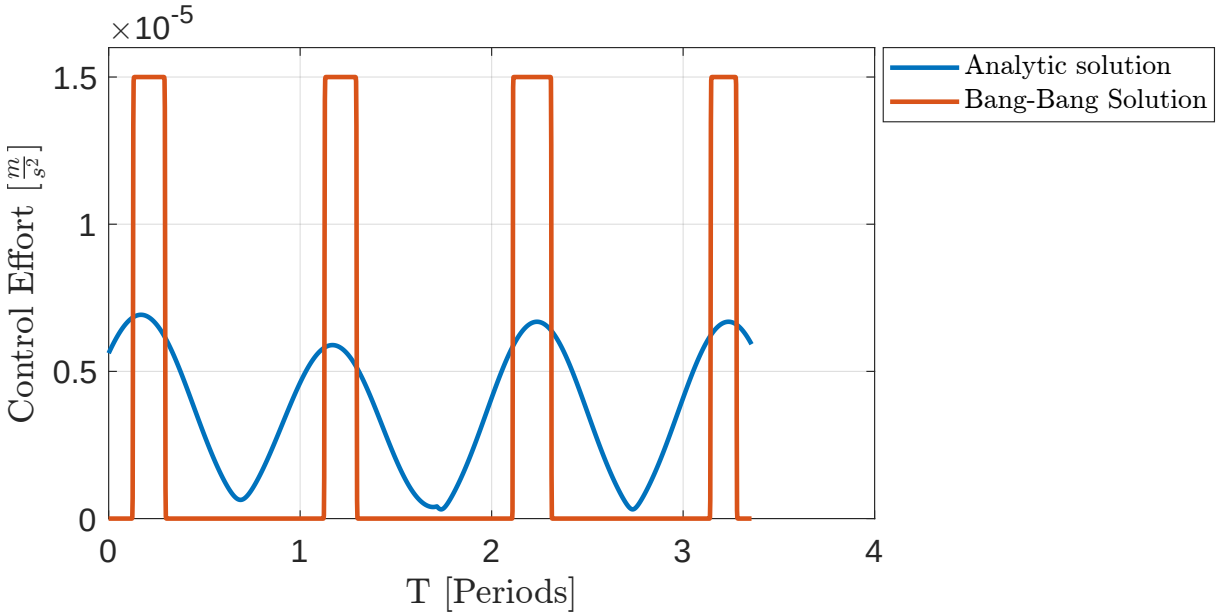

Figure 3.19: Comparison of PTO analytic acceleration profile and FOP solution

Point to Orbit vs Point to point

In this paragraph the benefits achieved without fixing the terminal point are presented in terms of Δv reduction (see Fig. 3.20).

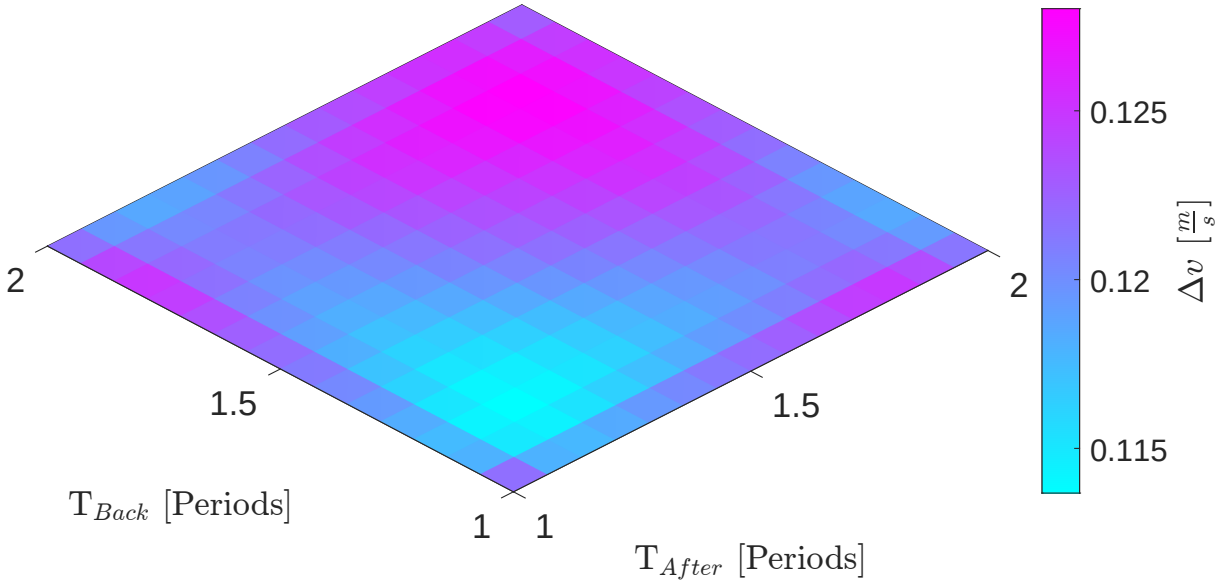

(a) PTO EOP cost.

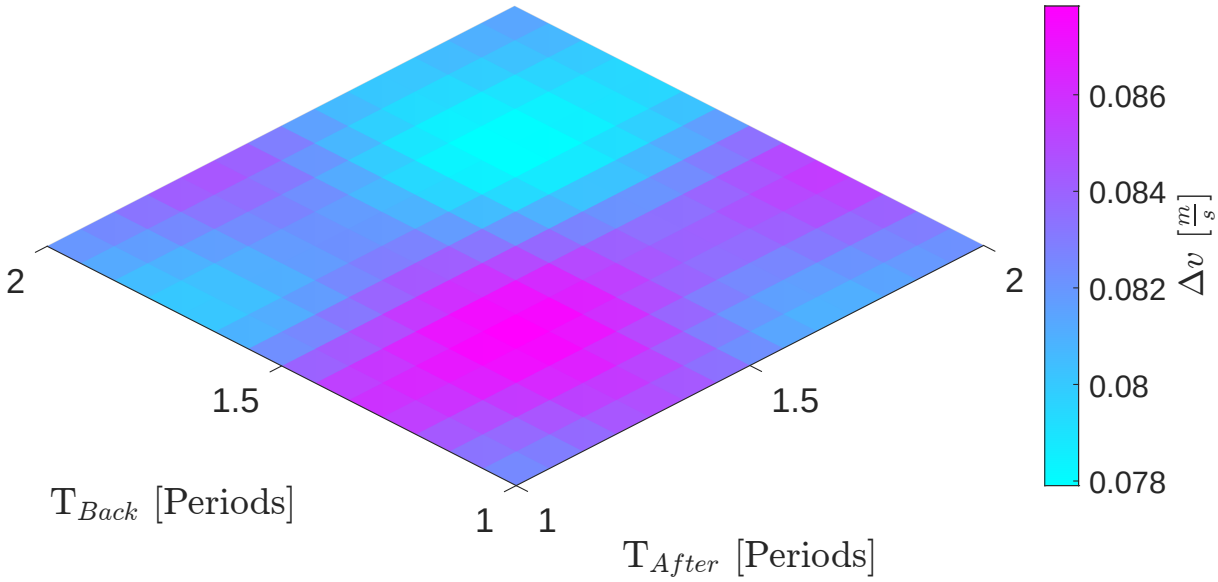

(b) PTP EOP cost.

Figure 3.20: PTO and PTP cost comparison for EOP solutions.

The PTOM case consumes less for the same PTPM time span at the expense of a delayed reentry in true anomaly terms. As can be seen in Fig. 3.21 the gap is almost negligible unless having constraints on the spacecraft station keeping.

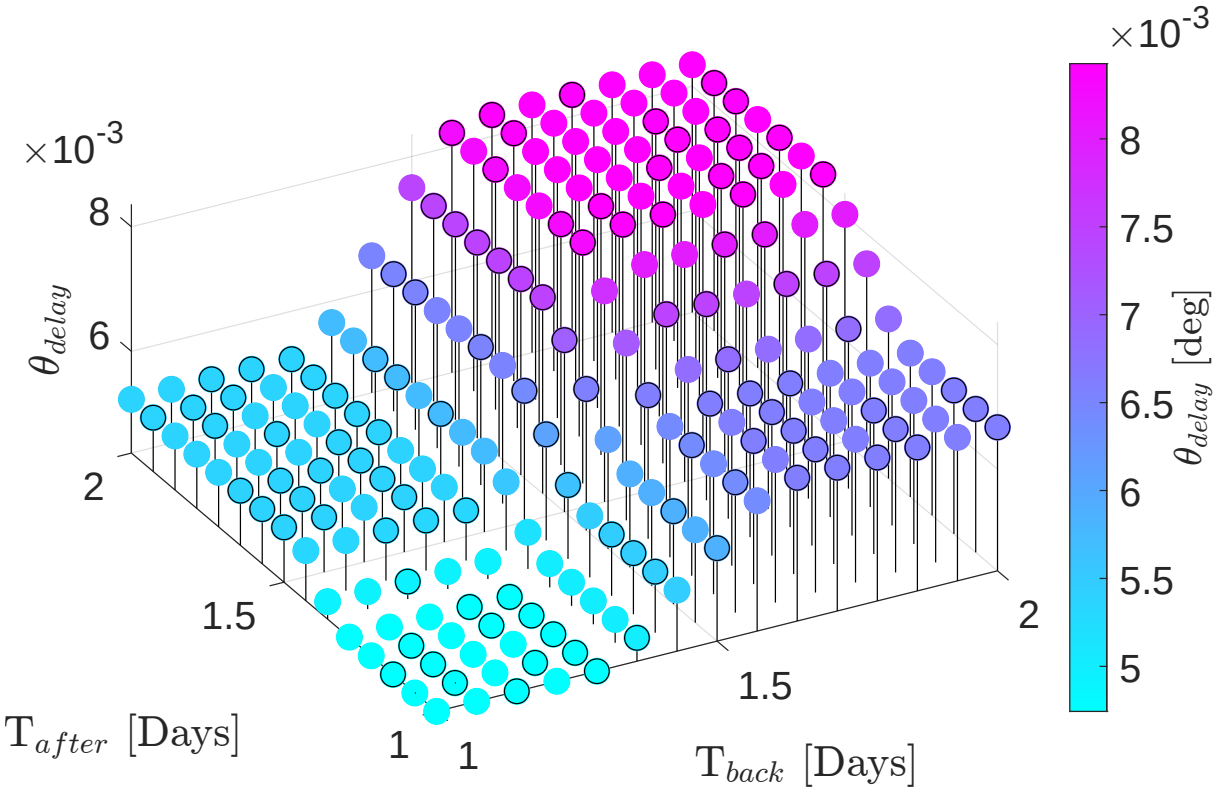

Figure 3.21: θ_{delay} difference.

4 | Low-Thrust CAM and SK EOP and FOP Design in GEO Orbit

In this chapter, the procedure to combine station-keeping with a collision avoidance maneuver is presented. The algorithm has to perform the SK maneuver. Moreover, it intervenes by modifying the trajectory if at TCA a threshold on the PoC is not respected. In the first part of the chapter, the analytical resolution of the EOP is obtained considering two polishes to find the optimal final target state. The second part provides the numerical transformation in FOP. Lastly, the more relevant results are reported.

4.1. Low-Thrust EOCP CAM and SK Formulation

Due to legal and practical reasons, the spacecraft position is constrained in the GEO orbital regime to lie in a given window of longitude and latitude. The evolution of the spacecraft's location inside the box is governed by the orbital perturbations. In particular, the non-spherical Earth perturbation affects mainly the longitude evolution, while the Solar and Moon perturbations modify the latitude behavior. In this thesis, the problem formulation is limited to considering the Earth's geopotential. To develop a more direct approach to the problem the dynamical model selected is different from the two used in Chapter 3. The EOE presented in Sec. 2.6 allow modeling the orbital dynamics directly with the reference parameters interested by the box limitation.

4.1.1. Problem Definition

In order to solve the problem the dynamical model is limited to include the non-spherical Earth geo-potential with harmonics up to J_{22}. Therefore the dynamics involves the EOE,

resumed in Eq. 4.1, and it is the one defined in Sect. 2.6.

$$\mathbf{x_{eoe}} = \begin{bmatrix} a \\ e_x = e\cos\omega + \Omega \\ e_y = e\sin\omega + \Omega \\ i_x = \tan\frac{i}{2}\cos\Omega \\ i_y = \tan\frac{i}{2}\sin\Omega \\ l_{M\Theta} = \Omega + \omega + M - \Theta \end{bmatrix} \qquad \mathbf{a_c} = \begin{bmatrix} a_n \\ a_t \\ a_h \end{bmatrix} \tag{4.1}$$

where $\Theta(t)$ represents Greenwich right ascension.

The EOP problem is defined as usual starting from the introduction of a cost function:

$$J := \nu\xi(t_{ca}, \mathbf{x}(t_{ca})) + \int_{t_i}^{t_f} \frac{1}{2}\mathbf{a_c}^T\mathbf{a_c}dt \tag{4.2a}$$

$$\xi(t_{ca}, \mathbf{x}(t_{ca})) = SMD(\mathbf{r}(t_{ca})) - \overline{SMD} \geq 0 \tag{4.2b}$$

The functional can be written introducing the Hamiltonian:

$$H := \frac{1}{2}\mathbf{a_c}^T\mathbf{a_c} + \boldsymbol{\lambda}^T\mathbf{f}(\mathbf{x}, \mathbf{a_c}) \tag{4.3a}$$

$$J := \nu\xi(t_{ca}, \mathbf{x}(t_{ca})) + \int_{t_i}^{t_f} \frac{1}{2}\mathbf{a_c}^T\mathbf{a_c} + \boldsymbol{\lambda}^T\left[\mathbf{f}(\mathbf{x}, \mathbf{a_c}) - \dot{\mathbf{x}}\right] dt \tag{4.3b}$$

As usual by imposing the first variation of the functional it is possible to reduce the problem to a set of differential-algebraic equations:

$$\begin{cases} \left.\dfrac{\partial\mathbf{x}}{\partial\eta}\right|_{t_i} = 0 \\ \left.\dfrac{\partial\mathbf{x}}{\partial\eta}\right|_{t_f} = 0 \\ \dfrac{\partial H}{\partial\mathbf{a_c}} = \mathbf{a_c}^T + \boldsymbol{\lambda}^T\mathbf{B}(t) = \mathbf{0} \Longrightarrow \mathbf{a_c} = -\mathbf{B}(t)^T\lambda \\ \dfrac{\partial H}{\partial\mathbf{x}} + \dot{\boldsymbol{\lambda}}^T = 0 \Longrightarrow \dot{\boldsymbol{\lambda}} = -\left[\dfrac{\partial H}{\partial\mathbf{x}}\right]^T = -\left[\dfrac{\partial\mathbf{f}}{\partial\mathbf{x}}\right]^T\boldsymbol{\lambda} = -\mathbf{A}(t)^T\boldsymbol{\lambda} \\ \dfrac{\partial H}{\partial\boldsymbol{\lambda}} = \dot{\mathbf{x}} = \mathbf{f}(\mathbf{x}, \mathbf{a_c}) \\ \nu\xi \geq 0 \end{cases} \tag{4.4}$$

Solving again the control equation it is possible to define an MPBVP:

$$\begin{cases} \dot{\mathbf{x}} = \mathbf{A}(t)\mathbf{x} - \mathbf{B}(t)\mathbf{B}(t)^T\boldsymbol{\lambda} + \mathbf{D}(t) \\ \dot{\boldsymbol{\lambda}} = -\mathbf{A}(\mathbf{t})^t\boldsymbol{\lambda} \end{cases} \qquad BCs: \begin{cases} \mathbf{x}(t_0) = \mathbf{x_0} \\ \mathbf{x}(t_f) = \mathbf{x_f} \\ \nu\dfrac{\partial\xi}{\partial\mathbf{x}(t_{ca})} - \boldsymbol{\lambda}^T(t_{ca}^-) + \boldsymbol{\lambda}^T(t_{ca}^+) = 0 \\ \xi(t_{ca}) \geq 0 \end{cases} \tag{4.5}$$

It is important to underline that, differently from chapter 3, it is impossible here to determine a-priori if the problem represents a ThPBVP or TwPBVP. The reason resides in the combination of the maneuver; in fact, if the perturbation due only to the SK reassessment is sufficient to respect the PoC constraint, the problem results in a simple TwPBVP in which the interior point conastraint is neglected.

4.1.2. Target Definition

The target parameters need to be defined in such a way as they maximize the resident time in the station-keeping box. In this thesis work, two different methodologies are implemented.

Numerical Definition

The first method proposed consists of a pure numerical optimization. The cost function is defined as the inverse of the resident time. The latter is computed by propagating the orbit with a numerical integrator until the spacecraft position, mediated along one orbital period results outside of the station keeping box.

The reliability of this method depends on the complexity of the dynamics used to model the spacecraft's motion. The main drawback of this strategy is the computational burden. In fact, the optimization requires a large number of numerical integrations; in addition, the numerical effort of the propagation increases with the model complexity; for this reason, obtaining a high-fidelity target state with this method is a cumbersome operation.

Analytic Definition

The second strategy adopted is an analytical method to determine the ideal target longitude to exploit the geopotential perturbation. This method does not provide the ideal target for all the six equinoctial elements; however, it can be implemented to identify the semi-major axis and the longitude. The other four parameters representative respectively of eccentricity and inclination are set to zero. The methodology used to determine the optimal longitude is taken from [28]. The longitudinal acceleration due to J_{22} is tabulated for different values of longitude. Therefore the evolution of the longitude in the station keeping box is represented as a ballistic motion.

$$\ddot{l}_m(t) = A = const \tag{4.6a}$$

$$\dot{l}_m(t) = At + \dot{l}_m(0) \tag{4.6b}$$

$$l_m(t) = \frac{1}{2}At^2 + \dot{l}_m(0)t + l_m(0) \tag{4.6c}$$

Acting on the semi-major axis it is possible to control the drift rate of the longitude. The complete mathematical formulation can be found in [28]:

$$\dot{l}_m = -\frac{3}{2}\frac{\omega_E}{a_{GEO}}\Delta a \tag{4.7}$$

These two informations are sufficient to determine analytically the ideal target longitude. The procedure can be resumed as follow:

1. For the assigned $\overline{l_m}$ compute the tabulated value of longitudinal acceleration.
2. Compute the initial longitude as:

$$\begin{cases} l_m(0) = \overline{l_m} + \dfrac{\delta}{2} \; if \; A > 0 \\ l_m(0) = \overline{l_m} - \dfrac{\delta}{2} \; if \; A < 0 \end{cases} \tag{4.8}$$

   Where δ is the admissible longitude window.

3. Use 4.6c to find $\dot{l}_m(0)$ and T by setting:

$$\begin{aligned} At \quad & t = T \quad && \Delta l_m(T) = \Delta l_m(0) \\ At \quad & t = \frac{T}{2} \quad && \Delta l_m\left(\frac{T}{2}\right) = -\Delta l_m(0) \end{aligned} \tag{4.9}$$

Leading to:

$$\begin{cases} \Delta l_m(0) = \frac{1}{2}AT^2 + \dot{l_m}(0)T + \Delta l_m(0) \\ -\Delta l_m(0) = \frac{1}{8}AT^2 + \dot{l_m}(0)\frac{T}{2} + \Delta l_m(0) \end{cases} \tag{4.10}$$

Solving the system the following results are obtained:

$$T = 4\sqrt{\frac{\Delta l_m(0)}{A}} = 4\sqrt{\frac{\delta}{2A}} \tag{4.11a}$$

$$\dot{l_m}(0) = -2sign(A)\sqrt{2A\delta} \tag{4.11b}$$

4. From the value of the initial drift compute the semi-major axis target using Eq. 4.7:

$$\Delta a = -\frac{3}{2}\frac{a_{GEO}}{\omega_E}\dot{l}_m(0) \tag{4.12}$$

State Transition Matrix

Even in this case, the linearization of the trajectory with respect to the unmaneuvered motion is achieved trough the STM. That is obtained with the following integration:

$$\begin{cases} \dot{\mathbf{\Phi}}(t) = \mathbf{A_{STM}}(t)\mathbf{\Phi}(\mathbf{x}(t_0), t) \\ \mathbf{\Phi}(\mathbf{x}(t_0), t_0) = \mathbf{I} \end{cases} \tag{4.13}$$

Where:

$$\mathbf{A_{STM}}(t) = \begin{bmatrix} \mathbf{A}(t) & -\mathbf{B}(t)\mathbf{B}(t)^T \\ \mathbf{0_{3\times 3}} & -\mathbf{A_{STM}}(t)^T \end{bmatrix} \tag{4.14}$$

First Trajectory Arc

Considering the linearization along the nominal trajectory in the interval $[t_0, t_{ca}^-]$:

$$\begin{bmatrix} \boldsymbol{\delta}\mathbf{x_{ca}} \\ \boldsymbol{\lambda}_{ca^-} \end{bmatrix} = \begin{bmatrix} \mathbf{\Phi}_{xx} & \mathbf{\Phi}_{x\lambda} \\ \mathbf{\Phi}_{\lambda x} & \mathbf{\Phi}_{\lambda\lambda} \end{bmatrix} \begin{bmatrix} \boldsymbol{\delta}\mathbf{x_0} \\ \boldsymbol{\lambda_0} \end{bmatrix} \tag{4.15}$$

Imposing $\boldsymbol{\delta}\mathbf{x_0} = 0$ after some algebraic manipulation the following expression is obtained:

$$\boldsymbol{\lambda}_{ca^-} = \mathbf{\Phi}_{\lambda\lambda}\mathbf{\Phi}_{x\lambda}^{-1}\boldsymbol{\delta}\mathbf{x_{ca}} = \mathbf{E}\boldsymbol{\delta}\mathbf{x_{ca}} \tag{4.16}$$

Costate Discontinuity

The co-state discontinuity equation imposed by the SMD constraints is represented by the following equations:

$$\frac{\partial \xi}{\partial \mathbf{x}(t_{ca})} = \boldsymbol{\varphi}(\mathbf{x_{ca}}) \tag{4.17a}$$

$$\boldsymbol{\lambda}_{ca^+} = \boldsymbol{\lambda}_{ca^-} - \nu \boldsymbol{\varphi}(\mathbf{x_{ca}}) \tag{4.17b}$$

Following the procedure executed in Sect. 3.4. To obtain the analytic solution of the problem, it is necessary to approximate the discontinuity by adopting a zero-order Taylor expansion:

$$\boldsymbol{\varphi}(\mathbf{x_{ca}}) \approx \boldsymbol{\varphi}(\mathbf{x_{ref}}(t_{ca})) = \boldsymbol{\varphi} \tag{4.18}$$

Second Trajectory Arc

Reasoning in a similar way as for the first arc, using the STM and the results obtained in the previous passages, it is possible to find the expression of the state perturbation at TCA:

$$\boldsymbol{\delta}\mathbf{x_{ca}} = \boldsymbol{\delta}\mathbf{x_{sk,ca}} + \nu \mathbf{h_{CAM}} \tag{4.19}$$

It is possible to notice that Eq. 4.19 is composed of two terms. The first one represents the perturbation of the state due to the station-keeping maneuver; the second one instead is the eventual additional contribution due to the collision avoidance maneuver.

SMD Constraints

Differently from the previous maneuver the PoC threshold represents an inequality constraint. In fact, during this operation, it is possible that the modification in the trajectory, induced by station-keeping maneuver, is sufficient to overcome SMD threshold. In this case, the constraint is totally neglected by setting $\nu = 0$ and the problem is transformed into the following TwPBVP.

$$\begin{cases} \dot{\mathbf{x}} = \mathbf{A}(t)\mathbf{x} - \mathbf{B}(t)\mathbf{B}(t)^T\boldsymbol{\lambda} + \mathbf{D}(t) \\ \dot{\boldsymbol{\lambda}} = -\mathbf{A}(\mathbf{t})^t\boldsymbol{\lambda} \end{cases} \qquad BCs: \begin{cases} \mathbf{x}(t_0) = \mathbf{x_0} \\ \mathbf{x}(t_f) = \mathbf{x_f} \end{cases} \tag{4.20}$$

In case the SK perturbation is not enough, the problem proceeds in a similar way to Sec. 3.4. Defining as $\boldsymbol{\varrho}(\mathbf{x})$ the transformation from equinoctial state elements to cartesian

position it is possible to define the SMD constraint equation:

$$[\boldsymbol{\varrho}(\mathbf{x_{ca}}) - \mathbf{r_s}(t_{ca})]^T \mathbf{Q} [\boldsymbol{\varrho}(\mathbf{x_{ca}}) - \mathbf{r_s}(t_{ca})] = \overline{SMD} \tag{4.21}$$

Once again without linearizing the transformation function $\boldsymbol{\varrho}(\mathbf{x})$ it is impossible to find an analytic solution. However in this case the first order expansion is performed around the SK perturbed state rather than about the nominal one. In this way, the error induced is lower.

$$\boldsymbol{\varrho}(\mathbf{x_{ca}}) \approx \mathbf{r_{sk,ca}}(t_{ca}) + \nu \mathbf{Jh} \tag{4.22}$$

This approximation brings the constraint equation to a second-degree expression that can be solved as a function of ν. Then this value is used to determine the initial co-state. The procedure is summarized in Alg. 4.1 and the full matematical procedure can be found in Appendix C.

Algorithm 4.1 EOP Point to orbit. Part 1

Input: $\mathbf{x}_{p_{TCA}}$, $\mathbf{r}_{s_{TCA}}$, $\overline{\text{SMD}}$, $\Delta\theta_1$,$\Delta\theta_2$, t_{ca}
Output: SMD, $\mathbf{a}_c$, $\mathbf{\Delta v}$
for i = length($\Delta\theta_1$) **do**
  T_1 time interval corresponding to the selected $\Delta\theta_1$
  Backward propagation
  tspan_backward = [0, $-T_1$]
  $\mathbf{y}_0 = \mathbf{x}_{p_{TCA}}$
  $\mathbf{x}_0 = eoe\_back\_propagation$
  for j = length($\Delta\theta_2$) **do**
    T_2 time interval corresponding to the selected $\Delta\theta_2$
    Forward propagation
    tspan_forward = [0, T_2]
    $\mathbf{x}_f = eoe\_forward\_propagation(\mathbf{y}_0,$ **tspan_forward**$)$
    STM$_1$ computation
    $tspan_1$ =[0, T_1]
    [**STM$_1$**] = $stateTrans\_eoe($**tspan$_1$**, $\mathbf{x}_0)$
    STM$_2$ computation
    $tspan_2$ =[0, T_2]
    [**STM$_2$**] = $stateTrans\_eoe($**tspan$_2$**, $\mathbf{x}_{pTCA})$

Algorithm 4.2 EOP Point to orbit. Part 2

Solve the non-linear system
compute $\boldsymbol{\delta}\mathbf{x}_{\mathbf{sk,ca}}$
$\mathbf{r}_{\mathbf{sk,ca}}$=$eoe2rv(\mathbf{x}_{\mathbf{sk,ca}})$
$\Delta\mathbf{r}_{\mathbf{sk,ca}} = \mathbf{r}_{sk,ca} - \mathbf{r}_s$
$[SMD_{sk}] = squared\_mahalanobis\_distance(\Delta\mathbf{r}_{\mathbf{sk,ca}})$
if SMD_{sk}>$\overline{\text{SMD}}$ **then**
$\nu = 0$
else
find ν from Eq. 4.21
end if
compute $\boldsymbol{\delta}\mathbf{x}_{ca}$ from Eq. 4.19
compute $\boldsymbol{\lambda}_0$
Controlled forward propagation
$tspan$=$[0, T_1 + T_2]$
$\mathbf{y}_0 = [\mathbf{x}_0, \boldsymbol{\lambda}_0]$
$[\mathbf{x}_f, \boldsymbol{\lambda}_f, \mathbf{x}_{\mathbf{ca}}] = control\_propagator\_eoe(\mathbf{y}_0, \mathbf{tspan\_forward})$
$\mathbf{r}_{\mathbf{ca}}$=$eoe2rv(\mathbf{x}_{\mathbf{ca}})$
$\Delta\mathbf{r} = \mathbf{r}_{ca} - \mathbf{r}_s$
$[\text{SMD}] = squared\_mahalanobis\_distance(\Delta\mathbf{r})$
$\mathbf{a}_c = f(\boldsymbol{\lambda})$
$\Delta v = trapz(\mathbf{a}_c, \Delta t)$
end for
end for

4.2. Low-Thrust CAM and SK FOP Transformation.

The solution procedure is strictly related to the ones presented in chapter 3. The main difference is the same which characterize all the solution obtained in this chapter. The final results represent a MPBVP, that would be represented with the interior point constraint active or inactive depending on the maneuver condition. This leads to a more complex algorithm. However, it does not influence the definition of the problem.

4.2.1. Problem Definition

The problem has an analogous solution technique of the FOP presented in Sec. 3.5. Obviously, the function explained below has a different expression compared to the ones

reported in the previous FOP problem, however, the mathematical structure and the physical concepts are the same. Starting from the cost function:

$$J := \nu\xi(t_{ca}, \mathbf{x}(t_{ca})) + u_{th}\int_{t_i}^{t_f} a_{max}\epsilon dt \tag{4.23}$$

Thanks to Pontryagin's maximum principle, the optimal control law (ϵ^*, α^*), providing $\mathbf{a_c} = a_{max}\epsilon^*\alpha^*$ is:

$$\begin{cases} \alpha^* = \dfrac{\mathbf{B}(t)^T\boldsymbol{\lambda}}{||\mathbf{B}(t)^T\boldsymbol{\lambda}||} \\ \epsilon^* = 1 \; if \; ||\mathbf{B}(t)^T\boldsymbol{\lambda}|| > u_{th} \Longrightarrow \epsilon = \dfrac{1}{2}\left[1 - \tanh\left(\dfrac{||\mathbf{B}(t)^T\boldsymbol{\lambda}|| - u_{th}}{\rho}\right)\right] \\ \epsilon^* = 0 \; if \; ||\mathbf{B}(t)^T\boldsymbol{\lambda}|| < u_{th} \end{cases} \tag{4.24}$$

The parameter u_{th} represents the threshold acceleration value on the continuous profile. It is obtained with the usual iterative procedure based on the bisection method and described in Sec. 3.5. The resolution of the optimal control problem leads to the following ThPBVP.

$$\begin{cases} \dot{\mathbf{x}} = \mathbf{A}(t)\mathbf{x} - \mathbf{B}(t)\left\{\dfrac{1}{2}\left[1 - \tanh\left(\dfrac{||\mathbf{B}(t)^T\boldsymbol{\lambda}|| - u_{th}}{\rho}\right)\right]\dfrac{\mathbf{B}(t)^T\boldsymbol{\lambda}}{||\mathbf{B}(t)^T\boldsymbol{\lambda}||}\right\} + \mathbf{D}(t) \\ \dot{\boldsymbol{\lambda}} = -\mathbf{A}(\mathbf{t})^t\boldsymbol{\lambda} \end{cases} \tag{4.25a}$$

$$BCs: \begin{cases} \mathbf{x}(t_0) = \mathbf{x_0} \\ \mathbf{x}(t_f) = \mathbf{x_f} \\ \nu\dfrac{\partial\xi}{\partial\mathbf{x}(t_{ca})} - \boldsymbol{\lambda}^T(t_{ca}^-) + \boldsymbol{\lambda}^T(t_{ca}^+) = 0 \\ \xi(t_{ca}) \geq 0 \end{cases} \tag{4.25b}$$

Or, if the station keeping contribution is sufficient to satisfy the SMD constraint, by the following TwPBVP.

$$\begin{cases} \dot{\mathbf{x}} = \mathbf{A}(t)\mathbf{x} - \mathbf{B}(t)\left\{\dfrac{1}{2}\left[1 - \tanh\left(\dfrac{||\mathbf{B}(t)^T\boldsymbol{\lambda}|| - u_{th}}{\rho}\right)\right]\dfrac{\mathbf{B}(t)^T\boldsymbol{\lambda}}{||\mathbf{B}(t)^T\boldsymbol{\lambda}||}\right\} + \mathbf{D}(t) \\ \dot{\boldsymbol{\lambda}} = -\mathbf{A}(\mathbf{t})^t\boldsymbol{\lambda} \end{cases} \tag{4.26a}$$

$$BCs: \begin{cases} \mathbf{x}(t_0) = \mathbf{x_0} \\ \mathbf{x}(t_f) = \mathbf{x_f} \end{cases} \tag{4.26b}$$

The algorithm corresponding to the FOP transformation is resumed in Fig. 4.1.

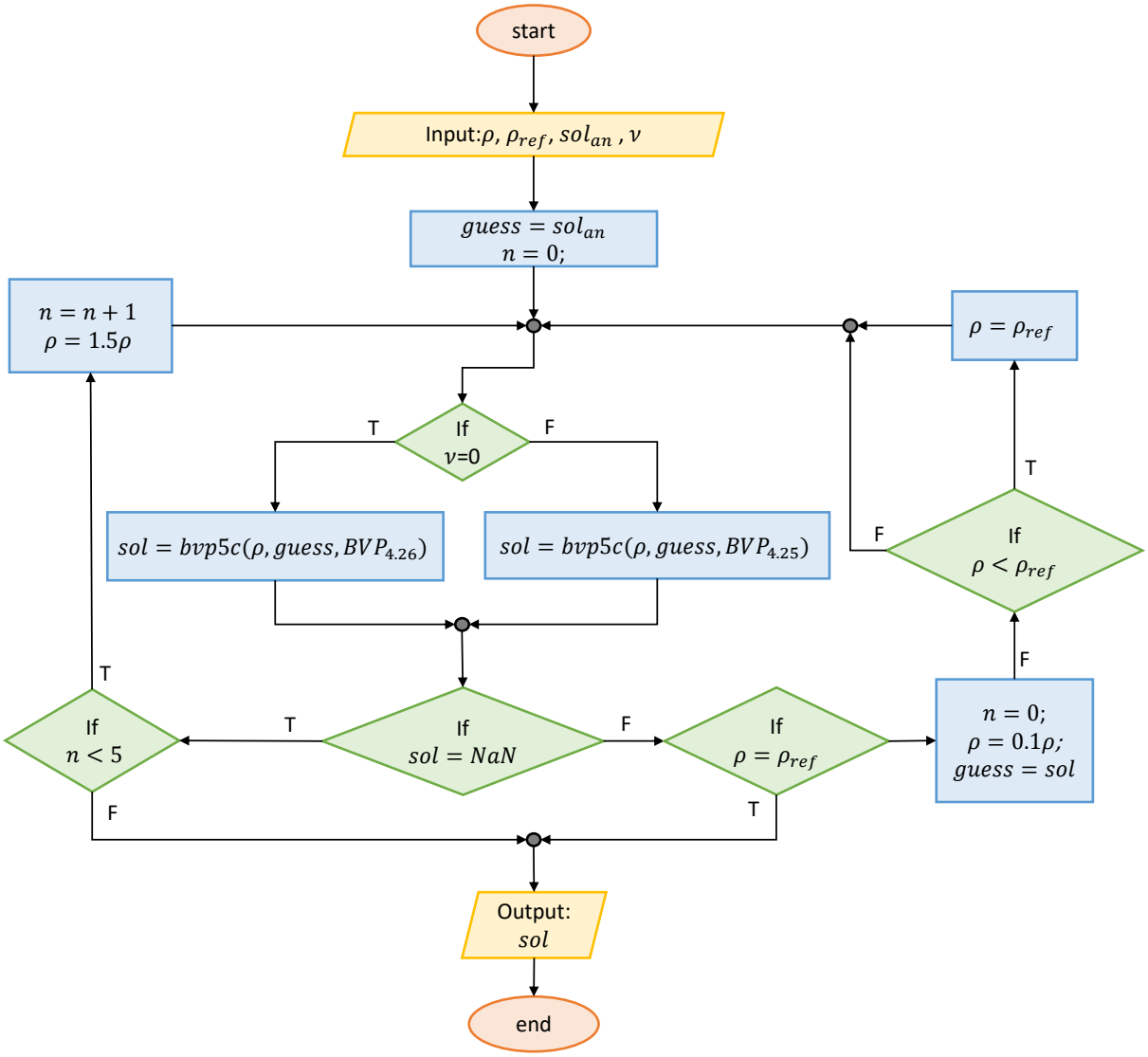

Figure 4.1: CAM and SK FOP algorithm.

4.3. Results

This section reports the results of the combination of the CAM with the station-keeping maneuver. In order to verify the reliability of the algorithm, the procedure is run both using a target state defined with the analytical method and with a target defined with the optimization procedure.

4.3.1. Test Case

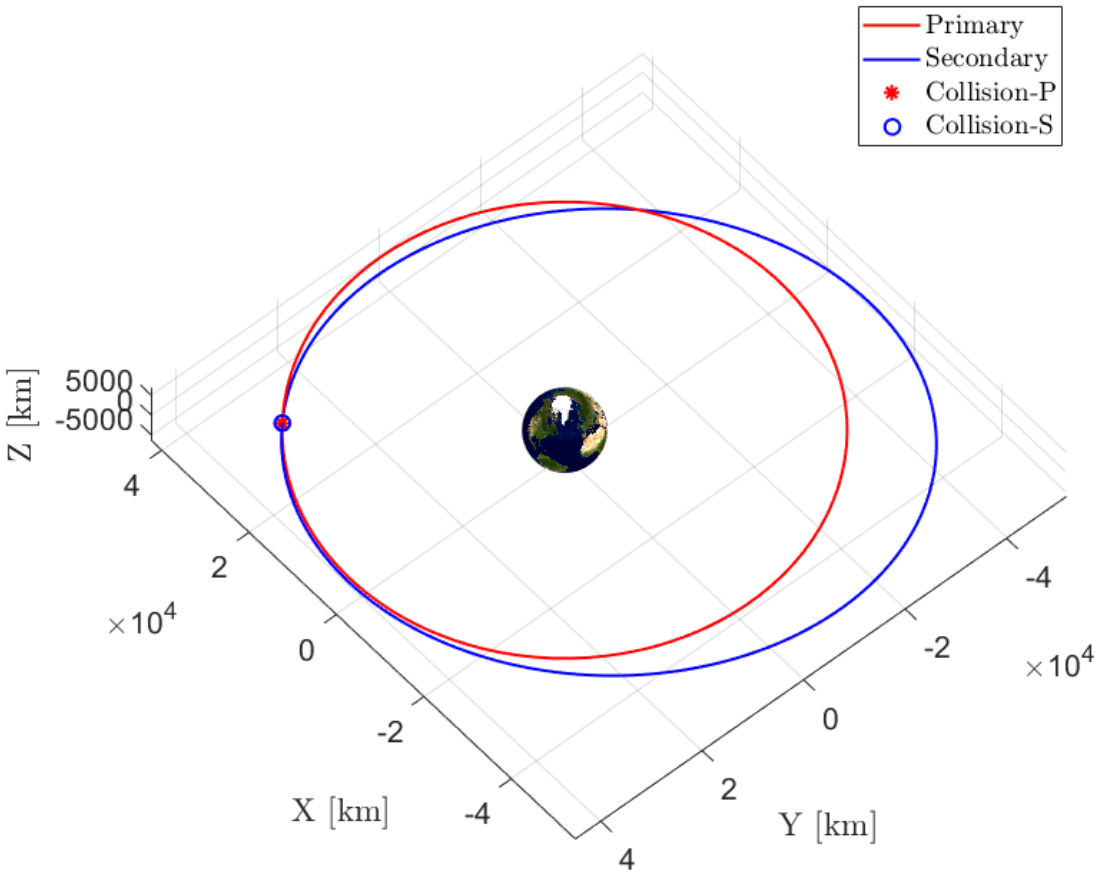

Figure 4.2: Test case GEO collision representation.

The method presented in chapter 4 is applied to a test case provided by GMV. A representation of the collision can be found in Figure 4.2. Table 4.1 reports the position and velocity vectors of the primary and secondary spacecraft at the conjunction in ECI frame, the PoC, the SMD and the miss distance d. The Keplerian elements of the two orbits are computed and displayed in Table 4.2.

Table 4.1: Test case conjunction data.

$\vec{r}_p$[km]	[2 8525, 3 1054, -42.4360]$^\top$
$\vec{r}_s$[km]	[2 8525, 3 1054, -42.4360]$^\top$
$\vec{v}_p$ [km/s]	[-2.2644, -2.0978, 0.0032]$^\top$
$\vec{v}_s$ [km/s]	[-2.3001, 2.2941, 0.4560]$^\top$
PoC	4.628e-02
SMD	0.2020
d [km]	0.0350

Table 4.2: Test case orbital elements, in order: semi-major axis, eccentricity, inclination, Right Ascension of the Ascending Node (RAAN), argument of the periapsis, true anomaly.

	a	e	i	Ω	ω	θ
O_p	42 165 km	4.4556e-05	0.8594 °	0 °	91.30 °	263.09 °
O_s	48 939 km	0.1441	8.00 °	340.92 °	184.41 °	18.67 °

The position covariance matrices of the two satellites, expressed in their respective ECI reference frame, are:

$$\vec{C}_p = \begin{bmatrix} 0.8085e-05 & -2.0477 & 6.55174 \\ -2.0477 & 137.6 & -1.8341e \\ 6.5517 & -1.8341 & 59.78 \end{bmatrix} \cdot 10^{-4} \text{ km}^2 \tag{4.27}$$

$$\vec{C}_s = \begin{bmatrix} 2.4481 & 7.2988 & 18.10 \\ 7.2988 & 0.1113 & -114.9 \\ 18.10 & -114.9 & 186.6 \end{bmatrix} \cdot 10^{-4} \text{ km}^2 \tag{4.28}$$

The corresponding combined covariance matrix in B-plane coordinates is:

$$\vec{C} = \begin{bmatrix} 687.7 & 564.7 \\ 0.0565 & 477.5 \end{bmatrix} \cdot 10^{-4} \text{ km}^2 \tag{4.29}$$

All the simulations presented in this dissertation are run with a processor "AMD RYZEN9 3900x" and 32 GB Ram Memory.

The results reported in this section are obtained from the application of the algorithms presented in 4.1, and Fig. 4.1. The collision probability is imposed as $PoC = 10^{-6}$

that leads to a threshold of $SMD = 17.1251$. The FOP is solved considering a level of acceleration of $a_{max} = 6.7 \cdot 10^{-5} \frac{m}{s^2}$.

4.3.2. Analytical Target

The analytical target is computed as described in Sect. 4.1.2. The value of the EOE achieved is shown in Tab. 4.3 and the prescribed longitude evolution, subjected to the geopotential perturbation, is represented in Fig. 4.3.

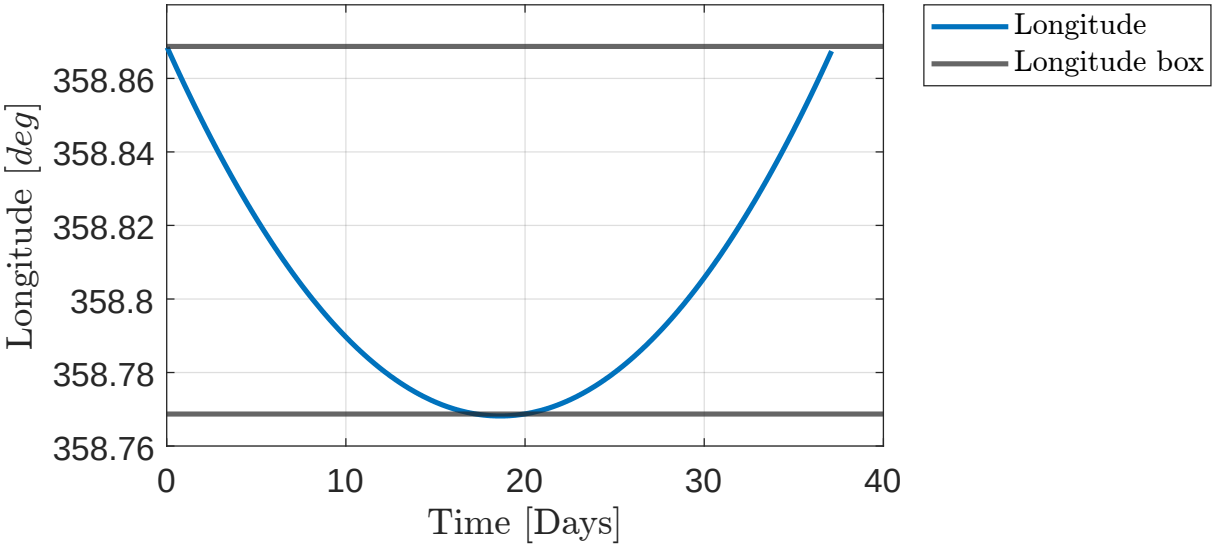

Figure 4.3: Target longitude evolution, and longitude box.

Table 4.3: Analytical target.

a [km]	e_x	e_y	i_x	i_y	l_m [deg]
42 166.34	0	0	0	0	358.86

Even in this case, the first verification is done by showing that none of the maneuvers computed allows the primary object to pass inside the PoC ellipse threshold. The position at TCA of the primary object, computed solving the EOP, is represented in Fig. 4.4.

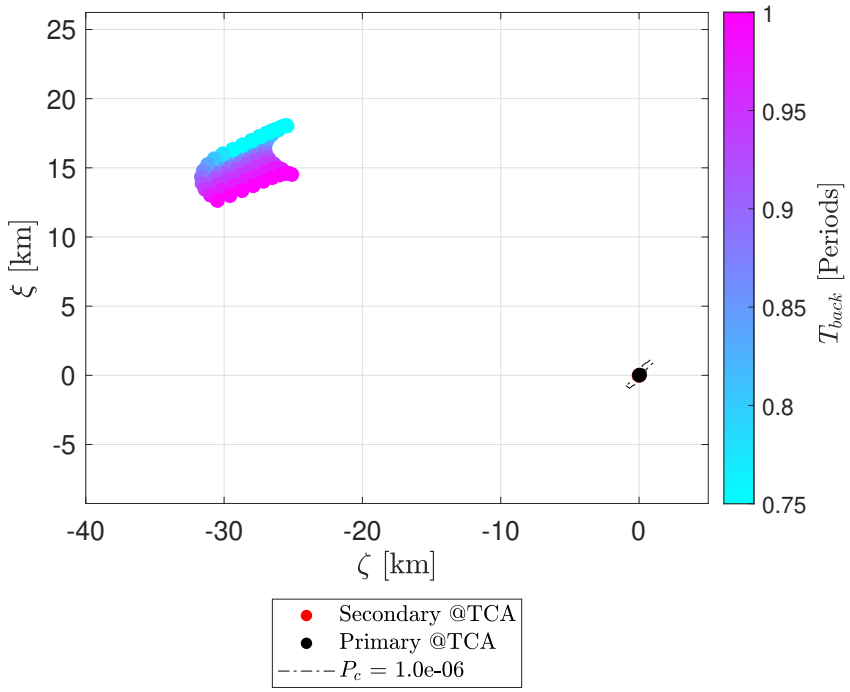

(a) First trajectory arc.

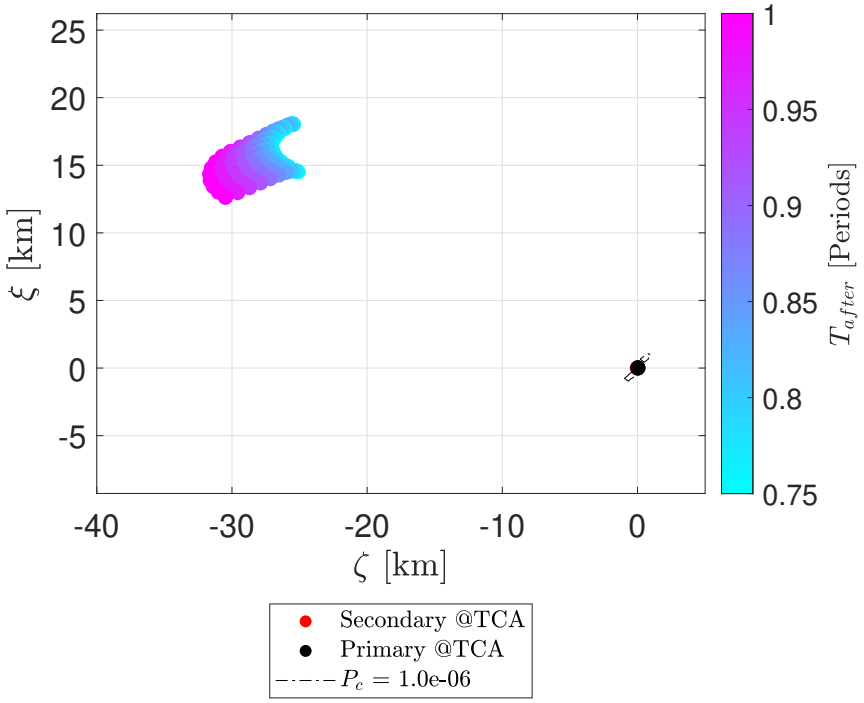

(b) Second trajectory arc.

Figure 4.4: Position of the primary object, achieved with the analytic solution, and represented in b-plane for the various values of the first and the second trajectory arc.

Then it is possible to compare the maneuver cost of the EOP and the FOP solutions. As it is shown in Fig 4.5, the maneuver corresponding to the FOP solution is generally cheaper than the analytic solution. However, in some specific cases, the previous property is not respected. The motivation behind this particular phenomenon is the same that generates the saturation effect explained in Sect. 3.3.3. The fixed level of acceleration available for the FOP can be very different from the magnitude of the acceleration required by the EOP solution. In the case of geostationary orbit, this takes more relevance due to the high difference in maneuvering time that leads to a strongly variation in maximum acceleration needed.

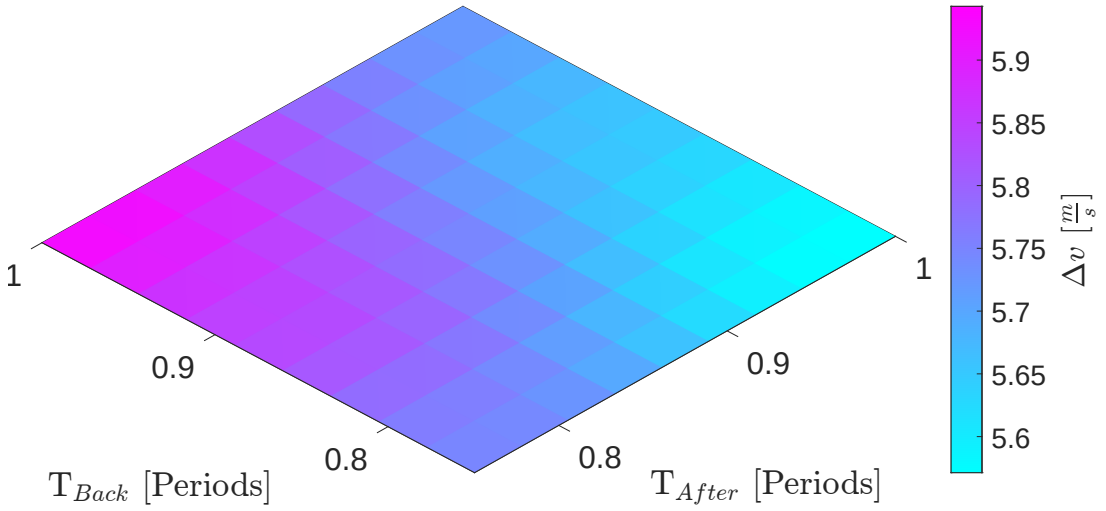

(a) Analytic Δv magnitude.

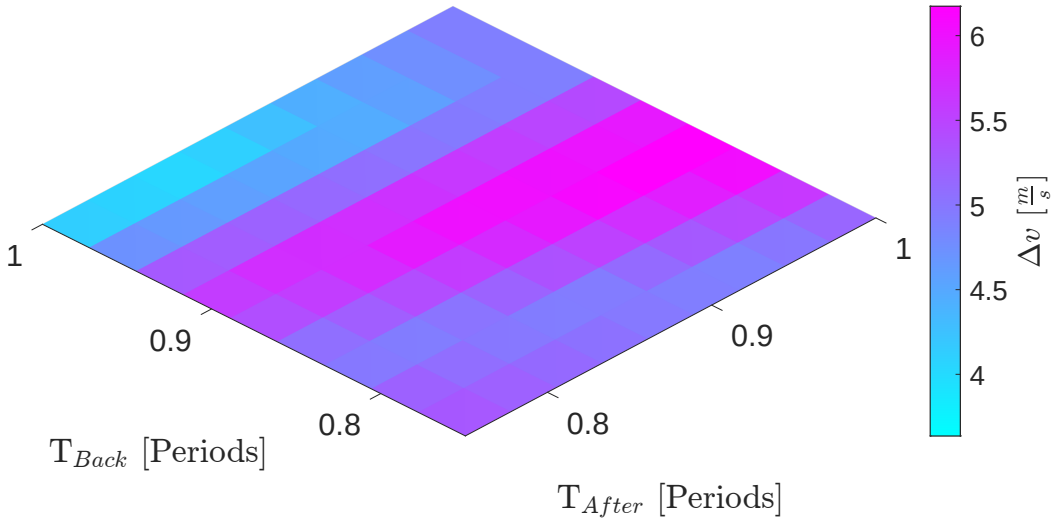

(b) Bang-bang Δv magnitude.

Figure 4.5: Δv results from FOP and EOP solutions.

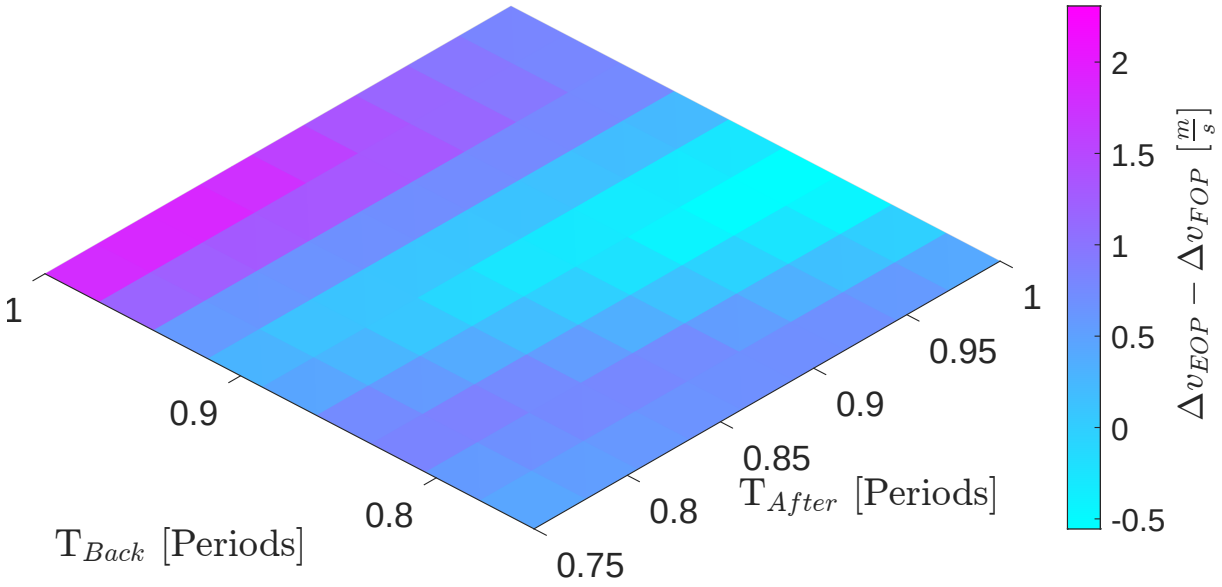

Figure 4.6: Δv difference between EOP and FOP solutions.

For what concerns the computational time, Fig 4.7 shows how the situation is similar to the previous chapter. It reveals a strong dependency on the propagation time for the EOP numerical effort, while the FOP computational time does not show any relevant trend.

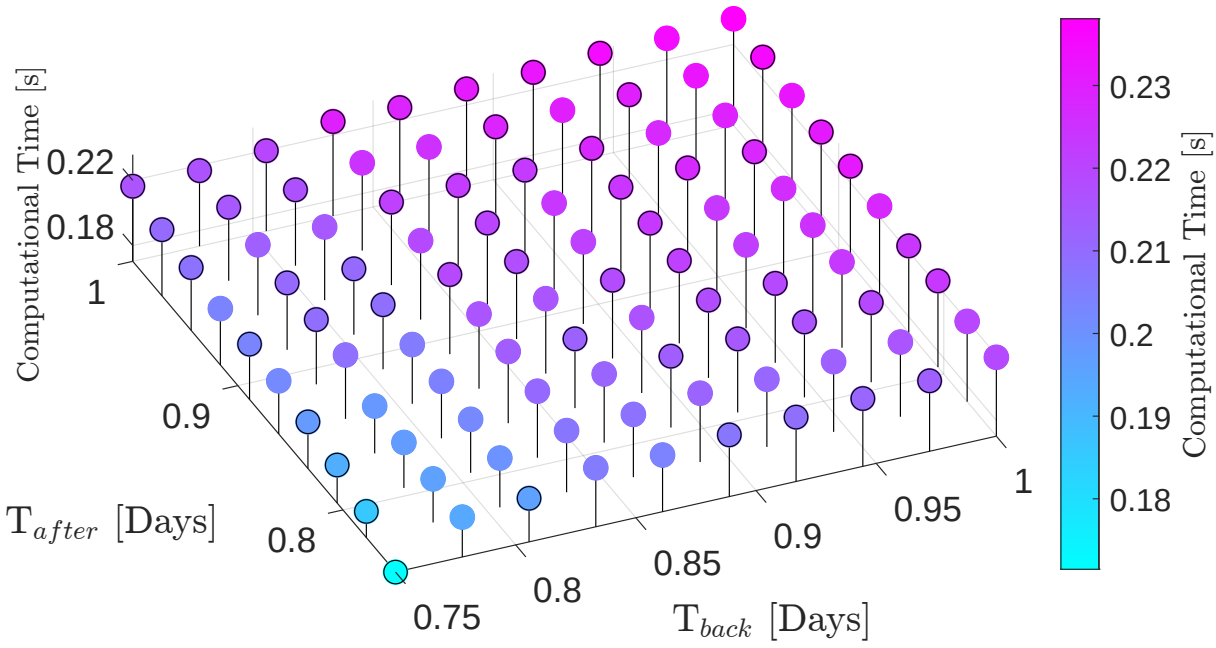

(a) EOP computational time.

Figure 4.7: Computational time for EOP and FOP solution.

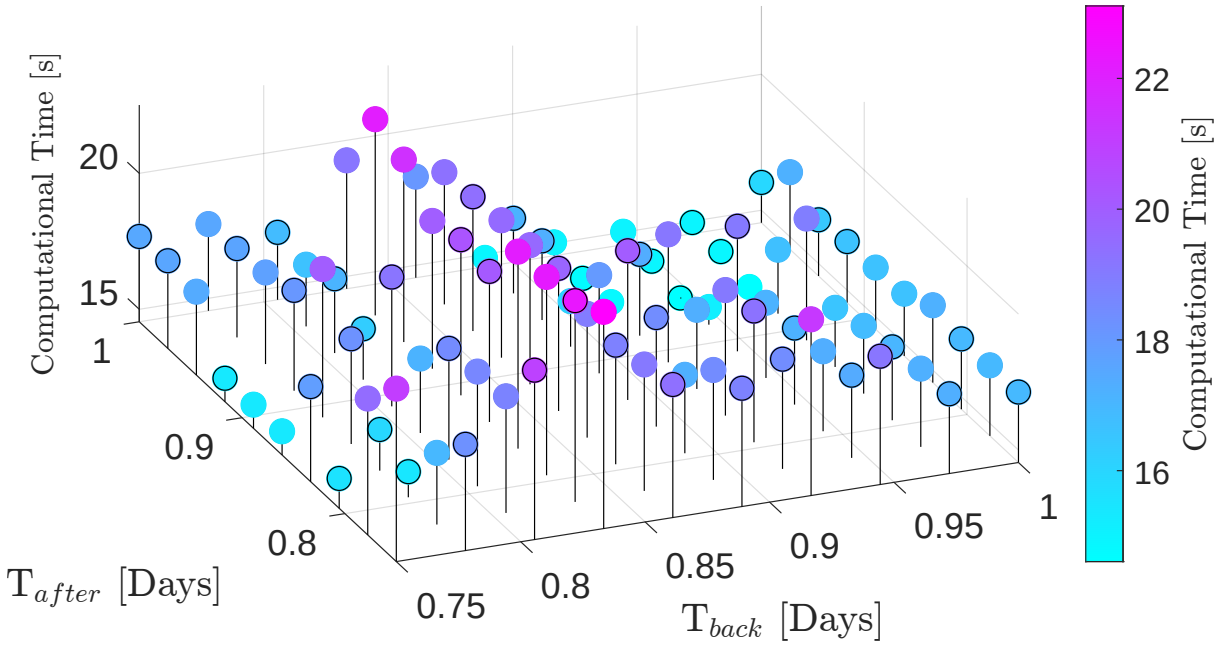

(b) FOP computational time.

Figure 4.7: Computational time for EOP and FOP solution.

Minimum Δv Maneuver

Once again the minimum Δv case can be analyzed to show some features of the EOP and FOP solutions. Figure 4.8 shows the acceleration profiles of the analytic result and the correspondent bang-bang transformation.

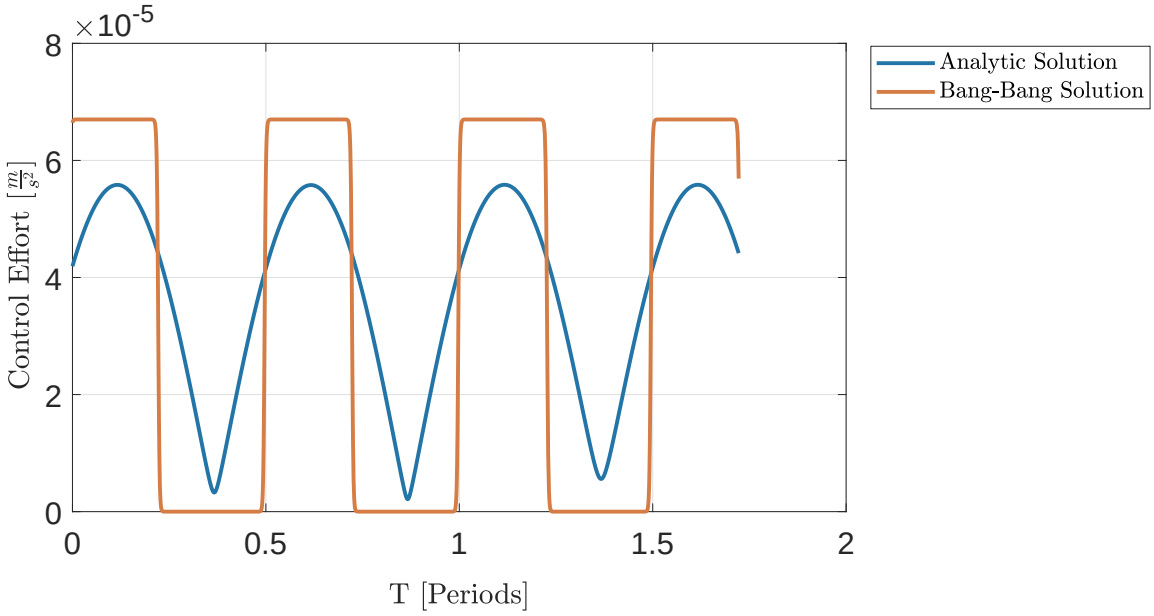

Figure 4.8: Comparison of analytic acceleration profile and FOP solution.

In addition, it is possible to represent the evolution of the longitude and the latitude during the maneuver. As can be seen in Fig.4.9, as far as the latitude is concerned, it remains inside the station keeping box during the entire maneuver. The longitude instead appears to exceed the longitude limits in order to match the target at the final time. The reason behind this behaviour lies in the perturbations. The optimal maneuver tends to use the geopotential effect to match the final target reducing the propulsion effort.

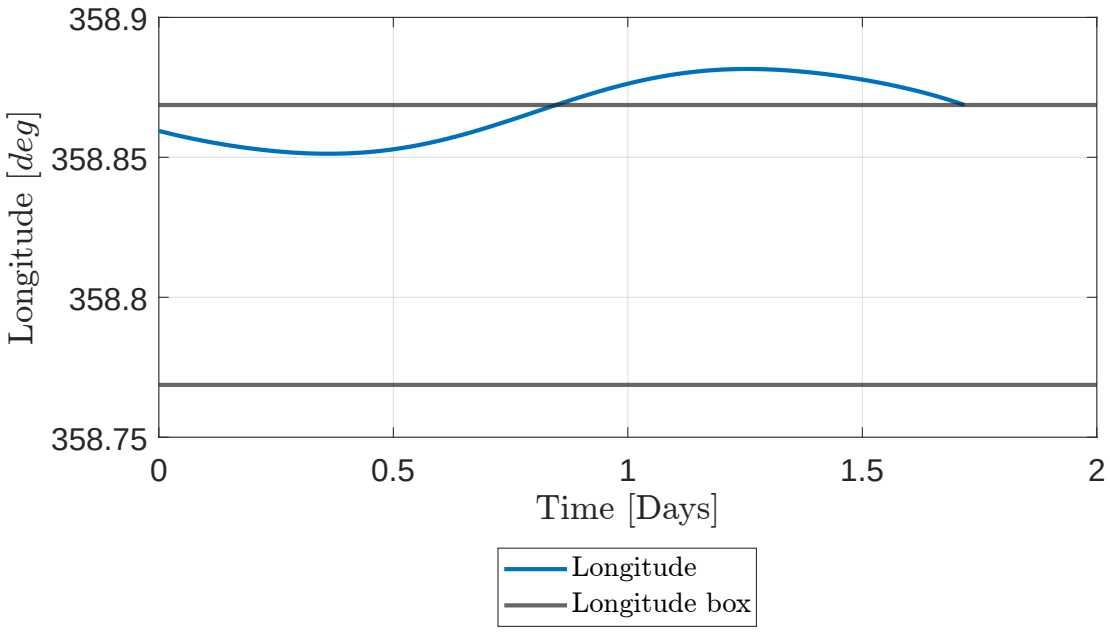

(a) Longitude.

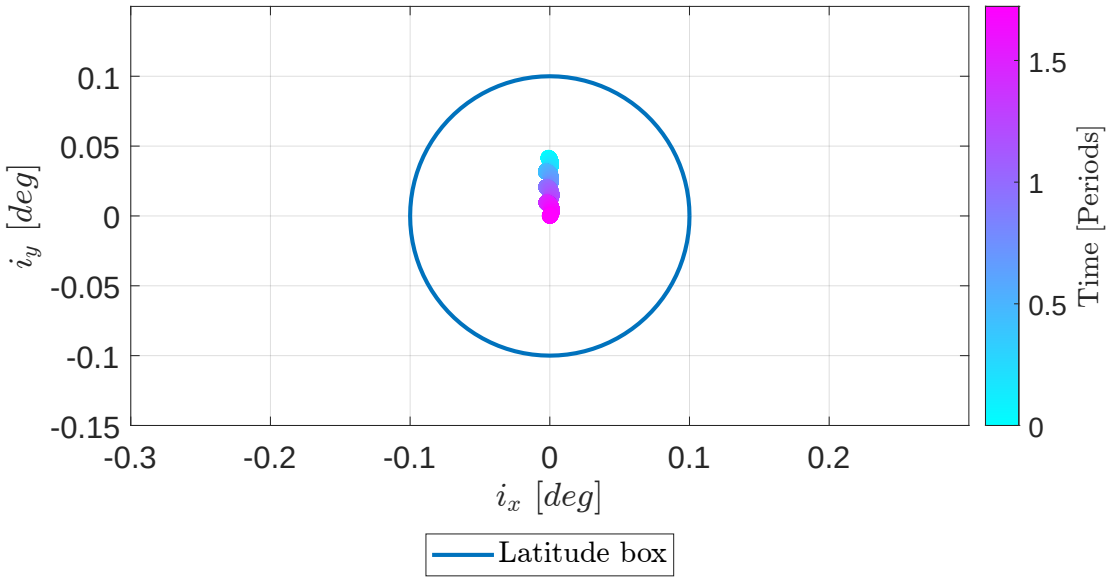

(b) Latitude.

Figure 4.9: Spacecraft latitude and longitude evolution during the maneuver.

Imposed CAM

As can be seen in Fig. 4.4, in all the cases analyzed the contribution due to the SK maneuver is always sufficient to respect the PoC constraint. To verify the ability of the algorithm in a situation in which the station-keeping contribution is not sufficient, or brings the spacecraft even nearer the secondary object. The position of the latter is changed in order to match the position reached by the primary object in the minimum cost maneuver at TCA. During this procedure all the other data presented in Sect. 4.3.1 remains the same.

Let's start by looking at the position of the primary object after the new maneuver at TCA. Figure 4.10 shows that, although the position of the bang-bang solution is slightly different from the one provided by the EOP maneuver, they both lie on the ellipse of PoC limit.

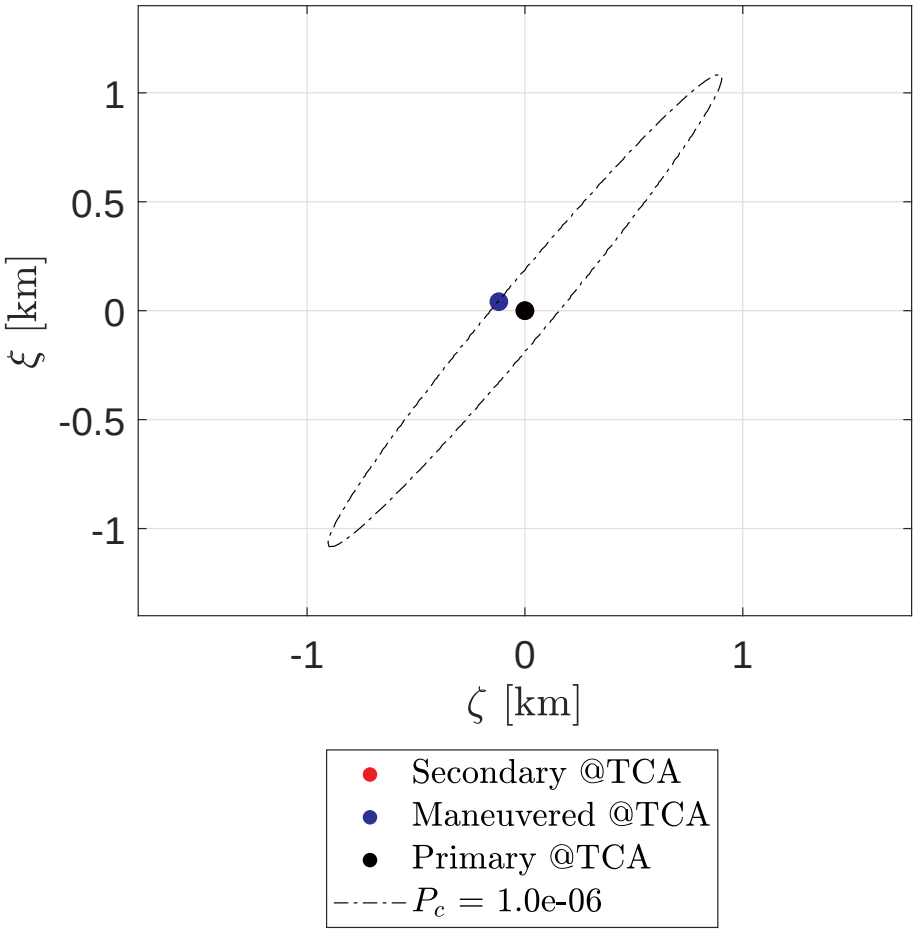

(a) Analytic.

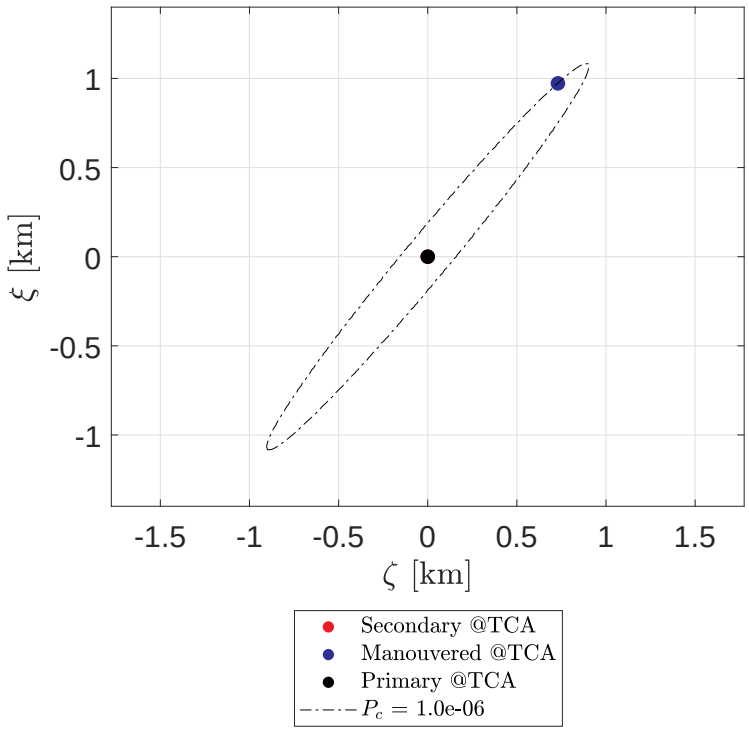

(b) Bang-bang.

Figure 4.10: B-plane position for the CAM maneuver.

Then, even in this case, it can be seen the difference between the analytical acceleration profile and the correspondent bang-bang transformation (Fig. 4.11).

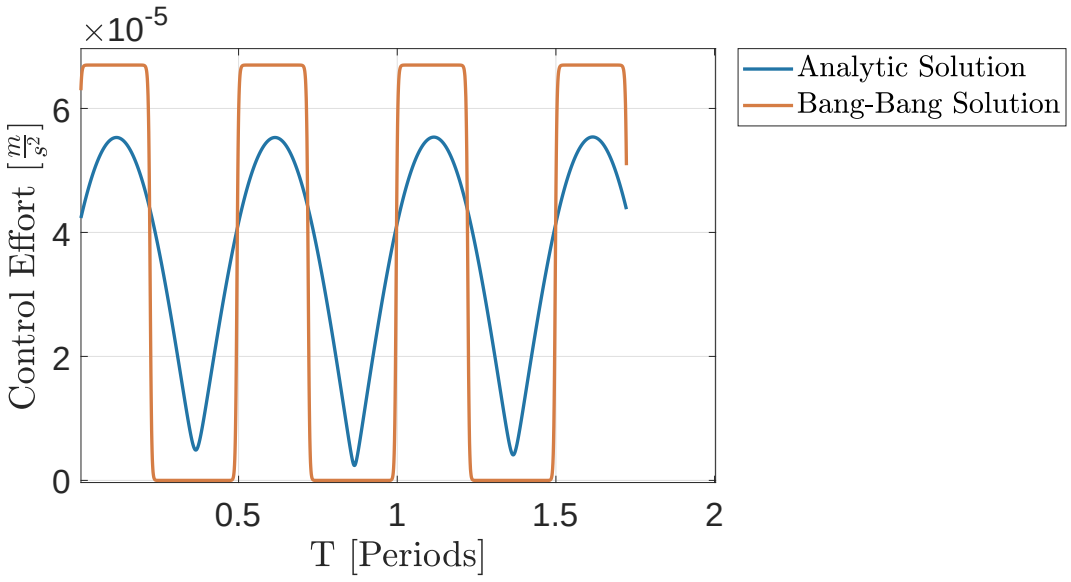

Figure 4.11: Comparison of analytic acceleration profile and FOP solution.

4.3.3. Numerical Target

The previous procedures is adopted even for the case of the numerical optimized targets. As before it is possible to represent the analytic position in B-plane for the various cases analyzed and the resulting transfer cost.

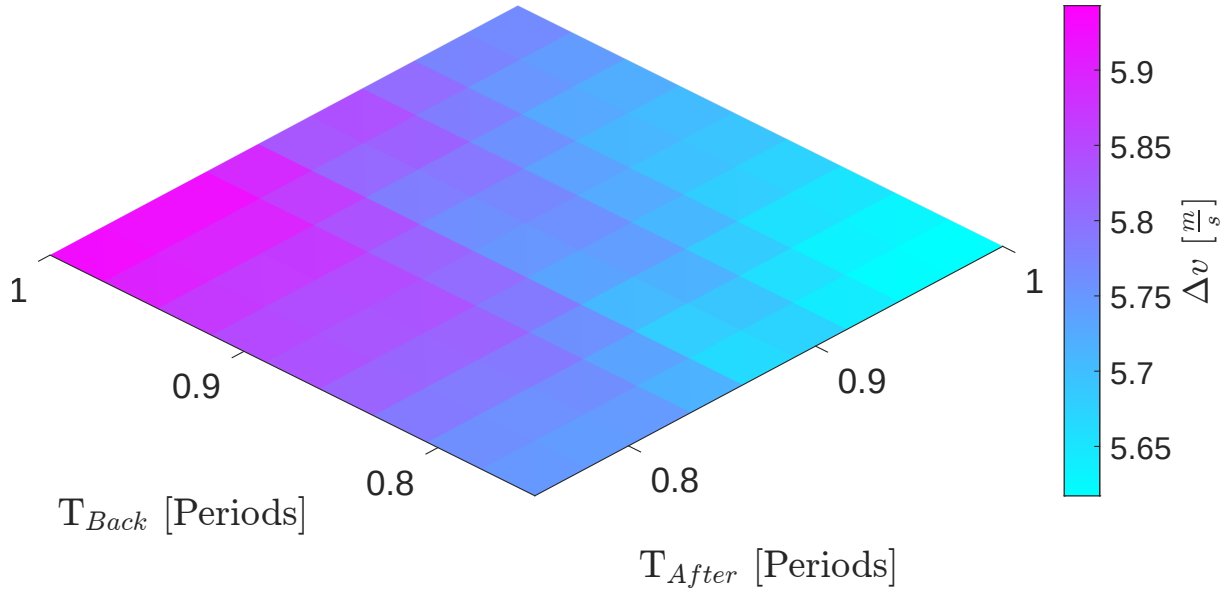

(a) Analytic Δv magnitude.

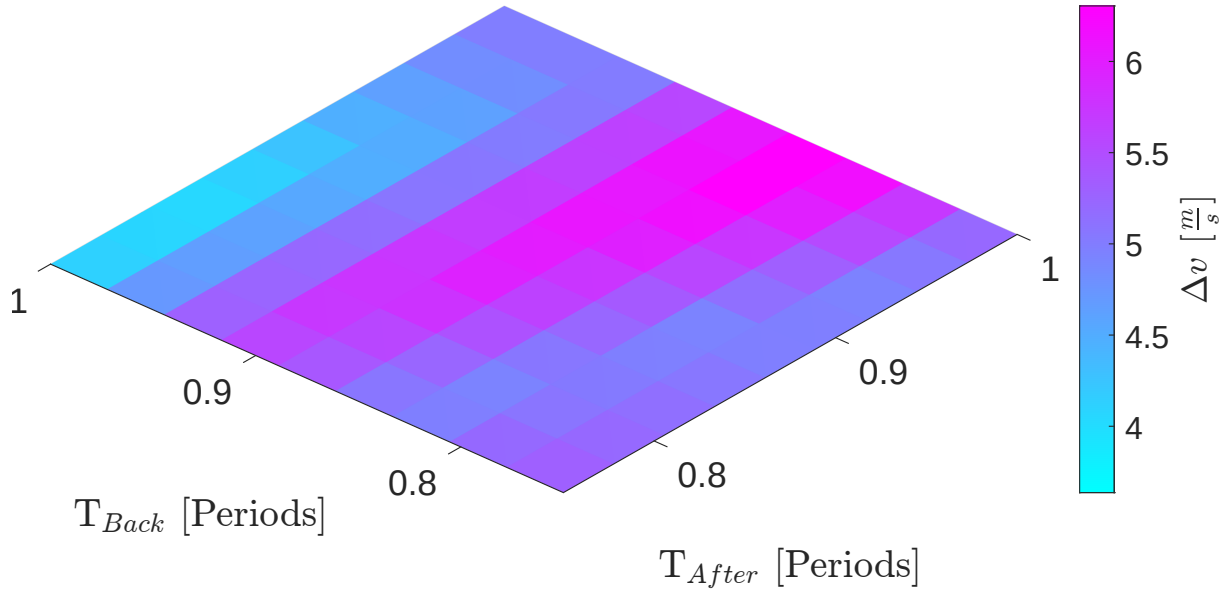

(b) Bang-bang Δv magnitude.

Figure 4.11: Δv results from FOP and EOP solutions.

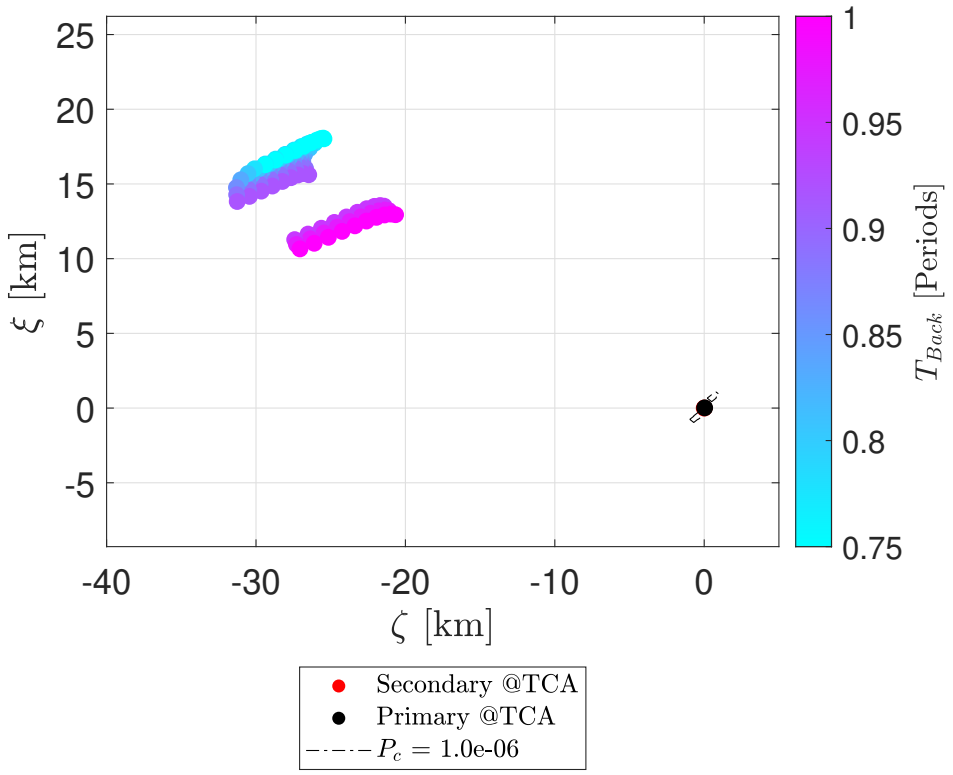

(c) First trajectory arc.

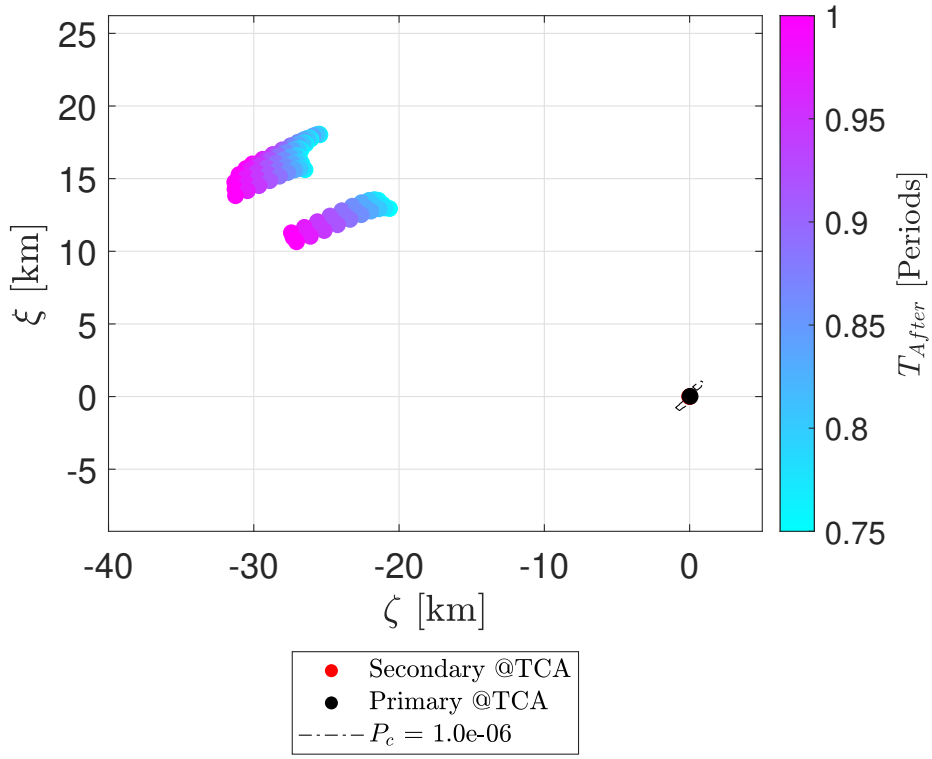

(d) Second trajectory arc.

Figure 4.12: Position of the primary object, achieved with the analytic solution, and represented in b-plane for the various values of the first and the second trajectory arc.

4.3.4. Minimum Δv Maneuver

The transfer with minimum cost is obtained with the following target:

Table 4.4: Numerical target.

a [km]	e_x	e_y	i_x	i_y	l_m [deg]
42 167.18	-1·10^{-4}	-1.1346·10^{-7}	-4.4491·10^{-6}	-6.3195·10^{-4}	358.87

The comparison between the two acceleration profiles is represented in Fig. 4.13

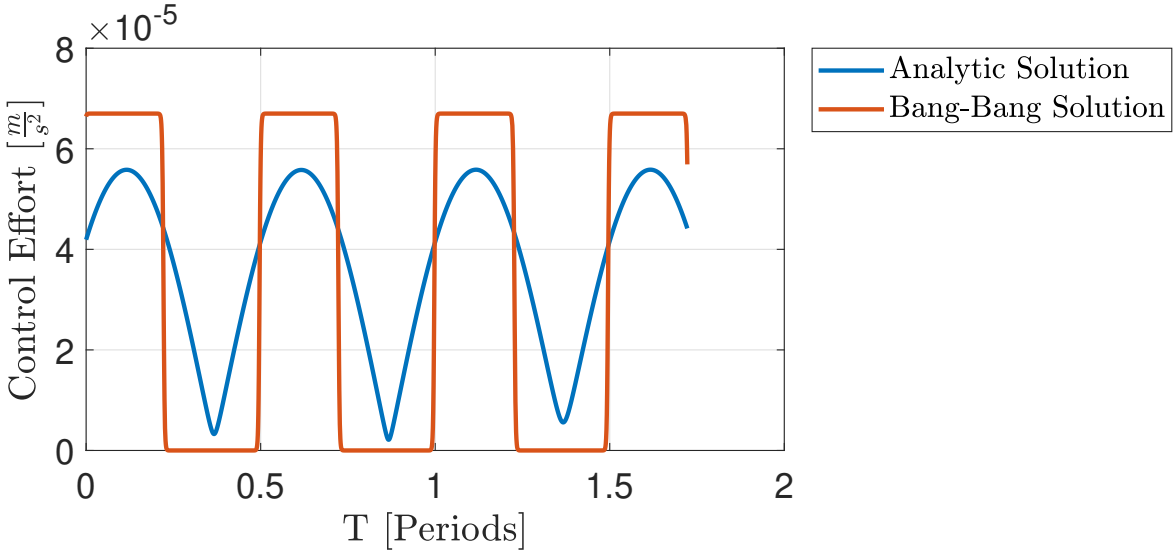

Figure 4.13: Comparison of analytic acceleration profile and FOP solution.

It is possible to notice that the results obtained from the numerical targeting are very similar to the one of Sec. 4.3.2. This confirms the validity of the elements computed with an analytical framework.

5 | Conclusions and Future Developments

This chapter deals with the conclusion and further developments. In particular, in Sect. 5.1 the achieved objectives of this work are presented, whereas in Sect. 5.2 some suggestions for future works are proposed.

5.1. Conclusions

The maneuver proposed in Sec. 3.1 of this thesis work started from an already existing control strategy, which has been extended including the spacecraft injection back into the nominal orbit.
In this case, the dynamical model used does not include the effect of any perturbations. The optimization of the maneuver is done by extending the optimal control problem to the reentry phase and by settling as PoC constraint an interior point one. In this way, the two trajectory segments can be seen as a unique path from the initial maneuvering point to the imposed final point. As evident from the graphs, the control action required by the analytic solution does not have a uniform shape. However, it does not affect the possibility to realize the transformation to a FOP with a bang-bang structure.

The CAM proposed in Sect. 3.4 has the objective of improving the performance in terms of computational effort and maneuver cost compared to the previous control problem. This is done by reducing the number of constraints, leaving free the final true anomaly and fixing only the return on the nominal orbit. The procedure is realized again by adopting Keplerian dynamics; however, in this case, the state variables used are the orbital elements instead of cartesian position and velocity. This allows for an easier mathematical formulation of the constraints, at the cost of more complex dynamical equations. The results shows a saving in the Δv compared to the previous maneuver for all the transfers analyzed with a very small variation on the final true anomaly. Moreover, the shape of the acceleration profiles obtained is more regular than before. Consequently, the FOP transformation turns out to be less cumbersome reducing the computational time.

Finally, in Chapter 4, a combined strategy of SK and CAM for a spacecraft in geostationary orbit is investigated. Basically, the maneuver is represented by an adaptation of the first one presented in this thesis work, in which the final state is computed in order to maximize the resident time inside the SK box. The optimal control problem is computed by adopting as state variables the equinoctial orbital elements that allow to menage easily the latitude and the longitude. Particular attention is devoted to the longitudinal behavior; consequently, the dynamical model adopted includes the geopotential perturbation until the j_{22} term. The target elements are computed both with an analytical strategy, that takes into consideration only the ballistic motion of the longitude due to the geopotential effect, and with an optimization procedure that has the objective to maximize the resident time. In both cases, for all the transfers analyzed the EOP and FOP problems are solved. However, due to the high variation of the maximum thrust needed for different values of the transfer time, the bang-bang transformation can be ineffective for what concerns fuel consumption savings.

In all the maneuvers analyzed, the computational times required are compatible with an onboard implementation. In particular, if the procedure adopted considers analyzing all the cases with the analytical procedure and realizes the FOP transformation only for the minimum Δv maneuver, the total computational time is restricted to a few minutes.

5.2. Further Developments

In this subsection, some suggestions for future developments are proposed. In particular:

- The bang-bang transformation leads to a reduction in the resolution of the maneuver cost due to the fixed level of acceleration available. In order to perform a more effective algorithm, the possibility to restrict the time window of the maneuvers in a particular range based on the level of the onboard thrust should be investigated.
- The possibility to realize the FOP with an analytic procedure should be taken into consideration.
- For all the analyzed cases, the satellite trajectory violates the station-keeping box during the execution of the maneuvers. One possible solution could be the implementation of the proposed methods by adding path constraints.
- The method developed here could be extended to other orbital regimes, e.g. the cislunar environment.
- In the last chapter, the dynamical model considered in this thesis work embeds a

second-order geopotential contribution (J_{22}). However, there is the possibility to increase the approximation order. Moreover, other perturbation contributions can be added: Solar Radiation Pressure and Soli-Lunar gravitational perturbations.

- The linear approximation of the dynamics can be overcome by employing differential algebra, increasing the accuracy of the method in describing the reality and the capacity to plan the maneuver sooner.
- One research topic could be the implementation of analytical multi-impulsive strategies.

Bibliography

[1] M. R. Akella and K. T. Alfriend. Probability of collision between space objects. *Journal of Guidance, Control, and Dynamics*, 23(5):769–772, Sept. 2000. doi: 10.2514/2.4611. URL https://doi.org/10.2514/2.4611.

[2] R. Armellin. Github, https://github.com/arma1978/conjunction/.

[3] A. E. Bryson. *Applied optimal control: optimization, estimation and control*. CRC Press, 1975.

[4] A. Cantoni. Numerically efficient methods for low-thrust collision avoidance maneuver design in geo regime. Master's thesis, School of industrial and information engineering, Department of aerospace science and technology, Politecnico di Milano, Italy, 2022.

[5] F. K. Chan et al. *Spacecraft collision probability*. Aerospace Press El Segundo, CA, 2008.

[6] R. Deakin. Derivatives of the earth's potentials. *Geomatics Research Australasia*, pages 31–60, 1998.

[7] ESA. Space debris problem, 2022. URL https://www.esa.int/Safety_Security/Space_Debris/The_current_state_of_space_debris.

[8] ESA. Ssa programme overview, 2022. URL https://www.esa.int/Safety_Security/SSA_Programme_overview.

[9] C. C. for Space Data System. Conjunction data message. CCSDS 508.0-B-1, Blue Book, 2013.

[10] C. Gazzino. Dynamics of a Geostationary Satellite. (Rapport LAAS n° 17432), Nov. 2017. URL https://hal.archives-ouvertes.fr/hal-01644934.

[11] C. Gazzino, D. Arzelier, L. Cerri, D. Losa, C. Louembet, and C. Pittet. A three-step decomposition method for solving the minimum-fuel geostationary station keeping of satellites equipped with electric propulsion. *Acta Astronautica*, 2019.

[12] J. Gonzalo Gomez, C. Colombo, and P. Di Lizia. A semi-analytical approach to low-thrust collision avoidance manoeuvre design. In *70th International Astronautical Congress (IAC 2019)*, pages 1–9, 2019.

[13] L. Hall. The history of space debris. *Embry-Riddle Aeronautical University Scholarly Commons*, 2014.

[14] J. Hernando-Ayuso and C. Bombardelli. Low-thrust collision avoidance in circular orbits. *Journal of Guidance, Control, and Dynamics*, pages 1–13, 2021.

[15] S.-C. Lee, H.-D. Kim, and J. Suk. Collision avoidance maneuver planning using ga for leo and geo satellite maintained in keeping area. *International Journal of Aeronautical and Space Sciences*, 13:474–483, 2012.

[16] LESICS. How do satellites work?, 2022. URL `https://www.lesics.com/how-do-satellites-work.html`.

[17] D. Losa, M. Lovera, R. Drai, T. Dargent, and J. Amalric. Electric station keeping of geostationary satellites: a differential inclusion approach. pages 7484 – 7489, 01 2006. doi: 10.1109/CDC.2005.1583369.

[18] Martínez Chamarro, C. Belmonte Hernandez, and R. Armellin. Design of collision avoidance maneuvers using optimal control theory and convex optimization. *31st Space Flight Mechanics Meeting*, 2021.

[19] K. Merz, B. B. Virgili, V. Braun, T. Flohrer, Q. Funke, H. Krag, S. Lemmens, and J. Siminski. Current collision avoidance service by esa's space debris office. In *7th European Conference on Space Debris, Darmstadt, Germany*, pages 18–21, 2017.

[20] M. F. Montaruli. Collision risk assessment and collision avoidance maneuver planning. Master's thesis, School of industrial and information engineering, Department of aerospace science and technology, Politecnico di Milano, Italy, 2019.

[21] A. Morselli, R. Armellin, P. Di Lizia, and F. Bernelli-Zazzera. Collision avoidance maneuver design based on multi-objective optimization. *Advances in the Astronautical Sciences*, 152(4):1819–1838, 2014.

[22] M. F. Palermo. Numerically efficient methods for impulsive and low-thrust collision avoidance manoeuvre design. Master's thesis, School of industrial and information engineering, Department of aerospace science and technology, Politecnico di Milano, Italy, 2021.

[23] M. Rasotto, R. Armellin, and P. Di Lizia. Multi-step optimization strategy for fuel-

optimal orbital transfer of low-thrust spacecraft. *Engineering Optimization*, 48(3): 519–542, 2016.

[24] J. A. Reiter and D. B. Spencer. Solutions to rapid collision-avoidance maneuvers constrained by mission performance requirements. *Journal of Spacecraft and Rockets*, 55(4):1040–1048, 2018.

[25] G. Salemme, P. Di Lizia, and R. Armellin. Continuous- thrust collision avoidance manoeuvres optimization. In *AIAA Scitech 2020 Forum*, 2020. doi: 10.2514/6.2020-0231.

[26] N. Sánchez-Ortiz, M. Belló-Mora, and H. Klinkrad. Collision avoidance manoeuvres during spacecraft mission lifetime: Risk reduction and required ΔV. *Advances in Space Research*, 38(9):2107–2116, Jan. 2006. doi: 10.1016/j.asr.2005.07.054. URL `https://doi.org/10.1016/j.asr.2005.07.054`.

[27] T. Schildknecht, M. Ploner, and U. Hugentobler. The search for debris in GEO. *Advances in Space Research*, 28(9):1291–1299, Jan. 2001. doi: 10.1016/s0273-1177(01)00399-4. URL `https://doi.org/10.1016/s0273-1177(01)00399-4`.

[28] E. Soop. Handbook of geostationary orbits. 1994.

[29] E. Taheri and J. L. Junkins. Generic smoothing for optimal bang-off-bang spacecraft maneuvers. *Journal of Guidance, Control, and Dynamics*, 41(11):2470–2475, 2018.

[30] T. Uriot, D. Izzo, L. Simoes, R. Abay, N. Einecke, S. Rebhan, J. Martinez-Heras, F. Letizia, J. Siminski, and K. Merz. Spacecraft collision avoidance challenge: design and results of a machine learning competition. *arXiv preprint arXiv:2008.03069*, 2020.

A | Appendix A

A.0.1. Problem Formulation

This appendix reports the detailed demonstration of the EOP reported in Sect. 3.1.2.

$$J := \nu\Psi(t_{ca}, \mathbf{x}(t_{ca})) + \int_{t_i}^{t_f} \frac{1}{2}\mathbf{a_c}^T\mathbf{a_c}dt \tag{A.1}$$

Where:

$$\Psi(t_{ca}, \mathbf{x}(t_{ca})) = SMD(\mathbf{r}(t_{ca})) - \overline{SMD} \geq 0 \tag{A.2}$$

The objective function can be rewritten by introducing the Hamiltonian:

$$H := \frac{1}{2}\mathbf{a_c}^T\mathbf{a_c} + \boldsymbol{\lambda}^T\mathbf{f}(\mathbf{x}, \mathbf{a_c}) \tag{A.3}$$

$$J := \nu\Psi(t_{ca}, \mathbf{x}(t_{ca})) + \int_{t_i}^{t_f} \frac{1}{2}\mathbf{a_c}^T\mathbf{a_c} + \boldsymbol{\lambda}^T\left[\mathbf{f}(\mathbf{x}, \mathbf{a_c}) - \dot{\mathbf{x}}\right] dt \tag{A.4}$$

In which: $\boldsymbol{\lambda}^T\dot{\mathbf{x}} = -\dot{\boldsymbol{\lambda}}^T\mathbf{x} + \frac{d(\boldsymbol{\lambda}^T\mathbf{x})}{dt}$

Splitting the integral it is possible to apply the necessary condition as described in 2.7.1:

$$\begin{aligned} J :=& \nu\Phi(t_{ca}, \mathbf{x}(t_{ca})) - \boldsymbol{\lambda}^T\mathbf{x}|_{t_i}^{t_{ca}^-} - \boldsymbol{\lambda}^T\mathbf{x}|_{t_{ca}^+}^{t_f} + \int_{t_i}^{t_{ca}^-} H(\mathbf{x}, \mathbf{a_c}, \boldsymbol{\lambda}, t) + \dot{\boldsymbol{\lambda}}^T\mathbf{x}dt \\ &+ \int_{t_{ca}^+}^{t_f} H(\mathbf{x}, \mathbf{a_c}, \boldsymbol{\lambda}, t) + \dot{\boldsymbol{\lambda}}^T\mathbf{x}dt \end{aligned} \tag{A.5}$$

$$\frac{\partial J}{\partial \eta} = \nu\frac{\partial \Psi}{\partial \tilde{\mathbf{x}}(t_{ca})}\frac{\partial \tilde{\mathbf{x}}(t_{ca})}{\partial \eta} - \boldsymbol{\lambda}^T\frac{\partial \tilde{\mathbf{x}}}{\partial \eta}\Big|_{t_i}^{t_{ca}^-} - \boldsymbol{\lambda}^T\frac{\partial \tilde{\mathbf{x}}}{\partial \eta}\Big|_{t_{ca}^+}^{t_f} + \int_{t_i}^{t_f} \frac{\partial H}{\partial \widetilde{\mathbf{a_c}}}\frac{\partial \widetilde{\mathbf{a_c}}}{\partial \eta} + \frac{\partial H}{\partial \tilde{\mathbf{x}}}\frac{\partial \tilde{\mathbf{x}}}{\partial \eta} + \dot{\boldsymbol{\lambda}}^T\frac{\partial \tilde{\mathbf{x}}}{\partial \eta}dt = 0 \tag{A.6}$$

The application of the necessary condition brings to a system of differential and algebraic equations:

$$\begin{cases} \nu \dfrac{\partial \Psi}{\partial \mathbf{x}(t_{ca})} - \boldsymbol{\lambda}^T(t_{ca}^-) + \boldsymbol{\lambda}^T(t_{ca}^+) = 0 \\ \left.\dfrac{\partial \mathbf{x}}{\partial \eta}\right|_{t_i} = 0 \\ \left.\dfrac{\partial \mathbf{x}}{\partial \eta}\right|_{t_f} = 0 \\ \dfrac{\partial H}{\partial \mathbf{a_c}} = \mathbf{a_c} + \boldsymbol{\lambda}_v = 0 \Longrightarrow \mathbf{a_c} = -\boldsymbol{\lambda}_v \\ \dfrac{\partial H}{\partial \mathbf{x}} + \dot{\boldsymbol{\lambda}}^T = 0 \Longrightarrow \dot{\boldsymbol{\lambda}} = -\left[\dfrac{\partial H}{\partial \mathbf{x}}\right]^T = -\left[\dfrac{\partial \mathbf{f}}{\partial \mathbf{x}}\right]^T \boldsymbol{\lambda} \\ \dfrac{\partial H}{\partial \boldsymbol{\lambda}} = \dot{\mathbf{x}} = \mathbf{f}(\mathbf{x}, \mathbf{a_c}) \\ \nu \geq 0 \\ \nu \Psi = 0 \end{cases} \tag{A.7}$$

Where:

$$\left[\frac{\partial \mathbf{f}}{\partial \tilde{\mathbf{x}}}\right] = \begin{bmatrix} \mathbf{0_{3\times 3}} & \mathbf{I_{3\times 3}} \\ \frac{3\mu}{r^5}\mathbf{r}\mathbf{r}^T - \frac{\mu}{r^3}\mathbf{I_{3\times 3}} & \mathbf{0_{3\times 3}} \end{bmatrix} \tag{A.8}$$

Solving the algebraic equation of the control acceleration as function of the co-state it is possible to obtain the following ThPBVP:

$$\begin{cases} \dot{\mathbf{r}} = \mathbf{v} \\ \dot{\mathbf{v}} = -\dfrac{mu}{r^3}\mathbf{r} - \boldsymbol{\lambda}_v \\ \dot{\boldsymbol{\lambda}}_r = \dfrac{\mu}{r^3}\boldsymbol{\lambda}_v - \dfrac{3\mu \mathbf{r}^T \boldsymbol{\lambda}_v}{r^5}\mathbf{r} \\ \dot{\boldsymbol{\lambda}}_v = -\boldsymbol{\lambda}_r \end{cases} \qquad BCs: \begin{cases} \mathbf{x}(t_0) = \mathbf{x_0} \\ \mathbf{x}(t_{ca^-}) = \mathbf{x}(t_{ca^+}) \\ \nu \dfrac{\partial \Psi}{\partial \tilde{\mathbf{x}}(t_{ca})} - \boldsymbol{\lambda}^T(t_{ca}^-) + \boldsymbol{\lambda}^T(t_{ca}^+) = 0 \\ \mathbf{x}(t_f) = \mathbf{x_f} \\ \Psi(t_{ca}) = 0 \end{cases} \tag{A.9}$$

A.0.2. EOP Solution: Single Linearization

In the previous section, the OCP is transformed into the problem of finding the initial co-state and the adjoined multiplicator. The resolution procedure requires to subdivide the trajectory in two segments in the intervals $[t_1; t_{ca}]$ and $[t_{ca}; t_f]$. This step is necessary to apply the interior point constraint. To obtain an analytical solution the two trajectories have to be linearized with respect to the Keplerian unperturbed motion by virtue of the STM.

$$\begin{cases} \dot{\mathbf{\Phi}}(t) = \mathbf{A}(t)\mathbf{\Phi}(\mathbf{x}(t_0), t) \\ \mathbf{\Phi}(\mathbf{x}(t_0), t_0) = \mathbf{I} \end{cases} \tag{A.10}$$

Where:

$$\mathbf{A} = \begin{bmatrix} \mathbf{0_{3\times3}} & \mathbf{I_{3\times3}} & \mathbf{0_{3\times3}} & \mathbf{0_{3\times3}} \\ \frac{3\mu}{r^5}\mathbf{r}\mathbf{r}^T - \frac{\mu}{r^3}\mathbf{I_{3\times3}} & \mathbf{0_{3\times3}} & \mathbf{0_{3\times3}} & -\mathbf{I_{3\times3}} \\ \mathbf{0_{3\times3}} & \mathbf{0_{3\times3}} & \mathbf{0_{3\times3}} & \frac{\mu}{r^3}\mathbf{I_{3\times3}} - \frac{3\mu}{r^5}\mathbf{r}\mathbf{r}^T \\ \mathbf{0_{3\times3}} & \mathbf{0_{3\times3}} & -\mathbf{I_{3\times3}} & \mathbf{0_{3\times3}} \end{bmatrix}$$

First Trajectory Arc

The linearization of the first arc brings to the following system of vectorial equations:

$$\begin{bmatrix} \boldsymbol{\delta}\mathbf{r_{ca}} \\ \boldsymbol{\delta}\mathbf{v_{ca}} \\ \boldsymbol{\delta\lambda}^-_{r_{ca}} \\ \boldsymbol{\delta\lambda}^-_{v_{ca}} \end{bmatrix} = \begin{bmatrix} \mathbf{\Phi_{11}} & \mathbf{\Phi_{12}} & \mathbf{\Phi_{13}} & \mathbf{\Phi_{14}} \\ \mathbf{\Phi_{21}} & \mathbf{\Phi_{22}} & \mathbf{\Phi_{23}} & \mathbf{\Phi_{24}} \\ \mathbf{\Phi_{31}} & \mathbf{\Phi_{32}} & \mathbf{\Phi_{33}} & \mathbf{\Phi_{34}} \\ \mathbf{\Phi_{41}} & \mathbf{\Phi_{42}} & \mathbf{\Phi_{43}} & \mathbf{\Phi_{44}} \end{bmatrix} \begin{bmatrix} \boldsymbol{\delta}\mathbf{r_0} \\ \boldsymbol{\delta}\mathbf{v_0} \\ \boldsymbol{\delta\lambda}_{r_0} \\ \boldsymbol{\delta\lambda}_{v_0} \end{bmatrix} \tag{A.11}$$

The symbol δ for the co-state variables is not necessary because along the unmaneuvered trajectory they assume a null value. For this reason, the symbol is now on omitted for these variables. The first vectorial equation can be expressed considering that the initial state is fixed $\boldsymbol{\delta}\mathbf{r_0} = \boldsymbol{\delta}\mathbf{v_0} = 0$.

$$\boldsymbol{\delta}\mathbf{r_{ca}} = \mathbf{\Phi_{13}}\boldsymbol{\lambda}_{r_0} + \mathbf{\Phi_{14}}\boldsymbol{\lambda}_{v_0} \tag{A.12a}$$

$$\boldsymbol{\lambda}_{r_0} = \mathbf{\Phi}_{13}^{-1}\boldsymbol{\delta}\mathbf{r_{ca}} - \mathbf{\Phi}_{13}^{-1}\mathbf{\Phi_{14}}\boldsymbol{\lambda}_{v_0} \tag{A.12b}$$

Substituting the expression in the Eq. A.12b it is possible to express the initial velocity co-state as a function of the perturbation on the state at TCA:

$$\boldsymbol{\delta}\mathbf{v_{ca}} = \mathbf{\Phi_{23}}\boldsymbol{\lambda}_{r_0} + \mathbf{\Phi_{24}}\boldsymbol{\lambda}_{v_0} \tag{A.13a}$$

$$\boldsymbol{\delta}\mathbf{v_{ca}} = \mathbf{\Phi_{23}}\mathbf{\Phi}_{13}^{-1}\boldsymbol{\delta}\mathbf{r_{ca}} + [\mathbf{\Phi_{24}} - \mathbf{\Phi_{23}}\mathbf{\Phi}_{13}^{-1}\mathbf{\Phi_{14}}]\boldsymbol{\lambda}_{v_0} \tag{A.13b}$$

$$\boldsymbol{\lambda}_{v_0} = [\mathbf{\Phi_{24}} - \mathbf{\Phi_{23}}\mathbf{\Phi}_{13}^{-1}\mathbf{\Phi_{14}}]^{-1}\boldsymbol{\delta}\mathbf{v_{ca}} - [\mathbf{\Phi_{24}} - \mathbf{\Phi_{23}}\mathbf{\Phi}_{13}^{-1}\mathbf{\Phi_{14}}]^{-1}\mathbf{\Phi_{23}}\mathbf{\Phi}_{13}^{-1}\boldsymbol{\delta}\mathbf{r_{ca}} \tag{A.13c}$$

The previous expression can be simplified by collecting the matrices:

$$\boldsymbol{\lambda}_{v_0} = \mathbf{M}\boldsymbol{\delta}\mathbf{r_{ca}} + \mathbf{B}\boldsymbol{\delta}\mathbf{v_{ca}} \tag{A.14a}$$

$$\mathbf{M} = -[\boldsymbol{\Phi}_{24} - \boldsymbol{\Phi}_{23}\boldsymbol{\Phi}_{13}^{-1}\boldsymbol{\Phi}_{14}]^{-1}\boldsymbol{\Phi}_{23}\boldsymbol{\Phi}_{13}^{-1} \qquad \mathbf{B} = [\boldsymbol{\Phi}_{24} - \boldsymbol{\Phi}_{23}\boldsymbol{\Phi}_{13}^{-1}\boldsymbol{\Phi}_{14}]^{-1} \tag{A.14b}$$

Expression A.14a can be substituted in Eq. A.12b to express the initial position constraint as function of the position and velocity perturbation of the nominal trajectory at TCA:

$$\boldsymbol{\lambda}_{r_0} = [\boldsymbol{\Phi}_{13}^{-1} - \boldsymbol{\Phi}_{13}^{-1}\boldsymbol{\Phi}_{14}\mathbf{M}]\boldsymbol{\delta}\mathbf{r_{ca}} - \boldsymbol{\Phi}_{13}^{-1}\boldsymbol{\Phi}_{14}\mathbf{B}\boldsymbol{\delta}\mathbf{v_{ca}} \tag{A.15a}$$

$$\mathbf{D} = [\boldsymbol{\Phi}_{13}^{-1} - \boldsymbol{\Phi}_{13}^{-1}\boldsymbol{\Phi}_{14}\mathbf{M}] \qquad \mathbf{E} = -\boldsymbol{\Phi}_{13}^{-1}\boldsymbol{\Phi}_{14}\mathbf{B} \tag{A.15b}$$

Now the two Eqs. A.14a and A.15a can be replaced in the initial system to find the expression of the co-state at t_{CA^-} respect to the state perturbations at TCA:

$$\begin{cases} \boldsymbol{\lambda}_{r_{ca}}^{-} = [\boldsymbol{\Phi}_{33}\mathbf{D} + \boldsymbol{\Phi}_{34}\mathbf{M}]\boldsymbol{\delta}\mathbf{r_{ca}} + [\boldsymbol{\Phi}_{34}\mathbf{B} + \boldsymbol{\Phi}_{33}\mathbf{E}]\boldsymbol{\delta}\mathbf{v_{ca}} \\ \boldsymbol{\lambda}_{v_{ca}}^{-} = [\boldsymbol{\Phi}_{43}\mathbf{D} + \boldsymbol{\Phi}_{44}\mathbf{M}]\boldsymbol{\delta}\mathbf{r_{ca}} + [\boldsymbol{\Phi}_{44}\mathbf{B} + \boldsymbol{\Phi}_{43}\mathbf{E}]\boldsymbol{\delta}\mathbf{v_{ca}} \end{cases} \Longrightarrow \begin{cases} \boldsymbol{\lambda}_{r_{ca}}^{-} = \mathbf{F}\boldsymbol{\delta}\mathbf{r_{ca}} + \mathbf{G}\boldsymbol{\delta}\mathbf{v_{ca}} \\ \boldsymbol{\lambda}_{v_{ca}}^{-} = \mathbf{H}\boldsymbol{\delta}\mathbf{r_{ca}} + \mathbf{L}\boldsymbol{\delta}\mathbf{v_{ca}} \end{cases} \tag{A.16a}$$

$$\mathbf{F} = [\boldsymbol{\Phi}_{33}\mathbf{D} + \boldsymbol{\Phi}_{34}\mathbf{M}] \qquad \mathbf{G} = [\boldsymbol{\Phi}_{34}\mathbf{B} + \boldsymbol{\Phi}_{33}\mathbf{E}] \tag{A.16b}$$

$$\mathbf{H} = [\boldsymbol{\Phi}_{43}\mathbf{D} + \boldsymbol{\Phi}_{44}\mathbf{M}] \qquad \mathbf{L} = [\boldsymbol{\Phi}_{44}\mathbf{B} + \boldsymbol{\Phi}_{43}\mathbf{E}] \tag{A.16c}$$

Second Trajectory Arc

The resolution procedure continues by considering the second trajectory arc. The state variables and the velocity co-state are continuous at TCA; while the interior point constraints generate a discontinuity in the position co-state. The final target point is considered the one obtained with a Keplerian propagation. For this reason the perturbation on the final state needs to be assumed as: $\boldsymbol{\delta}\mathbf{r_f} = \boldsymbol{\delta}\mathbf{r_f} = 0$

$$\begin{bmatrix} \boldsymbol{\delta}\mathbf{r_f} \\ \boldsymbol{\delta}\mathbf{v_f} \\ \boldsymbol{\lambda}_{r_f} \\ \boldsymbol{\lambda}_{v_f} \end{bmatrix} = \begin{bmatrix} \boldsymbol{\Phi}_{11} & \boldsymbol{\Phi}_{12} & \boldsymbol{\Phi}_{13} & \boldsymbol{\Phi}_{14} \\ \boldsymbol{\Phi}_{21} & \boldsymbol{\Phi}_{22} & \boldsymbol{\Phi}_{23} & \boldsymbol{\Phi}_{24} \\ \boldsymbol{\Phi}_{31} & \boldsymbol{\Phi}_{32} & \boldsymbol{\Phi}_{33} & \boldsymbol{\Phi}_{34} \\ \boldsymbol{\Phi}_{41} & \boldsymbol{\Phi}_{42} & \boldsymbol{\Phi}_{43} & \boldsymbol{\Phi}_{44} \end{bmatrix} \begin{bmatrix} \boldsymbol{\delta}\mathbf{r_{ca}} \\ \boldsymbol{\delta}\mathbf{v_{ca}} \\ \boldsymbol{\lambda}_{r_{ca}}^{+} \\ \boldsymbol{\lambda}_{v_{ca}} \end{bmatrix} \tag{A.17}$$

It is possible to proceed as done in the previous section by writing down the first two vectorial equations:

$$\boldsymbol{\delta \mathbf{r}_{\mathbf{f}}} = \boldsymbol{\Phi_{11}} \boldsymbol{\delta \mathbf{r}_{\mathbf{ca}}} + \boldsymbol{\Phi_{12}} \boldsymbol{\delta \mathbf{v}_{\mathbf{ca}}} + \boldsymbol{\Phi_{13}} \boldsymbol{\lambda}^{+}_{r_{ca}} + \boldsymbol{\Phi_{14}} \boldsymbol{\lambda}_{v_{ca}} = 0 \tag{A.18a}$$

$$[\boldsymbol{\Phi_{11}} + \boldsymbol{\Phi_{14}} \mathbf{H}] \boldsymbol{\delta \mathbf{r}_{\mathbf{ca}}} + [\boldsymbol{\Phi_{12}} + \boldsymbol{\Phi_{14}} \mathbf{L}] \boldsymbol{\delta \mathbf{v}_{\mathbf{ca}}} + \boldsymbol{\Phi_{13}} \boldsymbol{\lambda}^{+}_{r_{ca}} = 0 \tag{A.18b}$$

$$\boldsymbol{\delta \mathbf{v}_{\mathbf{f}}} = \boldsymbol{\Phi_{21}} \boldsymbol{\delta \mathbf{r}_{\mathbf{ca}}} + \boldsymbol{\Phi_{22}} \boldsymbol{\delta \mathbf{v}_{\mathbf{ca}}} + \boldsymbol{\Phi_{23}} \boldsymbol{\lambda}^{+}_{r_{ca}} + \boldsymbol{\Phi_{24}} \boldsymbol{\lambda}_{v_{ca}} = 0 \tag{A.19a}$$

$$[\boldsymbol{\Phi_{21}} + \boldsymbol{\Phi_{24}} \mathbf{H}] \boldsymbol{\delta \mathbf{r}_{\mathbf{ca}}} + [\boldsymbol{\Phi_{22}} + \boldsymbol{\Phi_{24}} \mathbf{L}] \boldsymbol{\delta \mathbf{v}_{\mathbf{ca}}} + \boldsymbol{\Phi_{23}} \boldsymbol{\lambda}^{+}_{r_{ca}} = 0 \tag{A.19b}$$

Then it is necessary to recall the co-state discontinuity expressed in A.9 by substituting the expression of the SMD constraint derivative:

$$\boldsymbol{\lambda}^{+}_{r_{ca}} = \boldsymbol{\lambda}^{-}_{r_{ca}} - 2\nu \mathbf{R_{2b}}^{T} \mathbf{C}^{-1} \mathbf{R_{2b}} \boldsymbol{\delta \mathbf{r}^{\mathbf{m}}_{\mathbf{imp}}} \tag{A.20}$$

Where $\boldsymbol{\delta \mathbf{r}^{\mathbf{m}}_{\mathbf{imp}}} = \mathbf{r}^{\mathbf{m}}_{\mathbf{ca}} - \mathbf{r_s}$ is the position vector from the secondary object at TCA to the primary in cartesian coordinates.

Eq. A.20 and A.16a can be substituted in Eq. A.19b obtaining:

$$\mathbf{N} \boldsymbol{\delta \mathbf{r}_{\mathbf{ca}}} + \mathbf{P} \boldsymbol{\delta \mathbf{v}_{\mathbf{ca}}} - \nu \mathbf{Q} \mathbf{R_{2b}} \boldsymbol{\delta \mathbf{r}^{\mathbf{m}}_{\mathbf{imp}}} = 0 \tag{A.21a}$$

$$\mathbf{N} = [\boldsymbol{\Phi_{21}} + \boldsymbol{\Phi_{24}} \mathbf{H} + \boldsymbol{\Phi_{23}} \mathbf{F}] \qquad \mathbf{P} = [\boldsymbol{\Phi_{22}} + \boldsymbol{\Phi_{24}} \mathbf{L} + \boldsymbol{\Phi_{23}} \mathbf{G}] \qquad \mathbf{Q} = 2\boldsymbol{\Phi_{23}} \mathbf{R_{2b}}^{T} \mathbf{C}^{-1} \tag{A.21b}$$

The same procedure can be used for Eq. A.18b:

$$\tilde{\mathbf{N}} \boldsymbol{\delta \mathbf{r}_{\mathbf{ca}}} + \tilde{\mathbf{P}} \boldsymbol{\delta \mathbf{v}_{\mathbf{ca}}} - \nu \tilde{\mathbf{Q}} \mathbf{R_{2b}} \boldsymbol{\delta \mathbf{r}^{\mathbf{m}}_{\mathbf{imp}}} = 0 \tag{A.22a}$$

$$\tilde{\mathbf{N}} = [\boldsymbol{\Phi_{11}} + \boldsymbol{\Phi_{14}} \mathbf{H} + \boldsymbol{\Phi_{13}} \mathbf{F}] \qquad \tilde{\mathbf{P}} = [\boldsymbol{\Phi_{12}} + \boldsymbol{\Phi_{14}} \mathbf{L} + \boldsymbol{\Phi_{13}} \mathbf{G}] \qquad \tilde{\mathbf{Q}} = 2\boldsymbol{\Phi_{13}} \mathbf{R_{2b}}^{T} \mathbf{C}^{-1} \tag{A.22b}$$

Eq. A.21 can be solved for $\boldsymbol{\delta \mathbf{v}_{\mathbf{ca}}}$ and substituted in Eq. A.22 in order to find the expression of $\boldsymbol{\delta \mathbf{r}_{\mathbf{ca}}}$ as function of the position vector $\boldsymbol{\delta \mathbf{r}^{\mathbf{m}}_{\mathbf{imp}}}$ and the multiplier ν:

$$\boldsymbol{\delta \mathbf{r}_{\mathbf{ca}}} = \nu \mathbf{S}^{-1} \mathbf{T} \mathbf{R_{2b}} \boldsymbol{\delta \mathbf{r}^{\mathbf{m}}_{\mathbf{imp}}} \tag{A.23a}$$

$$\mathbf{S} = [\tilde{\mathbf{N}} - \tilde{\mathbf{P}}\mathbf{P}^{-1}\mathbf{N}] \qquad \mathbf{T} = [\tilde{\mathbf{Q}} - \tilde{\mathbf{P}}\mathbf{P}^{-1}\mathbf{Q}] \tag{A.23b}$$

SMD Constraint

To find an analytic solution of the problem, it is necessary to apply the SMD constraint at TCA. This can be done by adding and subtracting $\mathbf{r_s}$ on the left term and premultipling Eq. A.23a by $\mathbf{R_{2b}}$. This allows to transfer the problem in B-plane reducing the dimension of the equation.

$$\mathbf{R_{2b}}[\mathbf{r^m_{ca}} - \mathbf{r_s} - \mathbf{r_{ca}} + \mathbf{r_s}] = \nu\mathbf{R_{2b}}\mathbf{S}^{-1}\mathbf{T}\mathbf{R_{2b}}\boldsymbol{\delta}\mathbf{r^m_{imp}} \tag{A.24a}$$

$$\mathbf{R_{2b}}[\boldsymbol{\delta}\mathbf{r^m_{imp}} - \boldsymbol{\delta}\mathbf{r_{imp}}] = \nu\mathbf{R_{2b}}\mathbf{S}^{-1}\mathbf{T}\mathbf{R_{2b}}\boldsymbol{\delta}\mathbf{r^m_{imp}} \tag{A.24b}$$

$$\mathbf{b^m_{imp}} - \mathbf{b_{imp}} = \nu\mathbf{R_{2b}}\mathbf{S}^{-1}\mathbf{T}\mathbf{b^m_{imp}} \tag{A.24c}$$

The previous equation can be inverted to obtain the expression of the maneuvered position vector in B-plane.

$$\mathbf{b^m_{imp}} = [\mathbf{I} - \nu\mathbf{U}]^{-1}\mathbf{b_{imp}} \tag{A.25a}$$

$$\mathbf{U} = \mathbf{R_{2b}}\mathbf{S}^{-1}\mathbf{T} \tag{A.25b}$$

Finally by using the following relation:

$$[\mathbf{I} - \nu\mathbf{U}]^{-1} = \frac{1}{det(\mathbf{I} - \nu\mathbf{U})}[\mathbf{I} - \nu det(\mathbf{U})\mathbf{U}^{-1}] \tag{A.26}$$

And applying the constraint on the SMD; it is possible to obtain a fourth-degree-equation that can be solved analytically as function of ν:

$$\nu^2\mathbf{b_{imp}}^T\mathbf{Z}^T\mathbf{C}^{-1}\mathbf{Z}\mathbf{b_{imp}} - \nu\mathbf{b_{imp}}^T[\mathbf{Z}^T\mathbf{C}^{-1} + \mathbf{C}^{-1}\mathbf{Z}]\mathbf{b_{imp}} = \alpha^2\overline{SMD} - \mathbf{b_{imp}}^T\mathbf{C}^{-1}\mathbf{b_{imp}} \tag{A.27a}$$

$$\alpha = det(\mathbf{I} - \nu\mathbf{U}) \qquad \mathbf{Z} = det(\mathbf{U})\mathbf{U}^{-1} \tag{A.27b}$$

A.0.3. EOP Solution: Iterative Linearizations

The analysis of the first trajectory arc is the same as the first linearization and brings to an analogous system of equations:

$$\begin{bmatrix} \boldsymbol{\delta r_{ca}} \\ \boldsymbol{\delta v_{ca}} \\ \boldsymbol{\delta \lambda_{r_{ca-}}} \\ \boldsymbol{\delta \lambda_{v_{ca-}}} \end{bmatrix} = \begin{bmatrix} \boldsymbol{\Phi_{11}} & \boldsymbol{\Phi_{12}} & \boldsymbol{\Phi_{13}} & \boldsymbol{\Phi_{14}} \\ \boldsymbol{\Phi_{21}} & \boldsymbol{\Phi_{22}} & \boldsymbol{\Phi_{23}} & \boldsymbol{\Phi_{24}} \\ \boldsymbol{\Phi_{31}} & \boldsymbol{\Phi_{32}} & \boldsymbol{\Phi_{33}} & \boldsymbol{\Phi_{34}} \\ \boldsymbol{\Phi_{41}} & \boldsymbol{\Phi_{42}} & \boldsymbol{\Phi_{43}} & \boldsymbol{\Phi_{44}} \end{bmatrix} \begin{bmatrix} \boldsymbol{\delta r_0} \\ \boldsymbol{\delta v_0} \\ \boldsymbol{\delta \lambda_{r_0}} \\ \boldsymbol{\delta \lambda_{v_0}} \end{bmatrix} \tag{A.28}$$

It is important to notice that in this case the Symbol δ for the co-state variables can't be omitted. In fact, the successive linearizations are performed respect to the maneuvered trajectory which has a non-null co-state.

Second Trajectory Arc

In this case, the linearization produces rather different results compared to the previous case. The principal modifications are due to two reasons. The first one is the consideration of a perturbation on the final state that is not present in the first linearization. This perturbation needs to be included in order to correct the state error obtained at the end of the previous iteration. The second reason that brings to different equations lies in the definition of co-state discontinuity due to interior point constraint. If we consider the discontinuity expression in the general iteration:

$$\boldsymbol{\delta \lambda_{r_{ca+}}} = \boldsymbol{\lambda^{k+1}_{r_{ca+}}} - \boldsymbol{\lambda^{k}_{r_{ca+}}} \tag{A.29}$$

Where k indicates the number of iterations already executed. Recalling Eq. 3.13:

$$\boldsymbol{\lambda^{k+1}_{r_{ca+}}} - \boldsymbol{\lambda^{k}_{r_{ca+}}} = \boldsymbol{\lambda^{k+1}_{r_{ca-}}} - \boldsymbol{\lambda^{k}_{r_{ca-}}} - 2\nu \mathbf{R_{2b}}^T \mathbf{C}^{-1} \mathbf{R_{2b}} (\mathbf{r^{m\,k+1}_{ca}} - \mathbf{r_s} - \mathbf{r^{m\,k}_{ca}} + \mathbf{r_s}) \tag{A.30}$$

That can be expressed as:

$$\boldsymbol{\delta \lambda^{+}_{r_{ca}}} = \boldsymbol{\delta \lambda^{-}_{r_{ca}}} - 2\nu \mathbf{R_{2b}}^T \mathbf{C}^{-1} \mathbf{R_{2b}} \boldsymbol{\delta r^{m}_{ca}} \tag{A.31}$$

The difference respect to the previous case is that the constraint perturbation is no longer expressed as a function of the position of the secondary object at TCA. Then the resolution proceeds as in the previous case with the only difference of the non-null final state perturbation. From the STM it is possible to obtain the expression of the perturbation

on the state at TCA following a procedure similar to the one reported before.

$$\begin{bmatrix} \boldsymbol{\delta r_f} \\ \boldsymbol{\delta v_f} \\ \boldsymbol{\delta \lambda_{r_f}} \\ \boldsymbol{\delta \lambda_{v_f}} \end{bmatrix} = \begin{bmatrix} \boldsymbol{\Phi_{11}} & \boldsymbol{\Phi_{12}} & \boldsymbol{\Phi_{13}} & \boldsymbol{\Phi_{14}} \\ \boldsymbol{\Phi_{21}} & \boldsymbol{\Phi_{22}} & \boldsymbol{\Phi_{23}} & \boldsymbol{\Phi_{24}} \\ \boldsymbol{\Phi_{31}} & \boldsymbol{\Phi_{32}} & \boldsymbol{\Phi_{33}} & \boldsymbol{\Phi_{34}} \\ \boldsymbol{\Phi_{41}} & \boldsymbol{\Phi_{42}} & \boldsymbol{\Phi_{43}} & \boldsymbol{\Phi_{44}} \end{bmatrix} \begin{bmatrix} \boldsymbol{\delta r_{ca}} \\ \boldsymbol{\delta v_{ca}} \\ \boldsymbol{\delta \lambda_{r_{ca+}}} \\ \boldsymbol{\delta \lambda_{v_{ca}}} \end{bmatrix} \tag{A.32}$$

Analyzing first two vectorial equations in which $\boldsymbol{\delta r_f}$ and $\boldsymbol{\delta v_f}$ are known:

$$\boldsymbol{\delta r_f} = \boldsymbol{\Phi_{11}} \boldsymbol{\delta r_{ca}} + \boldsymbol{\Phi_{12}} \boldsymbol{\delta v_{ca}} + \boldsymbol{\Phi_{13}} \boldsymbol{\delta \lambda_{r_{ca+}}} + \boldsymbol{\Phi_{14}} \boldsymbol{\delta \lambda_{v_{ca}}} \tag{A.33a}$$

$$\boldsymbol{\delta r_f} = [\boldsymbol{\Phi_{11}} + \boldsymbol{\Phi_{14}} \mathbf{H}] \boldsymbol{\delta r_{ca}} + [\boldsymbol{\Phi_{12}} + \boldsymbol{\Phi_{14}} \mathbf{L}] \boldsymbol{\delta v_{ca}} + \boldsymbol{\Phi_{13}} \boldsymbol{\delta \lambda_{r_{ca+}}} \tag{A.33b}$$

$$\boldsymbol{\delta v_f} = \boldsymbol{\Phi_{21}} \boldsymbol{\delta r_{ca}} + \boldsymbol{\Phi_{22}} \boldsymbol{\delta v_{ca}} + \boldsymbol{\Phi_{23}} \boldsymbol{\delta \lambda_{r_{ca+}}} + \boldsymbol{\Phi_{24}} \boldsymbol{\delta \lambda_{v_{ca}}} \tag{A.34a}$$

$$\boldsymbol{\delta v_f} = [\boldsymbol{\Phi_{21}} + \boldsymbol{\Phi_{24}} \mathbf{H}] \boldsymbol{\delta r_{ca}} + [\boldsymbol{\Phi_{22}} + \boldsymbol{\Phi_{24}} \mathbf{L}] \boldsymbol{\delta v_{ca}} + \boldsymbol{\Phi_{23}} \boldsymbol{\delta \lambda_{r_{ca+}}} \tag{A.34b}$$

Applying the co-state discontinuity relation A.31:

$$[\boldsymbol{\Phi_{21}} + \boldsymbol{\Phi_{24}} \mathbf{H}] \boldsymbol{\delta r_{ca}} + [\boldsymbol{\Phi_{22}} + \boldsymbol{\Phi_{24}} \mathbf{L}] \boldsymbol{\delta v_{ca}} + \boldsymbol{\Phi_{23}} \boldsymbol{\delta \lambda_{r_{ca-}}} - 2\nu \boldsymbol{\Phi_{23}} \mathbf{R_{2b}}^T \mathbf{C}^{-1} \mathbf{R_{2b}} \boldsymbol{\delta r_{ca}} = \boldsymbol{\delta v_f} \tag{A.35}$$

Substituting now the first equation of system A.16a:

$$\mathbf{N} \boldsymbol{\delta r_{ca}} + \mathbf{P} \boldsymbol{\delta v_{ca}} - \nu \mathbf{Q} \mathbf{R_{2b}} \boldsymbol{\delta r_{ca}} = \boldsymbol{\delta v_f} \tag{A.36}$$

Now it is possible to express $\boldsymbol{\delta v_{ca}}$:

$$\boldsymbol{\delta v_{ca}} = -\mathbf{P}^{-1} \mathbf{N} \boldsymbol{\delta r_{ca}} + \nu \mathbf{P}^{-1} \mathbf{Q} \mathbf{R_{2b}} \boldsymbol{\delta r_{ca}} + \mathbf{P^{-1}} \boldsymbol{\delta v_f} \tag{A.37}$$

The same process is repeated for Eq A.33b:

$$\tilde{\mathbf{N}} \boldsymbol{\delta r_{ca}} + \tilde{\mathbf{P}} \boldsymbol{\delta v_{ca}} - \nu \tilde{\mathbf{Q}} \mathbf{R_{2b}} \boldsymbol{\delta r_{ca}} = \boldsymbol{\delta r_f} \tag{A.38}$$

Substituting in the latter Eq. A.37

$$\mathbf{S}\boldsymbol{\delta}\mathbf{r_{ca}} - \nu\mathbf{T}\mathbf{R_{2b}}\boldsymbol{\delta}\mathbf{r_{ca}} = \boldsymbol{\delta}\mathbf{r_f} - \tilde{\mathbf{P}}\mathbf{P}^{-1}\boldsymbol{\delta}\mathbf{v_f} \tag{A.39}$$

Then by expressing $\boldsymbol{\delta}\mathbf{r_{ca}}$:

$$\boldsymbol{\delta}\mathbf{r_{ca}} = \nu\mathbf{S}^{-1}\mathbf{T}\mathbf{R_{2b}}\boldsymbol{\delta}\mathbf{r_{ca}} + \mathbf{S^{-1}}(\boldsymbol{\delta}\mathbf{r_f} - \tilde{\mathbf{P}}\mathbf{P}^{-1}\boldsymbol{\delta}\mathbf{v_f}) \tag{A.40}$$

SMD Constraint

Premultiplying the members for $\mathbf{R_{2b}}$:

$$\mathbf{R_{2b}}\boldsymbol{\delta}\mathbf{r_{ca}} = \nu\mathbf{R_{2b}}\mathbf{S}^{-1}\mathbf{T}\mathbf{R_{2b}}\boldsymbol{\delta}\mathbf{r_{ca}} + \mathbf{R_{2b}}\mathbf{S^{-1}}(\boldsymbol{\delta}\mathbf{r_f} - \tilde{\mathbf{P}}\mathbf{P}^{-1}\boldsymbol{\delta}\mathbf{v_f}) \tag{A.41}$$

Then defining:

$$\mathbf{k} = \mathbf{R_{2b}}\mathbf{S^{-1}}(\boldsymbol{\delta}\mathbf{r_f} - \tilde{\mathbf{P}}\mathbf{P}^{-1}\boldsymbol{\delta}\mathbf{v_f}) \qquad \mathbf{U} = \mathbf{R_{2b}}\mathbf{S}^{-1}\mathbf{T} \tag{A.42}$$

It is possible to obtain:

$$[\mathbf{I} - \nu\mathbf{U}]\boldsymbol{\delta}\mathbf{b_{ca}} = \mathbf{k} \tag{A.43}$$

Now expressing $\boldsymbol{\delta}\mathbf{b_{ca}}$:

$$\boldsymbol{\delta}\mathbf{b_{ca}} = [\mathbf{I} - \nu\mathbf{U}]^{-1}\mathbf{k} \tag{A.44}$$

Now consider the following trick:

$$\boldsymbol{\delta}\mathbf{b_{ca}} = \mathbf{b_{ca}}^{k+1} - \mathbf{b_{ca}}^{k} = \mathbf{b_{ca}}^{k+1} - \mathbf{b_s} + \mathbf{b_s} - \mathbf{b_{ca}}^{k} = \mathbf{b_{imp}}^{k+1} - \mathbf{b_{imp}}^{k} \tag{A.45}$$

Eq. A.45 can be substituted in Eq. A.44, considering that $\mathbf{b_{imp}}^{k}$ is known from the previous iteration:

$$\mathbf{b_{imp}}^{k+1} = [\mathbf{I} - \nu\mathbf{U}]^{-1}\mathbf{k} + \mathbf{b_{imp}}^{k} \tag{A.46}$$

Now applying SMD constraint:

$$\mathbf{b_{imp}}^{\mathbf{k+1}T}\mathbf{C}^{-1}\mathbf{b_{imp}}^{k+1} = \overline{SMD} \tag{A.47}$$

It is possible to obtain the following equation in ν:

$$\nu^2 \mathbf{k}^T \mathbf{Z}^T \mathbf{C}^{-1} \mathbf{Z}\mathbf{k} - \nu \mathbf{k}^T [\mathbf{Z}^T \mathbf{C}^{-1} + \mathbf{C}^{-1}\mathbf{Z}]\mathbf{k} = \alpha^2 \overline{SMD} - (\mathbf{b}_{\mathbf{imp}}^{\mathbf{k}} + \mathbf{k})^T \mathbf{C}^{-1} (\mathbf{b}_{\mathbf{imp}}^{\mathbf{k}} + \mathbf{k}) \tag{A.48}$$

B | Appendix B

This appendix reports the detailed demonstration of the sub-optimal Three Point Boundary Value Problem reported in Sect. 3.4.

B.0.1. Problem Formulation

First of all let's start by describing the dynamical model used for the orbital propagation:

$$\mathbf{x} = \begin{bmatrix} a \\ e \\ i \\ \Omega \\ \omega \\ \theta \end{bmatrix} \qquad \mathbf{a_c} = \begin{bmatrix} a_n \\ a_t \\ a_h \end{bmatrix} \tag{B.1}$$

$$\mathbf{f} = \begin{cases} \dot{a} = 2\sqrt{\dfrac{a^3}{\mu}\left(\dfrac{1+e\cos\theta+e^2}{1-e^2}\right)}a_t \\ \dot{e} = \sqrt{\dfrac{a}{\mu}\left(\dfrac{1-e^2}{1+e\cos\theta+e^2}\right)}\left[2(e+\cos\theta)a_t - \dfrac{(1-e)^2}{1+e\cos\theta}\sin\theta u_n\right] \\ \dfrac{di}{dt} = \sqrt{\dfrac{a}{\mu}(1-e^2)}\sin\theta + \omega a_h \\ \dot{\Omega} = \sqrt{\dfrac{a}{\mu}(1-e^2)}\dfrac{\sin\theta+\omega}{\sin i}a_h \\ \dot{\omega} = \sqrt{\dfrac{a}{\mu}\left(\dfrac{1-e^2}{1+e\cos\theta+e^2}\right)}\left[2\sin\theta a_t - \left(2e + \dfrac{(1-e)^2}{1+e\cos\theta}\cos\theta\right)a_n\right] + \\ \qquad\qquad - \sqrt{\dfrac{a}{\mu}(1-e^2)}\dfrac{\sin\theta+\omega\cos i}{\sin i}a_h \\ \dot{\theta} = \sqrt{\dfrac{\mu}{a^3(1-e^2)^3}}(1+e\cos\theta^2) + \dot{\omega} \end{cases} \tag{B.2}$$

Then assuming Keplerian orbit, knowing $\mathbf{x}(t_0) = \mathbf{x_0}$ initial state, t_0 starting time, t_{ca} time of closest approach, t_f final time. The problem is defined as the minimization of the following cost function:

$$J := \nu\Pi(t_{ca}, \mathbf{x}(t_{ca})) + \int_{t_i}^{t_f} \frac{1}{2}\mathbf{a_c}^T\mathbf{a_c}dt \tag{B.3a}$$

$$\Pi(t_{ca}, \mathbf{x}(t_{ca})) = SMD(\mathbf{r}(t_{ca})) - \overline{SMD} \geq 0 \tag{B.3b}$$

The functional can be expressed using the Hamiltonian:

$$H := \frac{1}{2}\mathbf{a_c}^T\mathbf{a_c} + \boldsymbol{\lambda}^T\mathbf{f}(\mathbf{x}, \mathbf{a_c}) \tag{B.4a}$$

$$J := \nu\Pi(t_{ca}, \mathbf{x}(t_{ca})) + \int_{t_i}^{t_f} \frac{1}{2}\mathbf{a_c}^T\mathbf{a_c} + \boldsymbol{\lambda}^T\left[\mathbf{f}(\mathbf{x}, \mathbf{a_c}) - \dot{\mathbf{x}}\right] dt \tag{B.4b}$$

Where: $\boldsymbol{\lambda}^T\dot{\mathbf{x}} = -\dot{\boldsymbol{\lambda}}^T\mathbf{x} + \frac{d(\boldsymbol{\lambda}^T\mathbf{x})}{dt}$

Splitting the integral:

$$\begin{aligned} J :=& \nu\Pi(t_{ca}, \mathbf{x}(t_{ca})) - \boldsymbol{\lambda}^T\mathbf{x}|_{t_i}^{\bar{t_{ca}}} - \boldsymbol{\lambda}^T\mathbf{x}|_{t_{ca}^+}^{t_f} + \int_{t_i}^{\bar{t_{ca}}} H(\mathbf{x}, \mathbf{a_c}, \boldsymbol{\lambda}, t) + \dot{\boldsymbol{\lambda}}^T\mathbf{x}dt \\ &+ \int_{t_{ca}^+}^{t_f} H(\mathbf{x}, \mathbf{a_c}, \boldsymbol{\lambda}, t) + \dot{\boldsymbol{\lambda}}^T\mathbf{x}dt \end{aligned} \tag{B.5}$$

Computing the first variation:

$$\frac{\partial J}{\partial \eta} = \nu\frac{\partial \Pi}{\partial \tilde{\mathbf{x}}(t_{ca})}\frac{\partial \tilde{\mathbf{x}}(t_{ca})}{\partial \eta} - \boldsymbol{\lambda}^T\frac{\partial \tilde{\mathbf{x}}}{\partial \eta}\bigg|_{t_i}^{\bar{t_{ca}}} - \boldsymbol{\lambda}^T\frac{\partial \tilde{\mathbf{x}}}{\partial \eta}\bigg|_{t_{ca}^+}^{t_f} + \int_{t_i}^{t_f} \frac{\partial H}{\partial \widetilde{\mathbf{a_c}}}\frac{\partial \widetilde{\mathbf{a_c}}}{\partial \eta} + \frac{\partial H}{\partial \tilde{\mathbf{x}}}\frac{\partial \tilde{\mathbf{x}}}{\partial \eta} + \dot{\boldsymbol{\lambda}}^T\frac{\partial \tilde{\mathbf{x}}}{\partial \eta}dt \tag{B.6}$$

Then it is possible to impose the necessary condition by forcing as null the first variation:

$$\begin{cases} \nu \dfrac{\partial \Pi}{\partial \mathbf{x}(t_{ca})} - \boldsymbol{\lambda}^T(t_{ca}^-) + \boldsymbol{\lambda}^T(t_{ca}^+) = 0 \\ \left.\dfrac{\partial \mathbf{x}}{\partial \eta}\right|_{t_i} = 0 \\ \left.\dfrac{\partial \mathbf{x}'}{\partial \eta}\right|_{t_f} = 0 \\ \lambda_\theta(t_f) = 0 \\ \dfrac{\partial H}{\partial \mathbf{a_c}} = 0 \\ \dfrac{\partial H}{\partial \mathbf{x}} + \dot{\boldsymbol{\lambda}}^T = 0 \Longrightarrow \dot{\boldsymbol{\lambda}} = -\left[\dfrac{\partial H}{\partial \mathbf{x}}\right]^T = -\left[\dfrac{\partial \mathbf{f}}{\partial \mathbf{x}}\right]^T \boldsymbol{\lambda} \\ \dfrac{\partial H}{\partial \boldsymbol{\lambda}} = \dot{\mathbf{x}} = \mathbf{f}(\mathbf{x}, \mathbf{a_c}) \\ \nu \geq 0 \\ \nu \Pi = 0 \end{cases} \tag{B.7}$$

where:

$$\mathbf{x}' = \begin{bmatrix} a \\ e \\ i \\ \Omega \\ \omega \end{bmatrix} \tag{B.8}$$

Once the algebraic control solution is obtained the problem is again translated in a Th-PBVP:

$$\begin{cases} \dot{\mathbf{x}} = \mathbf{f}(\mathbf{x}, \mathbf{a_c}) \\ \dot{\boldsymbol{\lambda}} = -\left[\dfrac{\partial \mathbf{f}}{\partial \mathbf{x}}\right]^T \boldsymbol{\lambda} \end{cases} \qquad BCs: \begin{cases} \mathbf{x}(t_0) = \mathbf{x_0} \\ \mathbf{x}(t_{ca^-}) = \mathbf{x}(t_{ca^+}) \\ \nu \dfrac{\partial \Pi}{\partial \tilde{\mathbf{x}}(t_{ca})} - \boldsymbol{\lambda}^T(t_{ca}^-) + \boldsymbol{\lambda}^T(t_{ca}^+) = 0 \\ \mathbf{x}'(t_f) = \mathbf{x}'_\mathbf{f} \\ \boldsymbol{\lambda_\theta}(t_f) = 0 \\ \Pi(t_{ca}) = 0 \end{cases} \tag{B.9}$$

B.0.2. EOP Solution

Once the ThPBVP is obtained the resolution procedure follows the one described in Appendix A.

First Trajectory Arc

As usual, the first arc is the easier to deal with. The objective is to find the expression of the co-state at TCA as a function of the state perturbation at the same time:

$$\begin{bmatrix} \boldsymbol{\delta \mathbf{x}_{ca^-}} \\ \boldsymbol{\lambda_{ca^-}} \end{bmatrix} = \begin{bmatrix} \boldsymbol{\Phi_{xx}} & \boldsymbol{\Phi_{x\lambda}} \\ \boldsymbol{\Phi_{\lambda x}} & \boldsymbol{\Phi_{\lambda\lambda}} \end{bmatrix} \begin{bmatrix} \boldsymbol{\delta \mathbf{x}_0} \\ \boldsymbol{\lambda_0} \end{bmatrix} \tag{B.10}$$

By imposing $\boldsymbol{\delta \mathbf{x}_0} = 0$:

$$\boldsymbol{\lambda_{ca^-}} = \boldsymbol{\Phi_{\lambda\lambda}} \boldsymbol{\lambda_0} \tag{B.11a}$$

$$\boldsymbol{\delta \mathbf{x}_{ca^-}} = \boldsymbol{\Phi_{x\lambda}} \boldsymbol{\lambda_0} \tag{B.11b}$$

Substituting Eq. B.11b in Eq. B.11a:

$$\boldsymbol{\lambda_{ca^-}} = \boldsymbol{\Phi_{\lambda\lambda}} \boldsymbol{\Phi_{x\lambda}^{-1}} \boldsymbol{\delta \mathbf{x}_{ca^-}} \tag{B.12}$$

Even the co-state can be split with the same philosophy of the state:

$$\boldsymbol{\lambda'_{ca^-}} = \mathbf{E} \boldsymbol{\delta \mathbf{x}'_{ca^-}} + \mathbf{w} \theta_{ca^-} \tag{B.13a}$$

$$\lambda_{\theta_{ca^-}} = \mathbf{g} \boldsymbol{\delta \mathbf{x}'_{ca^-}} + P \theta_{ca^-} \tag{B.13b}$$

Where:

$$\boldsymbol{\lambda'} = \begin{bmatrix} \lambda_a \\ \lambda_e \\ \lambda_i \\ \lambda_\Omega \\ \lambda_\omega \end{bmatrix} \qquad \boldsymbol{\Phi_{\lambda\lambda}} \boldsymbol{\Phi_{x\lambda}^{-1}} = \begin{bmatrix} \mathbf{E} & \mathbf{w} \\ \mathbf{g} & P \end{bmatrix} \tag{B.14}$$

Co-state Discontinuty

In this problem, the application of the interior point constraints leads to a more complex discontinuity equation. Analyzing C.4:

$$\frac{\partial \Pi}{\partial \mathbf{x}(t_{ca})} = \boldsymbol{\varphi}(\mathbf{x_{ca}}) \tag{B.15}$$

The discontinuity can be expressed as:

$$\boldsymbol{\lambda_{ca}}_{+} = \boldsymbol{\lambda_{ca}}_{-} - \nu \boldsymbol{\varphi}(\mathbf{x_{ca}}) \tag{B.16}$$

As before the vectorial equation can be decomposed:

$$\boldsymbol{\lambda'_{ca}}_{+} = \boldsymbol{\lambda'_{ca}}_{-} - \nu \boldsymbol{\varphi'}(\mathbf{x_{ca}}) \tag{B.17a}$$

$$\lambda_{\theta_{ca^+}} = \lambda_{\theta_{ca^-}} - \nu \varphi_\theta(\mathbf{x_{ca}}) \tag{B.17b}$$

In order to find an analytic solution, the discontinuity expression has to be approximated by adopting zero order Taylor's expansion.

$$\boldsymbol{\varphi'}(\mathbf{x_{ca}}) \approx \boldsymbol{\varphi'}(\mathbf{x_{ref}}(t_{ca})) = \boldsymbol{\varphi'} \tag{B.18a}$$

$$\varphi_\theta(\mathbf{x_{ca}}) \approx \varphi_\theta(\mathbf{x_{ref}}(t_{ca})) = \varphi_\theta \tag{B.18b}$$

Second Trajectory Arc

The previous decomposition of state and co-state is fundamental and reveals its importance in this phase. As can be seen in the boundary condition of Eq. B.9 the boundary condition at the final time includes the first five orbital elements and the last co-state variable.

$$\begin{bmatrix} \boldsymbol{\delta \mathbf{x}'_f} \\ \delta\theta_f \\ \boldsymbol{\lambda'_f} \\ \lambda_{\theta_f} \end{bmatrix} = \begin{bmatrix} \boldsymbol{\Phi_{x'x'}} & \boldsymbol{\Phi_{x'\theta}} & \boldsymbol{\Phi_{x'\lambda'}} & \boldsymbol{\Phi_{x'\lambda_\theta}} \\ \boldsymbol{\Phi_{\theta x'}} & \boldsymbol{\Phi_{\theta\theta}} & \boldsymbol{\Phi_{\theta\lambda'}} & \boldsymbol{\Phi_{\theta\lambda_\theta}} \\ \boldsymbol{\Phi_{\lambda' x'}} & \boldsymbol{\Phi_{\lambda'\theta}} & \boldsymbol{\Phi_{\lambda'\lambda'}} & \boldsymbol{\Phi_{\lambda'\lambda_\theta}} \\ \boldsymbol{\Phi_{\lambda_\theta x'}} & \boldsymbol{\Phi_{\lambda_\theta\theta}} & \boldsymbol{\Phi_{\lambda_\theta\lambda'}} & \boldsymbol{\Phi_{\lambda_\theta\lambda_\theta}} \end{bmatrix} \begin{bmatrix} \boldsymbol{\delta \mathbf{x}'_{ca}} \\ \delta\theta_{ca} \\ \boldsymbol{\lambda'_{ca}}_{+} \\ \lambda_{\theta_{ca^+}} \end{bmatrix} \tag{B.19}$$

To impose the orbit reentry $\boldsymbol{\delta \mathbf{x}'_f} = \mathbf{0}$ e $\lambda_{\theta_f} = 0$.

So let's continue analyzing the first vectorial equation:

$$\boldsymbol{\Phi}_{x'x'}\boldsymbol{\delta}\mathbf{x}'_{\mathbf{ca}} + \boldsymbol{\Phi}_{x'\theta}\delta\theta_{ca} + \boldsymbol{\Phi}_{x'\lambda'}\boldsymbol{\lambda}'_{ca^+} + \boldsymbol{\Phi}_{x'\lambda_\theta}\lambda_{\theta_{ca^+}} = \mathbf{0} \tag{B.20}$$

By applying the co-state discontinuity described in Eqs. B.17 and B.18:

$$\boldsymbol{\Phi}_{x'x'}\boldsymbol{\delta}\mathbf{x}'_{\mathbf{ca}} + \boldsymbol{\Phi}_{x'\theta}\delta\theta_{ca} + \boldsymbol{\Phi}_{x'\lambda'}\left[\boldsymbol{\lambda}'_{ca^-} - \nu\boldsymbol{\varphi}'\right] + \boldsymbol{\Phi}_{x'\lambda_\theta}\left[\lambda_{\theta_{ca^-}} - \nu\varphi_\theta\right] = 0 \tag{B.21}$$

Then substituting Eq. B.13 e reassemble the terms:

$$\mathbf{B}\boldsymbol{\delta}\mathbf{x}'_{\mathbf{ca}} + \mathbf{d}\delta\theta_{ca} - \nu\left(\boldsymbol{\Phi}_{x'\lambda'}\boldsymbol{\varphi}' + \boldsymbol{\Phi}_{x'\lambda_\theta}\varphi_\theta\right) = 0 \tag{B.22}$$

Where:

$$\mathbf{B} = \boldsymbol{\Phi}_{x'x'} + \boldsymbol{\Phi}_{x'\lambda'}\mathbf{E} + \boldsymbol{\Phi}_{x'\lambda_\theta}\mathbf{g} \qquad \mathbf{d} = \boldsymbol{\Phi}_{x'\theta} + \boldsymbol{\Phi}_{x'\lambda'}\mathbf{w} + P\boldsymbol{\Phi}_{x'\lambda_\theta} \tag{B.23}$$

The previous relation can be inverted to express $\boldsymbol{\delta}\mathbf{x}'_{\mathbf{ca}}$

$$\boldsymbol{\delta}\mathbf{x}'_{\mathbf{ca}} = -\mathbf{B}^{-1}\mathbf{d}\delta\theta_{ca} + \nu\mathbf{B}^{-1}\left(\boldsymbol{\Phi}_{x'\lambda'}\boldsymbol{\varphi}' + \boldsymbol{\Phi}_{x'\lambda_\theta}\varphi_\theta\right) \tag{B.24}$$

It is now the moment to work on the last equation of the system B.19:

$$\tilde{\mathbf{b}}\boldsymbol{\delta}\mathbf{x}'_{\mathbf{ca}} + \tilde{D}\delta\theta_{ca} - \nu\left(\boldsymbol{\Phi}_{\lambda_\theta\lambda'}\boldsymbol{\varphi}' + \boldsymbol{\Phi}_{\lambda_\theta\lambda_\theta}\varphi_\theta\right) = 0 \tag{B.25}$$

Where:

$$\tilde{\mathbf{b}} = \boldsymbol{\Phi}_{\lambda_\theta x'} + \boldsymbol{\Phi}_{\lambda_\theta\lambda'}\mathbf{E} + \boldsymbol{\Phi}_{\lambda_\theta\lambda_\theta}\mathbf{g} \qquad \tilde{D} = \boldsymbol{\Phi}_{\lambda_\theta\theta} + \boldsymbol{\Phi}_{\lambda_\theta\lambda'}\mathbf{w} + P\boldsymbol{\Phi}_{\lambda_\theta\lambda_\theta} \tag{B.26}$$

Substituting B.24 and reassamble the terms:

$$L\delta\theta_{ca} - \nu M = 0 \tag{B.27}$$

In which:

$$\mathbf{l} = \tilde{D} - \tilde{\mathbf{b}}(\mathbf{B}^{-1}\mathbf{d}) \qquad M = \boldsymbol{\Phi}_{\lambda_\theta\lambda'}\boldsymbol{\varphi}' + \boldsymbol{\Phi}_{\lambda_\theta\lambda_\theta}\varphi_\theta - \tilde{\mathbf{b}}\left[\mathbf{B}^{-1}\left(\boldsymbol{\Phi}_{x'\lambda'}\boldsymbol{\varphi}' + \boldsymbol{\Phi}_{x'\lambda_\theta}\varphi_\theta\right)\right] \tag{B.28}$$

Expressing $\delta\theta_{ca}$:

$$\delta\theta_{ca} = \nu\frac{M}{L} \tag{B.29}$$

And so:

$$\boldsymbol{\delta}\mathbf{x}'_{\mathbf{ca}} = \nu\mathbf{B}^{-1}\mathbf{n} \tag{B.30}$$

Where:

$$\mathbf{n} = \boldsymbol{\Phi}_{\boldsymbol{x'\lambda'}}\boldsymbol{\varphi'} + \boldsymbol{\Phi}_{\boldsymbol{x'\lambda_\theta}}\varphi_\theta - \frac{M}{L}\mathbf{d} \tag{B.31}$$

Assemble the Eqs. B.30 e B.29:

$$\boldsymbol{\delta}\mathbf{x}_{\mathbf{ca}} = \nu\mathbf{h} \qquad \mathbf{h} = \begin{bmatrix}\mathbf{B}^{-1}\mathbf{n}\\ \frac{M}{L}\end{bmatrix} \tag{B.32}$$

SMD Constraint

The state obtained at TCA is the following:

$$\mathbf{x}(t_{ca}) = \mathbf{x}_{\mathbf{ref}}(t_{ca}) + \nu\mathbf{h} \tag{B.33}$$

Defining $\boldsymbol{\rho}(\mathbf{x})$ as the transformation function from orbital parameters to cartesian position, it is possible to apply the SMD constraints.

$$\left[\boldsymbol{\rho}(\mathbf{x}_{\mathbf{ca}}) - \mathbf{r}_{\mathbf{s}}(t_{ca})\right]^T \mathbf{Q}\left[\boldsymbol{\rho}(\mathbf{x}_{\mathbf{ca}}) - \mathbf{r}_{\mathbf{s}}(t_{ca})\right] = \overline{SMD} \tag{B.34}$$

Where:

$$\mathbf{Q} = \mathbf{R_{2b}}^T\mathbf{C}^{-1}\mathbf{R_{2b}} \tag{B.35}$$

However, it is not possible to solve analytically this equation. Therefore equation is linearized using the first order Taylor expansion $\boldsymbol{\rho}(\mathbf{x})$:

$$\boldsymbol{\rho}(\mathbf{x}_{\mathbf{ca}}) \approx \mathbf{r}_{\mathbf{ref}}(t_{ca}) + \nu\mathbf{J}(\mathbf{x}_{\mathbf{ref}}(t_{ca}))\mathbf{h} \tag{B.36}$$

Abbreviating the notation:

$$\boldsymbol{\rho}(\mathbf{x}_{\mathbf{ca}}) \approx \mathbf{r}_{\mathbf{p}}(t_{ca}) + \nu\mathbf{J}\mathbf{h} \tag{B.37}$$

Substituting in the constraint equation:

$$\left[\mathbf{r_p}(t_{ca}) + \nu\mathbf{Jh} - \mathbf{r_s}(t_{ca})\right]^T \mathbf{Q} \left[\mathbf{r_p}(t_{ca}) + \nu\mathbf{Jh} - \mathbf{r_s}(t_{ca})\right] = \overline{SMD} \tag{B.38}$$

C | Appendix C

C.0.1. Problem Formulation

The last appendix reports the accurate mathematical computation of the energy optimal problem proposed in Sect. 4.1

The dynamical model used for the orbital propagation is the one presented in Sect. 2.6. It includes the Non-spherical Earth perturbation until the J22 harmonical effect.

The optimal control problem starts like the other ones:

$$J := \nu\Pi(t_{ca}, \mathbf{x}(t_{ca})) + \int_{t_i}^{t_f} \frac{1}{2}\mathbf{a_c}^T\mathbf{a_c} + \boldsymbol{\lambda}^T\left[\mathbf{f}(\mathbf{x}, \mathbf{a_c}) - \dot{\mathbf{x}}\right] dt \tag{C.1}$$

Where: $\boldsymbol{\lambda}^T\dot{\mathbf{x}} = -\dot{\boldsymbol{\lambda}}^T\mathbf{x} + \frac{d(\boldsymbol{\lambda}^T\mathbf{x})}{dt}$

Splitting the integral:

$$\begin{aligned} J :=& \nu\Pi(t_{ca}, \mathbf{x}(t_{ca})) - \boldsymbol{\lambda}^T\mathbf{x}|_{t_i}^{t_{ca}^-} - \boldsymbol{\lambda}^T\mathbf{x}|_{t_{ca}^+}^{t_f} + \int_{t_i}^{t_{ca}^-} H(\mathbf{x}, \mathbf{a_c}, \boldsymbol{\lambda}, t) + \dot{\boldsymbol{\lambda}}^T\mathbf{x}dt \\ &+ \int_{t_{ca}^+}^{t_f} H(\mathbf{x}, \mathbf{a_c}, \boldsymbol{\lambda}, t) + \dot{\boldsymbol{\lambda}}^T\mathbf{x}dt \end{aligned} \tag{C.2}$$

Now it is possible to compute the first variation of J.

$$\frac{\partial J}{\partial \eta} = \nu\frac{\partial \Pi}{\partial \tilde{\mathbf{x}}(t_{ca})}\frac{\partial \tilde{\mathbf{x}}(t_{ca})}{\partial \eta} - \boldsymbol{\lambda}^T\frac{\partial \tilde{\mathbf{x}}}{\partial \eta}\Big|_{t_i}^{t_{ca}^-} - \boldsymbol{\lambda}^T\frac{\partial \tilde{\mathbf{x}}}{\partial \eta}\Big|_{t_{ca}^+}^{t_f} + \int_{t_i}^{t_f} \frac{\partial H}{\partial \widetilde{\mathbf{a_c}}}\frac{\partial \widetilde{\mathbf{a_c}}}{\partial \eta} + \frac{\partial H}{\partial \tilde{\mathbf{x}}}\frac{\partial \tilde{\mathbf{x}}}{\partial \eta} + \dot{\boldsymbol{\lambda}}^T\frac{\partial \tilde{\mathbf{x}}}{\partial \eta}dt \tag{C.3}$$

Then by imposing $\frac{\partial J}{\partial \eta} = 0$ the following system of algebraic and differential equations is

obtained:

$$\begin{cases} \left.\dfrac{\partial \mathbf{x}}{\partial \eta}\right|_{t_i} = 0 \\ \left.\dfrac{\partial \mathbf{x}}{\partial \eta}\right|_{t_f} = 0 \\ \dfrac{\partial H}{\partial \mathbf{a_c}} = \mathbf{a_c}^T + \boldsymbol{\lambda}^T \mathbf{B}(t) = \mathbf{0} \Longrightarrow \mathbf{a_c} = -\mathbf{B}(t)^T \lambda \\ \dfrac{\partial H}{\partial \mathbf{x}} + \dot{\boldsymbol{\lambda}}^T = 0 \Longrightarrow \dot{\boldsymbol{\lambda}} = -\left[\dfrac{\partial H}{\partial \mathbf{x}}\right]^T = -\left[\dfrac{\partial \mathbf{f}}{\partial \mathbf{x}}\right]^T \boldsymbol{\lambda} = -\mathbf{A}(t)^T \boldsymbol{\lambda} \\ \dfrac{\partial H}{\partial \boldsymbol{\lambda}} = \dot{\mathbf{x}} = \mathbf{f}(\mathbf{x}, \mathbf{a_c}) \\ \nu \Pi \geq 0 \end{cases} \tag{C.4}$$

From which is possible to determine the following MPBVP:

$$\begin{cases} \dot{\mathbf{x}} = \mathbf{A}(t)\mathbf{x} - \mathbf{B}(t)\mathbf{B}(t)^T \lambda + \mathbf{D}(t) \\ \dot{\boldsymbol{\lambda}} = -\mathbf{A}(\mathbf{t})^t \boldsymbol{\lambda} \end{cases} \qquad BCs : \begin{cases} \mathbf{x}(t_0) = \mathbf{x_0} \\ \mathbf{x}(t_f) = \mathbf{x_f} \\ \nu \dfrac{\partial \Pi}{\partial \mathbf{x}(t_{ca})} - \boldsymbol{\lambda}^T(t_{ca}^-) + \boldsymbol{\lambda}^T(t_{ca}^+) = 0 \\ \xi(t_{ca}) \geq 0 \end{cases} \tag{C.5}$$

C.0.2. EOP Solution

In the previous section, the OCP is transformed in the problem of finding the initial costate and the adjointed multiplicator. The resolution procedure requires to subdivide the trajectory in two segments in the intervals $[t_1; t_{ca}]$ and $[t_{ca}; t_f]$. This step is necessary to apply the interior point constraint. To obtain an analytical solution the two trajectories have to be linearized respect to Keplerian unperturbed motion by virtue of the STM.

$$\begin{cases} \dot{\boldsymbol{\Phi}}(t) = \mathbf{A_{STM}}(t)\boldsymbol{\Phi}(\mathbf{x}(t_0), t) \\ \boldsymbol{\Phi}(\mathbf{x}(t_0), t_0) = \mathbf{I} \end{cases} \tag{C.6}$$

Dove:

$$\mathbf{A_{STM}}(t) = \begin{bmatrix} \mathbf{A}(t) & -\mathbf{B}(t)\mathbf{B}(t)^T \\ \mathbf{0_{3\times 3}} & -\mathbf{A_{STM}}(t)^T \end{bmatrix} \tag{C.7}$$

First Arc

Considering the linearization respect to the un-maneuvered trajectory in the interval $[t_0, t_{ca}^-]$.

$$\begin{bmatrix} \boldsymbol{\delta}\mathbf{x_{ca}} \\ \boldsymbol{\lambda}_{ca^-} \end{bmatrix} = \begin{bmatrix} \boldsymbol{\Phi}_{xx} & \boldsymbol{\Phi}_{x\lambda} \\ \boldsymbol{\Phi}_{\lambda x} & \boldsymbol{\Phi}_{\lambda\lambda} \end{bmatrix} \begin{bmatrix} \boldsymbol{\delta}\mathbf{x_0} \\ \boldsymbol{\lambda_0} \end{bmatrix} \tag{C.8}$$

Imposing $\boldsymbol{\delta}\mathbf{x_0} = 0$:

$$\boldsymbol{\lambda}_{ca^-} = \boldsymbol{\Phi}_{\lambda\lambda}\boldsymbol{\lambda_0} \tag{C.9a}$$

$$\boldsymbol{\delta}\mathbf{x_{ca^-}} = \boldsymbol{\Phi}_{x\lambda}\boldsymbol{\lambda_0} \tag{C.9b}$$

Substituting the second equation inside the first one:

$$\boldsymbol{\lambda}_{ca^-} = \boldsymbol{\Phi}_{\lambda\lambda}\boldsymbol{\Phi}_{x\lambda}^{-1}\boldsymbol{\delta}\mathbf{x_{ca}} = \mathbf{E}\boldsymbol{\delta}\mathbf{x_{ca}} \tag{C.10}$$

Co-state discontinuity

$$\frac{\partial \Pi}{\partial \mathbf{x}(t_{ca})} = \boldsymbol{\varphi}(\mathbf{x_{ca}}) \tag{C.11}$$

The co-state discontinuity can be expressed as:

$$\boldsymbol{\lambda}_{ca^+} = \boldsymbol{\lambda}_{ca^-} - \nu\boldsymbol{\varphi}(\mathbf{x_{ca}}) \tag{C.12}$$

In order to find an analytic solution, the co-state discontinuity has to be approximated. In this case a zero order Taylor series expansion is adopted:

$$\boldsymbol{\varphi}(\mathbf{x_{ca}}) \approx \boldsymbol{\varphi}(\mathbf{x_{ref}}(t_{ca})) = \boldsymbol{\varphi} \tag{C.13}$$

Second Arc

In a similar way to what is done in the first arc. The resolution proceeds by linearizing the second arc using the STM.

$$\begin{bmatrix} \boldsymbol{\delta x_f} \\ \boldsymbol{\lambda}_f \end{bmatrix} = \begin{bmatrix} \boldsymbol{\Phi}_{xx} & \boldsymbol{\Phi}_{x\lambda} \\ \boldsymbol{\Phi}_{\lambda x} & \boldsymbol{\Phi}_{\lambda\lambda} \end{bmatrix} \begin{bmatrix} \boldsymbol{\delta x_{ca}} \\ \boldsymbol{\lambda}_{ca^+} \end{bmatrix} \tag{C.14}$$

Analyzing the first vectorial equation:

$$\boldsymbol{\delta x_f} = \boldsymbol{\Phi}_{xx}\boldsymbol{\delta x_{ca}} + \boldsymbol{\Phi}_{x\lambda}\boldsymbol{\lambda}_{ca^+} \tag{C.15}$$

Substituting EQ. C.13, C.10 and working on the equation:

$$\boldsymbol{\delta x_f} = \mathbf{F}\boldsymbol{\delta x_{ca}} - \nu\boldsymbol{\Phi}_{x\lambda}\boldsymbol{\varphi} \tag{C.16}$$

Where:

$$\mathbf{F} = \boldsymbol{\Phi}_{xx} + \boldsymbol{\Phi}_{x\lambda}\mathbf{E}$$

The expression of the state at TCA as a function of ν can be obtained from the previous relationship:

$$\boldsymbol{\delta x_{ca}} = \boldsymbol{\delta x_{sk,ca}} + \nu\mathbf{h_{CAM}} \tag{C.17}$$

The two terms represent respectively the contribution due to station keeping maneuver and to the CAM and are expressed as:

$$\boldsymbol{\delta x_{sk,ca}} = \mathbf{F}^{-1}\boldsymbol{\delta x_f} \qquad\qquad \mathbf{h_{CAM}} = \mathbf{F}^{-1}\boldsymbol{\Phi}_{x\lambda}\boldsymbol{\varphi} \tag{C.18}$$

SMD Constraint

Once the expression of the perturbation at TCA is computed, it is necessary to consider the SMD constraint. The first step is to verify if the contribution of the SK maneuver is sufficient to respect the PoC constraint. In this case:

$$\Pi(\mathbf{x_{sk,ca}}) \geq 0 \tag{C.19}$$

It is sufficient to impose $\nu = 0$, and compute the initial co-state.

If the previous inequality is not respected, the procedure follows an approach similar to

the one reported in Appendix A and Appendix B.

Defining $\boldsymbol{\varrho}(\mathbf{x})$ as the function that allows to convert the equinoctial orbital elements in the cartesian position it is possible to impose the SMD constraint.

$$[\boldsymbol{\varrho}(\mathbf{x_{ca}}) - \mathbf{r_s}(t_{ca})]^T \mathbf{Q} [\boldsymbol{\varrho}(\mathbf{x_{ca}}) - \mathbf{r_s}(t_{ca})] = \overline{SMD} \tag{C.20}$$

Where:

$$\mathbf{Q} = \mathbf{R_{2b}}^T \mathbf{C}^{-1} \mathbf{R_{2b}} \tag{C.21}$$

However, it is not possible to solve analytically the equation. Therefore it is necessary to linearize using the first order Taylor expansion respect to $\mathbf{x_{sk,ca}}$, the function $\boldsymbol{\varrho}(\mathbf{x})$:

$$\boldsymbol{\varrho}(\mathbf{x_{ca}}) \approx \mathbf{r_{sk,ca}}(t_{ca}) + \nu \mathbf{J}(\mathbf{x_{sk,ca}}(t_{ca}))\mathbf{h_{CAM}} \tag{C.22}$$

By abbreviating the notation:

$$\boldsymbol{\varrho}(\mathbf{x_{ca}}) \approx \mathbf{r_{sk,ca}}(t_{ca}) + \nu \mathbf{Jh} \tag{C.23}$$

Substituting inside the constraint equation:

$$[\mathbf{r_{sk,ca}}(t_{ca}) + \nu \mathbf{Jh} - \mathbf{r_s}(t_{ca})]^T \mathbf{Q} [\mathbf{r_{sk,ca}}(t_{ca}) + \nu \mathbf{Jh} - \mathbf{r_s}(t_{ca})] = \overline{SMD} \tag{C.24}$$

It represents a second-degree equation as function of ν that can be resolved in closed form.

List of Figures

List of Tables

Acronyms

CAM Collision Avoidance Maneuver

CCSDS Consultative Committee for Space Data Systems

CDM Conjunction Data Message

CSM Conjunction Summary Message

DFD Discontinue Finite Difference

ECI Earth Centered Inertial

EOE Equinoctial Orbital Element

EOP Energy Optimal Problem

ESA European Space Agency

FOP Fuel Optimal Problem

GA Genetic Algorithm

GEO Geostationary Earth Orbit

JSpOC Joint Space Operations Center

LEO Low Earth Orbit

MD Miss Distance

MPBVP Multi-Point Boundary Value Problem

NEO Near-Earth Object

OCP Optimal Control Problem

PDF Probability density function

PoC collision probability

PTOM Point To Orbit Maneuver

PTPM Point To Point Maneuver

r.f. reference frame

SDO Space Debris Office

SFD Smooth Finite Difference

SK Station Keeping

SMD Squared Mahalanobis Distance

SSA Space Situational Awareness

SST Space Surveillance and Tracking

STM State Transition Matrix

TCA Time of Closest Approach

ThPBVP Three Point Boundary Value Problem

TLE Two-Line Element set

TwPBVP Two Point Boundary Value Problem

USSTRATCOM US Strategic Command

Variable	Description	SI unit
a	Scalar	[-]
$\mathbf{a}$	Vector	[-]
$\mathbf{A}$	Matrix	[-]
ΔV	Velocity Variation	[km/s]
μ	Earth Gravitational Constant	[km^3/s^2]
$\boldsymbol{\lambda}$	Costate Vector	[-]
$\boldsymbol{\Phi}$	State Transition Matrix	[-]
$\mathbf{S\tilde{T}M}$	First Trajectory State Transition Matrix	[-]
STM	Second Trajectory State Transition Matrix	[-]
$\mathbf{a}_c$	Control Acceleration	[m/s^2]
$\mathbf{a}_p$	Perturbing Acceleration	[m/s^2]
$\mathbf{a}_{geo}$	Geopotential Acceleration	[m/s^2]
$\mathbf{b}$	Position Vector in B-Plane Coordinates	[km]
$\mathbf{C}$	Combined Covariance Matrix	[km^2]
$\mathbf{r}$	Position Vector in ECI coordinates	[km]
$\mathbf{R}_b$	Rotation Matrix between ECI frame and B-Plane	[-]
$\mathbf{v}$	Velocity Vector	[km/s]
g_0	Earth's Standard Gravity Acceleration	[km/s^2]
I_{sp}	Specific Impulse	[s]
t	Time	[s]
PoC	Probability of Collision	[-]
SMD	Squared Mahalanobis Distance	[km^2]
0	Initial Manoeuvering Point	[-]
f	Final Manoeuvering Point	[-]
p	Primary Object	[-]
s	Secondary Object	[-]
m	Quantities Belonging To Maneuvered Trajectories	[-]

Acknowledgements

First of all, a special thank goes to GMV for providing me the conjunction data message used as test case for the GEO maneuver. Without your help, I should have spent so much time to model the collision, with the risk of reproducing a non-relevant case.

I would like to thank all the people that have been close to me on this journey. First of all, a special thanks to my advisor Professor Pierluigi di Lizia. I had the pleasure of being inspired by him in two courses during my academic formation and finally he gave me the possibility to conclude my path with this master thesis, motivating and putting me in the condition to express my best. I would also like to thank my co-advisor, Professor Roberto Armellin, for his availability and collaboration in this work. A special thanks goes to the Ph.D. candidate Andrea De Vittori for supplying all the necessary material allowing me to focus on my work, and for his continuous support that accompanied me during this trip.

Then I would like to thank all my friends from the town where I grew up for never letting me alone during my experience in Milan. A thought goes to Manfredi, Andrea, Simone, Davide, and Silvia that alleviated my days at university, and with whom I shared all my best moments during these five academic years. Thanks especially to Davide for representing the perfect victim of Simone's jokes and mine.

Thanks to AC Milan, that after making me suffer like hell since my transfer to Milan, during my last year gave me the joy of celebrating the scudetto in this city.

Then I would like to thank Valentina, Nadia, and Giuseppe: despite we don't have blood ties, you are certainly part of my family.

Thanks to my uncles, Fabrizio and Giampaolo, for making me have fun during all my life. I probably spent with you the best days of my life. Thanks to my cousins, Francesco e Filippo, whom I saw growing up until they become men, but remember I will always be stronger than you both.

A special thank is given to Margherita who in the last two years endured me and gave me all the affection that I needed, only asking for the same. Thank you for always being

by my side, for convincing me to do something that I would never thought about such as taking a vacation, and for helping me in all my worst moments.

I am extremely grateful to my mother, Laura, and my father, Gian Luca, for all the sacrifices they made in these past years. Thanks also to the values that you both transmit to me without whom I could have never reached this goal. I hope I made you proud of me.

Finally, the most important thanks goes to my grandfathers, Michele and Gabriele, who have represented the most important people in my life. I don't know if you can read this message, surely you need someone who translates it. Anyway, I would like to tell you both that I was inspired by you every day of my life, hoping to become half the men you were.